INFORMATION TO USERS

This manuscript has been reproduced from the microfilm master. UMI films the text directly from the original or copy submitted. Thus, some thesis and dissertation copies are in typewriter face, while others may be from any type of computer printer.

The quality of this reproduction is dependent upon the quality of the copy submitted. Broken or indistinct print, colored or poor quality illustrations and photographs, print bleedthrough, substandard margins, and improper alignment can adversely affect reproduction.

In the unlikely event that the author did not send UMI a complete manuscript and there are missing pages, these will be noted. Also, if unauthorized copyright material had to be removed, a note will indicate the deletion.

Oversize materials (e.g., maps, drawings, charts) are reproduced by sectioning the original, beginning at the upper left-hand corner and continuing from left to right in equal sections with small overlaps.

Photographs included in the original manuscript have been reproduced xerographically in this copy. Higher quality 6" x 9" black and white photographic prints are available for any photographs or illustrations appearing in this copy for an additional charge. Contact UMI directly to order.

ProQuest Information and Learning
300 North Zeeb Road, Ann Arbor, MI 48106-1346 USA
800-521-0600

UMI®

An X- and Q-Band Electron Paramagnetic Resonance Study of Mn^{2+} in a Single Crystal of $NH_4Cl_{0.9}I_{0.1}$ in the Temperature Range 77-295 K

Gino Rinaldi

A Thesis

in

The Department

of

Physics

Presented in Partial Fulfillment of the Requirements

for the Degree of Master of Science at

Concordia University

Montreal, Quebec, Canada

August 2001

ABSTRACT

An X- and Q-Band Electron Paramagnetic Resonance Study of Mn^{2+} in a Single Crystal of $NH_4Cl_{0.9}I_{0.1}$ in the Temperature Range 77-295 K

Gino Rinaldi

This work is an electron paramagnetic resonance study of the mixed ammonium chloride-iodide host crystal doped with divalent manganese. The studies presented here were carried out at X-band and Q-band microwave frequencies, and at various microwave cavity temperatures. The resonance spectrum of this crystal is described by a set of spin-Hamiltonian parameters, whose parameters are determined by fitting the various resonance line positions obtained for several angular orientations of the magnetic field relative to the crystal axes. A set of initial parameters is then determined by second-order perturbation theory. These are then rigorously evaluated by a computer subroutine using the least-squares-fitting technique.

The spectra obtained through angular variation of the crystal within the static magnetic field confirm the cubic symmetry of the crystal, and the existence of three magnetically equivalent sites having their axes along the [100], [010], and [001] directions.

The final set of spin-Hamiltonian parameters were interpreted using the superposition model, which is a mathematical approach used to evaluate the intrinsic parameters of the crystal, based on the sum of nearest neighbor ligand contributions.

Acknowledgements

It is with great pleasure that I wish to express my gratitude and appreciation to Dr. S. K. Misra for his suggestion of the research topic, for his guidance, advice, critical comments, and patience in the preparation of this thesis.

I would also like to express my sincere appreciation and gratitude to Dr. Serguei Andronenko whose knowledge, insights, and discussions, both professional and personal, helped me with this project.

I would also like to acknowledge and thank Dr. Prem Chand from the Indian Institute of Technology for his help in this research, and for supplying us with the mixed ammonium chloride-iodide crystals and crystal data.

I am also grateful to Mr. Mostafa Showleh and Gurnum Manku for their friendship and for their technical expertise which on more than one occasion managed to keep the equipment running. I would also like to thank Aldo Dissegna, Richard Allix, Bob Pisarsky, and Claude Lamarche from the science technical center of Concordia University, for their help with equipment and electronics, and for their friendly doses of sarcasm.

My heartfelt thanks go to my colleagues and friends Manas Dan, Kevin Shannon, Mario Venditti, Yuxing Zhang, Julien Banchet, Derek Nelligan, Cicylia Kereh, Margareta Murwaningsih, Victor Erb, Peter Chau, Gilbert Melanson, Sara Chen, Michelle Baryliuk Raimbert, Svetlana Pidasheva, Ulle Doettling, Louise Laflamme, Pierre Raymond, Leonardo Nastasi, Carlos Melo, and Sarah Powis.

A big thank you goes out to Odette Dias who monitored my caffeine levels during the course of my studies at Concordia University.

I would also like to express my special appreciation to Ms. Gloria Thomson and Ms. Lynn Chapman of the Physics Department of Concordia University for their friendly smiles and encouragement during my studies.

I would like to say a special thank you to Dr. Mariana Frank, Professor Joseph Shin, Professor Zuoqing Wang, Dr. Ramesh Sharma, Dr. Calvin Kalman, Dr. Arlin Kipling, Dr. Petros Vassilopoulos, Dr. Barry Frank, Dr. M. Stephen Dubas, Dr. Nelson Eddy, Dr. Eli Cohen, and Dr. David Cheeke for the many stimulating non academic discussions over these past few years.

Finally, I wish to express my deepest gratitude to my parents and family for their love, affection, and moral support, without which I would not be where I am today.

Financial support from Dr. S. K. Misra NSERC grant is gratefully acknowledged, in addition to T. A. support from the Department of Physics of Concordia University.

Table of Contents

List of Figures

List of Tables

Preface

Motivation and Organization of Thesis

The motivation behind the research required for this thesis was the opportunity to apply the knowledge of electron paramagnetic resonance (EPR), also referred to as electron spin resonance (ESR), acquired in the classroom to the laboratory and to perform a study on an actual crystal on my part. An EPR course taught by Dr. Misra heightened my interest for the field of paramagnetic resonance. The initial feelings of intimidation of all the electronic, magnetic, energetic, components soon gave way to an appreciation of how all these different and varied pieces of equipment operate together to make up a magnetic resonance spectrometer. In this respect, an EPR spectrometer really is the sum of its parts.

In this thesis, an experimental study with appropriate theoretical interpretation of divalent manganese (Mn^{2+}), a transition metal ion, embedded in the mixed ammonium chloride-iodide ($NH_4Cl_{0.9}I_{0.1}$) host crystal is presented. The EPR spectrum of Mn^{2+} in the pure compounds ammonium chloride (NH_4Cl), and ammonium iodide (NH_4I) host crystals were initially studied by Forman and van Wyk (1966), and by Chand and Upreti (1983), respectively. It was reported that the Mn^{2+} cation substitutes for a NH_4^+ cation, and that "most probably", the overall charge compensation is achieved by having the next nearest cation site vacant in the crystal. The spin-Hamiltonian parameters (SHP) reported by Chand and Upreti (1983) for the NH_4I host crystal closely match those in the NH_4Cl

host crystal even though the two crystals have different lattice structures, the NH_4I crystal possessing the face-centered-cubic (FCC), while the NH_4Cl crystal possessing the body-centered-cubic (BCC) structure. The SHP of these two crystals, as well as those determined for the $NH_4Cl_{0.9}I_{0.1}$ crystal, will be interpreted by the superposition model (SM) of Newman (1971) where the intrinsic parameter, $\bar{b}_2$ is a function of the sum of, and spatial orientation of the ligands surrounding the Mn^{2+} cation in these crystals.

The X-band spectra of Mn^{2+} in NH_4Cl and NH_4I are very similar, and it was felt that because of these similarities it would be interesting to investigate the EPR spectrum of Mn^{2+} in the mixed $NH_4Cl_{0.9}I_{0.1}$ crystal. The zero-field splitting (ZFS) parameter, b_2^0, reported in these works for Mn^{2+} in NH_4Cl and NH_4I, has been observed to be rather large ($\approx$ 4.5 GHz) in these inorganic crystals, leading to some unusual features of the X-band spectrum, especially the forbidden hyperfine (HF) transitions [Chand and Upreti, 1983]. One of the motivations is to study this large ZFS in the $NH_4Cl_{0.9}I_{0.1}$ crystal by using a multi-frequency approach, X-band ($\approx$ 9.6 GHz), and Q-band ($\approx$ 35 GHz), at various temperatures: 295K, 120K and 77K. It is hoped that the $NH_4Cl_{0.9}I_{0.1}$ crystal will be further investigated by higher frequencies appropriate to study large ZFS.

The research for this thesis consisted of several experiments carried out at various temperatures and microwave frequencies where the crystal was rotated in the applied magnetic field. The Mn^{2+} first-derivative absorption line positions were used to evaluate the SHP for Mn^{2+} in the mixed $NH_4Cl_{0.9}I_{0.1}$ crystal.

The organization of this thesis is as follows. Chapter 1 provides an introduction to this thesis where a general discussion of EPR will be given and how it can be used to

analyze the energy transitions of paramagnetic ions embedded in suitable host crystals. This is followed by a discussion of the spin-Hamiltonian (SH) in chapter 2, which deals with a theoretical analysis of the energy-Hamiltonian equation. The specific SH for Mn^{2+} is determined based upon the crystal structure of the host lattice, and the local symmetry about the Mn^{2+} ion. The SHP are evaluated using EPR line positions. An historical overview of the evolution of EPR is given in chapter 3, where the workings of a general EPR spectrometer are discussed, including the specific spectrometer components for X-band and Q-band used in this research are introduced. The equipment used in low temperature measurements is also discussed in this section. In chapter 4, the preparation and structure of the $NH_4Cl_{0.9}I_{0.1}$ crystal are discussed, and the experimental results are analyzed to estimate the SHP for Mn^{2+} in $NH_4Cl_{0.9}I_{0.1}$, and compared to those published for NH_4Cl and NH_4I. The experimental results obtained are interpreted by using the SM in chapter 5. The SM is applied to the $NH_4Cl_{0.9}I_{0.1}$ crystal for both the FCC and BCC structures. The results obtained are the compared to those of the NH_4I and NH_4Cl crystals in order to establish a consistency with the published results for the intrinsic parameter $\bar{b}_2$ for Mn^{2+} with iodide ligands, and with chloride ligands. A summary and concluding remarks are given in chapter 6, as well as the future perspectives of EPR research on the Mn^{2+}-doped mixed $NH_4Cl_{0.9}I_{0.1}$ crystal. Appendix A gives the SM calculations for the NH_4I and NH_4Cl host crystals, Appendix B gives a derivation of second order energy perturbation, and Appendix C includes a listing of the computer program used in the determination of the SHP using the least-squares fitting method as developed by Dr. Misra.

The references cited in this work are listed at the end of this thesis, and are organized in the following way. They will be listed alphabetically. If a reference is cited within a sentence, for example, "...will be analyzed using the SM of Newman (1971)...", then the author's name will be followed by the year of publication in round brackets Newman (1971). All other references are presented with the author's name and year in square brackets eg. [Newman, 1971] when referring to a particular publication., When there are two authors given, both names will appear eg. [Newman and Urban, 1975], if there are more than two authors the rejoinder *et al.* will follow the first author's name eg. [Oseguera *et al.*, 1980].

Chapter 1

Introduction

Electron paramagnetic resonance is the study of the magnetic property of atoms, molecules, and solids that have unfilled electron d and f shells [M. Bersohn and J.C. Baird, 1966, Misra, 1999]. EPR is an experimental technique employed in the study of the ground state energy levels of a particular paramagnetic ion embedded in a host-crystal. The electron energy levels of the paramagnetic ion are describable in terms of an effective SH, which includes both electron and nuclear spin operators. The term "electron paramagnetic resonance" was coined by H. E. Weaver of Varian Associates, as a phrase that would take into account contributions from the orbital as well as spin angular momentum of an electron [Wertz and Bolton, 1972]. The study of EPR combines both of these contributions to the angular momentum into an "effective" spin. A notable exception is for certain gaseous systems that exhibit a net orbital angular momentum and zero spin angular momentum. Most of the electrons in an atom do not give an EPR signal, the reason being that the vast majority of electrons are paired. This means that for an electron in the $m_s = +1/2$ spin-state, there is a corresponding electron in the same orbital with a spin-state of $m_s = -1/2$, thus neutralizing its paramagnetism. The transition metal ions on the other hand have unpaired electrons in their unfilled 3d and 4f shells [Misra, 1999] and specifically the Mn^{2+} ion has 5 unpaired electrons. Each one of these five electrons occupies an orbital of equal energy within the 3d shell, so that one may

apply Hund's rule which states that "*when an atom has orbitals of equal energy, the order in which they are filled by electrons is such that a maximum number of electrons have unpaired spins*" [Kittel, 1961]. In this regard Mn^{2+} has a high-spin electron orbital configuration.

When a substance is placed in a magnetic field, it acquires a magnetic dipole moment given by

$$\vec{\mu} = V\vec{M} \qquad [1.1]$$

where V is the volume of the sample, and $\vec{M}$ is the magnetization per unit volume given by

$$\vec{M} = \chi_m \vec{B} \qquad [1.2]$$

where χ_m is the volume magnetic susceptibility and $\vec{B}$ is the applied magnetic field. Using

Eqs. [1.1] and [1.2] an expression for the magnetic susceptibility is found,

$$\chi_m = \frac{\vec{M}}{\vec{B}} = \frac{\vec{\mu}}{V\vec{B}} \qquad [1.3]$$

The magnetic susceptibility of a substance gives a clue as to the nature of the substance. For example if the value of χ_m is negative the material is said to be diamagnetic, that is the induced magnetic moment is in the direction opposing the applied magnetic field. For paramagnetic materials the value for χ_m is positive, and is independent of the applied magnetic field. In cases where χ_m is large and dependent upon the applied magnetic field, the substance is said to be ferromagnetic [Derring, 1967]. The difference between a

paramagnetic substance and a ferromagnetic one is that in a ferromagnetic material the magnetic dipoles are already strongly oriented within the domains even in the absence of an applied magnetic field, whereas as in a paramagnetic material the dipoles are randomly oriented. When the host crystal is diamagnetic, as the one studied here, its magnetic dipoles constitute an extremely small negative magnetic moment to oppose the direction of the applied magnetic field. Its influence on the EPR spectrum is thus negligible.

The EPR technique uses an externally applied static magnetic field, the so called Zeeman field, and a radio-frequency field inducing the transitions. The electron transitions take place between energy levels whose separation is dependent upon the externally applied magnetic field. These energy levels are called Zeeman levels, and the external static magnetic field is varied to adjust the energy separation of these levels to become equal to that of the energy of the microwave frequency being used.

Electron spin resonance is a term used mainly by chemists, dealing with only the pure electron spin of a sample, and not in general, those of transition metal ions wherein both the orbital and electron spins are coupled. Today, the terms EPR, ESR and EMR (electron magnetic resonance) are used interchangeably.

Chapter 2

Spin-Hamiltonian and Evaluation of Spin-Hamiltonian Parameters

In this chapter the Hamiltonian-energy equation will be introduced and applied to Mn^{2+} in $NH_4Cl_{0.9}I_{0.1}$. The spin-Hamiltonian parameters are evaluated using experimental data.

2.1 The Spin-Hamiltonian

Measurements carried out in EPR are most often done at temperatures where only the lowest energy levels are populated, therefore quantum numbers describing all the energy states are not necessary in order to effectively describe the EPR spectrum [Dering, 1967]. The populated energy levels can be taken into account by a fictitious spin, S, which describes only those levels pertinent to EPR spectroscopy. By equating the number of observed energy levels to 2S + 1, the value of S can be obtained, which for Mn^{2+} in the high spin state is 5/2.

The SH is a way of characterizing the energy levels and corresponding wave functions participating in transitions in EPR, including implicitly the effect of those energy levels higher than the ground state, and is usually made up of spin-operator terms capable of describing EPR absorption lines consistent with the crystal symmetry. The coefficients of these spin-operators are determined experimentally, and the orientation of

the crystal axes can be determined by analyzing the EPR spectra obtained for rotations of the crystal with respect to the external magnetic field about three mutually perpendicular axes [Misra, 1999]. This task is simplified if one uses rotation planes perpendicular to crystal axes as deduced for the morphology of the crystal. For a SH to be useful in interpreting an EPR spectrum, it should in general include terms which account for the following interactions,

(i). The effect that the applied magnetic field will have on the electron magnetic dipole moment (electronic Zeeman term).

(ii). The effect that the applied magnetic field will have on the nuclear magnetic dipole moment (nuclear Zeeman term).

(iii). The effect that the nuclear magnetic dipole moment will have on the electron magnetic dipole moment (hyperfine interaction).

(iv). The effect that the nuclear quadrupole moment will have on the electron magnetic dipole moment (quadrupole interaction).

(v). The effect of the crystal field on the electron magnetic dipole moment (crystal field interaction).

The SH is an approximate way of interpreting the interaction between the paramagnetic ion and its environment the ligands in the crystal. In general, the complexity of the interactions involved does not allow for the solution of the complete Hamiltonian, as the nature of these interactions is not fully known. It is often the case for

certain transition metal ions that the spectrum produced through EPR is quite complex. Among others, it consists mainly of lines due to different transitions between electronic energy levels called "fine structure". For electron spin greater than one-half, the energy levels remain split in zero magnetic field. One can also observe "forbidden" transitions which are not normally allowed by the selection rules of quantum mechanics in zero-order of perturbation. The spectrum may be further complicated by the interaction of electron-spin with the nuclear-spin (hyperfine interaction) [Abragam and Bleaney, 1970]. The terms that must be included in the SH are those which represent transitions leading to ZFS of the energy levels. The ZFS energy levels of the paramagnetic ion, are the eigenvalues, E_n of the Schrödinger equation applied to the paramagnetic ion [Merzbacher, 1998].

$$\mathcal{H}\psi_n = E_n\psi_n \qquad [2.1]$$

where ψ_n are the eigenfunctions representing the spin-states of the Hamiltonian $\mathcal{H}$.

The magnetic fields at which these first derivative absorption lines occur, depends explicitly upon the frequency of the applied microwave radiation, and also upon the orientation of the crystal's axes relative to the applied magnetic field. One way to treat the effect of the crystal lattice is to think of it as a perturbation to the solution of the Hamiltonian for a free ion, which is given by [Condon and Shortley, 1935]

$$\mathcal{H}_{Free} = \mathcal{H}_{elect} + \mathcal{H}_{SL} + \mathcal{H}_{SS} + \mathcal{H}_{Zee} + \mathcal{H}_{hfs} + \mathcal{H}_{Q} + \mathcal{H}_{N} \qquad [2.2]$$

where,

$\mathcal{H}_{elect}$ is the electronic energy of the paramagnetic ion in the free state.

$\mathcal{H}_{SL}$ is the electron-spin, electron-orbit interaction energy.

$\mathcal{H}_{SS}$ is the interaction energy of the electron magnetic dipole momnets.

$\mathcal{H}_{Zee}$ is the interaction energy between the Zeeman levels.

$\mathcal{H}_{hfs}$ is the interaction energy of the electron spin with the nuclear spin.

$\mathcal{H}_{Q}$ is the interaction energy of the electrons with the electric quadrupole moment of the nucleus.

$\mathcal{H}_{N}$ is the nuclear spin energy.

If now the paramagnetic ion is embedded in a crystal lattice Eq. [2.2] becomes,

$$\mathcal{H} = \mathcal{H}_{Free} + \mathcal{H}_{cf} \qquad [2.3]$$

where,

$\mathcal{H}_{cf}$ is the interaction energy of the electron with the crystalline electric field [Poole, 1967].

For Mn^{2+}, which is an S-state, $3d^5$ transition-metal ion there are 5 unpaired electrons in its 3d shell. The S-state is a definition meaning that the ion has only electron spin interaction, and no spin-orbit interaction. Each electron in the valence orbital contributes 1/2 to the spin, for a total spin S = 5/2. The electron magnetic quantum number m_s ranges from –5/2 to +5/2 in integral steps,

$$m_s = -5/2,\ -3/2,\ -1/2,\ 1/2,\ 3/2,\ 5/2 \qquad [2.4]$$

The spin-Hamiltonian for the S-state, $3d^5$ ions (Cr^{+}, Mn^{2+}, Fe^{3+}) in an arbitrary symmetry is expressed by [Misra, 1999],

$$\mathcal{H} = \mu_B \vec{S} \cdot \vec{g} \cdot \vec{B} + A\vec{S} \cdot \vec{I} + \sum_m B_2^m O_2^m + \sum_m B_4^m O_4^m \qquad [2.5]$$

The zero-field operator coefficients, B_n^m, and the spin-operators, O_n^m, in Eq. [2.5] depend upon the crystal's symmetry, and are specifically for the cubic symmetry determined for the $NH_4Cl_{0.9}I_{0.1}$ crystal, B_2^0, B_4^0, O_2^0 and O_4^0. The spin-operators are given by [Abragam and Bleaney, 1970],

$$O_2^0 = 3S_z^2 - S(S+1) \qquad [2.6]$$

$$O_4^0 = 35S_z^4 - 30S(S+1)S_z^2 + 25S_z^2 - 6S(S+1) + 3S^2(S+1)^2 \qquad [2.7]$$

There are several considerations to take into account, as have been determined through experiment on different S-state ions, before an accurate determination of the g value, and the zero-field operator coefficients can be made. The most important of which are [Misra, 1986],

(i) There is a large variation in the ground state field splitting for a given ion in different host lattices.

(ii) The zero-field coefficients are temperature sensitive, increasing with an increase in temperature.

(iii) The g value for the S-state (orbital angular momentum L = 0) ions (Fe^{3+}, Mn^{2+}) deviates only slightly from that of the free electron value (2.00232).

Rewriting Eq. [2.4] in terms of Eqs. [2.5, 2.6], and with S = 5/2, the Hamiltonian then becomes,

$$\mathcal{H} = \mu_B g(B_x S_x + B_y S_y + B_z S_z) + B_2^0 O_2^0 + B_4^0 O_4^0 + A(S_x I_x + S_y I_y + S_z I_z) \qquad [2.7]$$

The last term in Eq. [2.7] represents the hyperfine (electron-spin—nuclear-spin) interaction. Here I_x, I_y, I_z are the Cartesian components of the nuclear spin of manganese, I = 5/2. The variable A is called the hyperfine-interaction parameter. The so called "allowed" transitions have large transition probabilities, they are between levels differing in electron magnetic quantum number M by one unit: $\Delta M = \pm 1$. The "forbidden" transitions are those for which $\Delta M \neq 1$ and the transition probability between level 1 and level 2, $P_{12} = |\langle \psi_1 | \mathcal{H}_{int} | \psi_2 \rangle|^2$, has a small non-zero value. A computer simulation of an energy level scheme showing allowed EPR transitions is shown in Fig.2.1 below for an ion with S = 5/2 and **B** parallel to the x-axis of the crystal.

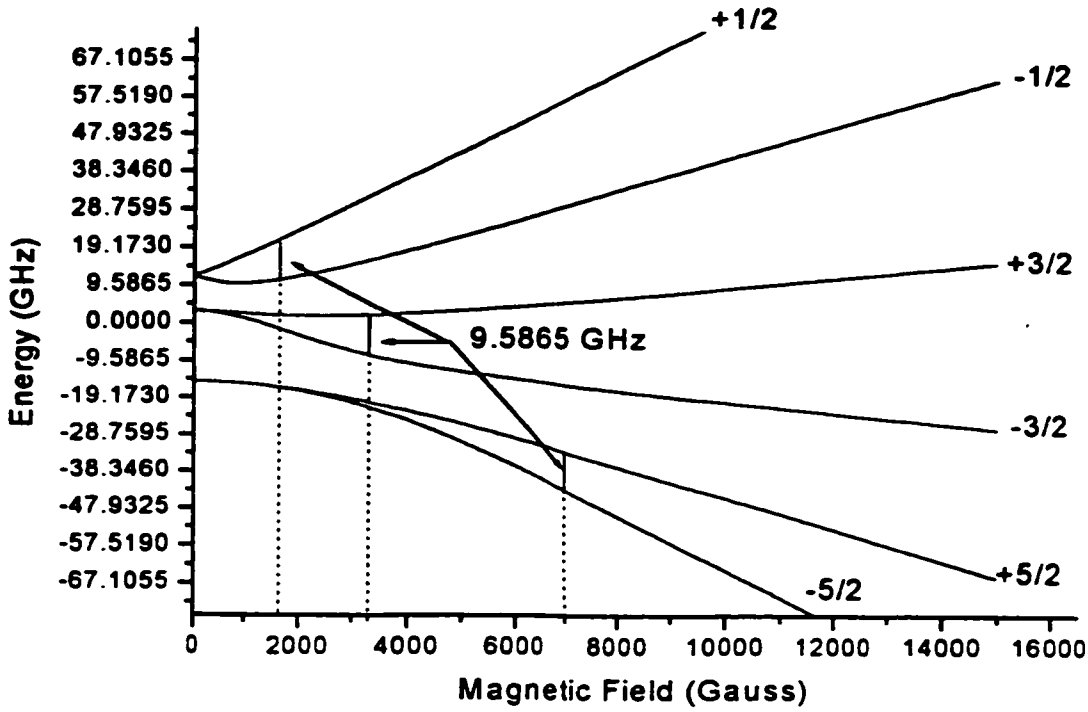

Fig 2.1: A computer simulation of the allowed energy level transitions for a spin 5/2 ion, with the microwave frequency of 9.5865 GHz, and the corresponding magnetic field values where the resonant transitions occur.

The EPR spectrum of the Mn^{2+} ion (S = I = 5/2) in $NH_4Cl_{0.9}I_{0.1}$ can be characterized by the following SH for axial symmetry [Forman and van Wyk, 1966].

$$\mathcal{H} = \mu_B(g_{\parallel}B_zS_z + g_{\perp}B_xS_x + g_{\perp}B_yS_y) + AS_zI_z + B(S_xI_x + S_yI_y) +$$

$$1/3\, b_2^0[3S_z^2 - S(S+1)] + 1/60\, b_4^0\,[35S_z^4 - 30S(S+1)S_z^2 +$$

$$25S_z^2 - 6S(S+1) + 3S^2(S+1)^2] \qquad [2.8]$$

For axial symmetry $g_{\perp} = g_x = g_y$.

The expressions for the transitions $M \leftrightarrow M'$, $\Delta E = E_M - E_{M'}$ to fourth order in perturbation for the various transitions are given by [Misra, 1986]

$$(\pm 5/2 \leftrightarrow \pm 3/2)\colon \Delta E = B \mp 12B_2^0 + \{4(B_2^2)^2/B\} \pm \{18B_2^0(B_2^2)^2/B^2\} + \{325(B_2^0)^2(B_2^2)^2/B^3\} + 28(B_2^2)^4/B^3 \qquad [2.9a]$$

$$(\pm 3/2 \leftrightarrow \pm 1/2)\colon \Delta E = B \mp 6B_2^0 - \{5(B_2^2)^2/B\} \pm \{99B_2^0(B_2^2)^2/B^2\} + \{405(B_2^0)^2(B_2^2)^2/B^3\} - 5/4(B_2^2)^4/B^3 \qquad [2.9b]$$

$$(1/2 \leftrightarrow -1/2)\colon \Delta E = B - 8(B_2^2)^2/B + 648(B_2^0)^2(B_2^2)^2/B^3 + 56(B_2^2)^4/B^3 \qquad [2.9c]$$

In Eqs. [2.9a – 2.9c], B is the magnetic field value at which the $M \leftrightarrow M'$ transition occurs.

Chapter 3

Experimental Arrangement in EPR

This chapter will give a brief historical background to EPR equipment, followed by the makeup of a general EPR spectrometer, and the specific experimental equipment used in this research.

3.1 A Brief History of EPR Equipment

In the early years of EPR, researchers were severely restricted by the quality of the experimental equipment available to them, and sadly, it took World War II to induce a substantial advance in scientific equipment technology!

The big breakthrough came with the advent of radar. Magnetrons, which are nothing more than high power microwave generators were developed to produce the radar signal. This development led in turn to the need for highly directional antennae to transmit the signal, and also to receive the echo, which then led to the development of sophisticated electronic methods to distinguish between the echo and the transmitted signal. Improvements were also made to amplifiers, detectors, noise reducing circuits, and data display systems such as oscilloscopes. By the end of the war, microwave, and electronic technology had advanced far enough, so that spectrometers with higher resolution and sensitivity could be constructed.

The very first experimental EPR observations were done in Russia in 1945 by Zavoisky [Pake and Estle,1973]. These initial experiments observed the power

absorption of bulk matter from a 12 mega-Hertz (MHz) radio frequency, which yielded absorption lines roughly 50 Gauss (G) wide or more. At such low frequencies the estimated field width for resonance is about 4G, where the condition for resonance is given by,

$$h\upsilon = g\mu_B B \qquad [3.1]$$

where B is the magnetic field, h is Planck's constant (6.626×10^{-34} Joules•Second (J•S)), υ is the incident microwave frequency, μ_B is called the Bohr-magneton (9.274×10^{-24} Joules/Tesla (J/T), 1 Tesla = 10000 Gauss), g is a dimensionless quantity called the Landé splitting factor, which is a combination of the spin (S), orbital (L), and total angular momentum (J) of an electron, given by

$$g = 1 + \frac{J(J+1) + S(S+1) - L(L+1)}{2J(J+1)} \qquad [3.2]$$

$$\vec{J} = \vec{L} + \vec{S} \qquad [3.3]$$

According to angular momentum theory J can have values ranging from L + S to | L – S | in discrete steps [Wertz and Bolton, 1972]. (For a free electron it has a value of 2.00 since L = 0, and J = S). Eq. [3.3] is included in order to show that the spin, orbital, and total angular momentum are vector quantities with magnitudes given by [Wertz and Bolton, 1972],

$$\left|\vec{J}\right| = \sqrt{J(J+1)} \qquad [3.3a]$$

$$\left|\vec{L}\right| = \sqrt{L(L+1)} \qquad [3.3b]$$

$$\left|\vec{S}\right| = \sqrt{S(S+1)} \qquad [3.3c]$$

In later work, Zavoisky extended the EPR technique to microwave frequencies, and he was able to observe well-defined resonances with line widths of about 250 G on samples with the Cu^{2+} ion.

3.2 General Details of an EPR Spectrometer

In this section the general details of an EPR spectrometer are described. This is followed by the specific details of the two commercial spectrometers, Bruker and Varian used to collect data presented in this thesis.

A typical EPR spectrometer is a combination of different electronic components, which may be combined in several different ways to satisfy the particular needs of the user in their EPR experiments. An illustrative example is given in Fig. 3.1 [Wertz and Bolton, 1972].

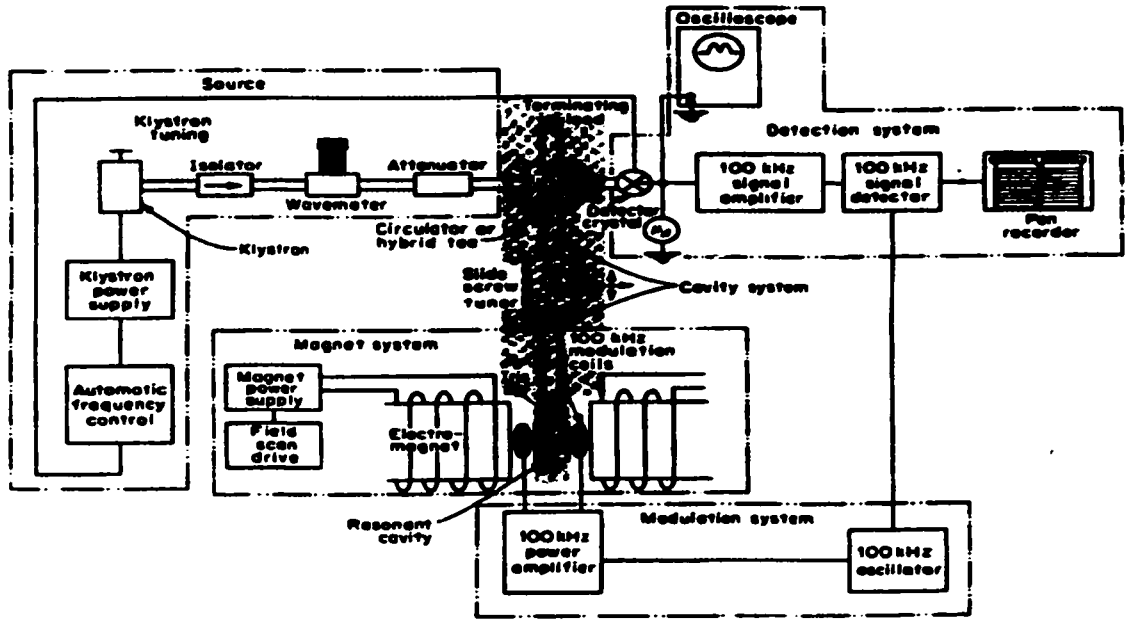

Fig. 3.1: A block diagram representation of a typical X-band spectrometer's major components. The sample is placed inside the resonant cavity.

An EPR spectrometer is designed to induce transitions among the eigenstates of magnetic dipole moments. This ability to induce transitions through the application of microwave radiation at a given frequency, and an external magnetic field, is what distinguishes EPR spectroscopy from other spectroscopic methods, which do not induce magnetic dipole moment transitions. In order to observe an EPR absorption signal, the resonance condition given by Eq. [3.1], rewritten here in terms of changes in energy, must be satisfied,

$$h\upsilon = \Delta E \qquad [3.4]$$

where h is Planck's constant, υ is the klystron frequency, and $\Delta E = | E_M - E_{M'} |$ is the energy difference between the levels participating in resonance, provided that the

transition probability, $P_{12} = |\langle\psi_M | \mathcal{H}_{int} |\psi_{M'}\rangle|^2 \neq 0$. Here ψ_M and $\psi_{M'}$ are the wave functions for the two energy levels E_M and $E_{M'}$, and

$$\mathcal{H}_{int} = g\mu_B \vec{B}_1 \cdot \vec{S} \qquad [3.5]$$

is the interaction Hamiltonian between the radio-frequency field $B_1 \cos\omega t$, with $\omega = 2\pi\upsilon$, inducing transition, and the magnetic moment of the ion $\mu = g\mu_B S$. Here S is the electron-spin of the ion.

The microwave frequency is tunable over a small range, in order to compensate for different cavity geometries, sample sizes, and temperatures. There are several considerations, which limit the choice of the radiation frequency [Wertz and Bolton, 1972], the most important of which is sensitivity. The sensitivity of an EPR spectrometer increases as υ^2. Thus in order to increase the signal-to-noise ratio, the frequency of the incident radiation should be as high as possible. However, high frequencies require high magnetic fields that should be uniform over the sample volume. For very high magnetic fields, of the order of 20,000-30,000 G, a homogenous field is difficult to maintain [Wertz and Bolton, 1972]. Another important consideration involves samples in aqueous solutions that have a high dielectric absorption. The high absorption factor seriously affects the sensitivity, as good microwave-sample-coupling becomes difficult. This results in a signal that is very difficult to detect even after amplification. These considerations dictate the choice of a working frequency of about 9.5 GHz for commercial spectrometers. The frequency range of these spectrometers is known as X-band (8.2-12.4 GHz) in the jargon of EPR experimentalists, where the X-band designation is in reference to the particular waveguide structure used at these frequencies.

Higher frequencies (33-50 GHz) are called Q-band. The Q-band waveguide differs from the X-band in that it is narrower in order to accommodate higher frequency, shorter wavelength microwave radiation. The other commonly used high frequency is 95 GHz (W-band).

The EPR instruments that analyze the signal from the resonance cavity give the data output in the form of the first (small modulation amplitude) or second (large modulation amplitude) derivative of the power absorption of the sample [Bersohn and Baird, 1966]. This is due to the fact that the DC signal from the sample represents a very small change in the overall absorption of the incident microwave power into the cavity. In other words, at the detector, the DC signal output from the cavity is a very small part of the overall DC magnetic field. An AC signal is from an experimental point of view simpler to amplify. It is then necessary to convert the DC signal due to the spins into an AC one. This can be achieved by modulating the external magnetic field by a small oscillating magnetic field at the sample. The smaller modulating magnetic field alternately adds to, and subtracts from the larger field, and as the resultant field increases and decreases, so does the absorption curve. It is this alternating increase and decrease in the DC signal, which provides an AC signal that may be amplified and recorded, on a x-y recorder or in the form of a data array on a digitized micro computer for different values of the external field during sweep.

The detection method used in the ER series is called homodyne detection. This means that the microwave frequency is split into two channels, one leading to the cavity and the other to a reference arm. The two branches are then recombined at the detector

diode. The self-mixed signal is then used to encode the signal response at the particular modulating frequency being used. A 100 kHz modulation frequency was used for these experiments. The EPR signal is then decoded by phase sensitive detection, that is, the signal will be detected at a harmonic of the applied modulation frequency, and it will be in or out of phase with the frequency in the reference arm. An in phase signal leading to a maximum, and an out of phase signal to a minimum. This form of encoding and detection is known as Zeeman modulation with phase sensitive detection. The signal is then amplified and a further reduction in noise is achieved by limiting all noise to ±1Hz around the 100 kHz modulating signal. The signal channel processes and enhances the incoming signal-to-noise ratio by virtue of its bandwidth limitation capacities. The operation of the phase sensitive detector can be understood with the help of Fig. 3.2 [Wertz and Bolton, 1972].

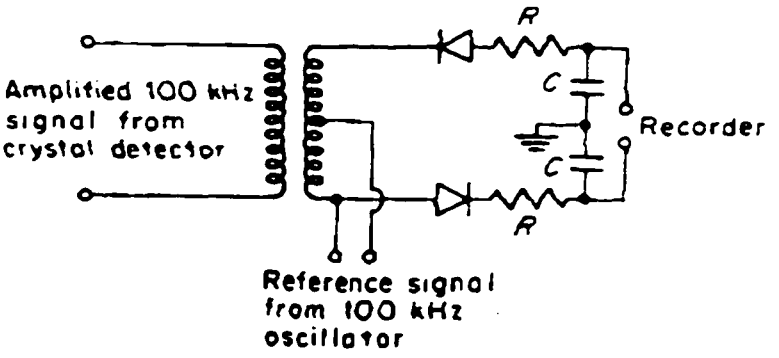

Fig. 3.2: Schematic diagram of a phase sensitive detector. The transformer has a split secondary coil, which is used to combine the amplified output of the crystal detector with a part of the output of the oscillator driven modulation coils. The combined signal is then rectified, filtered (resistor-capacitor combination, the filter time constant is given by RC) and recorded.

When the amplitude of the 100 kHz field modulation is kept small in comparison to the linewidth of the absorption curve, the amplitude of the detected signal will be proportional to the slope of the absorption curve at the center of the modulating field. As the modulating field varies between two values, H_a and H_b, the crystal current varies sinusoidally between i_a and i_b. The points at which the slope of the absorption curve is zero, the 100 kHz component at the detector will be zero. At the points of inflection, the slope is at its maximum, and the output signal will also be at maximum. The sign of the slope determines the output polarity of the detector, so that for small modulation amplitudes the output signal appears as the first derivative of the absorption curve. The second derivative of the absorption curve may be obtained by doubling the modulation frequency, for example 200 kHz. This is shown in Figs. 3.3 and 3.4.

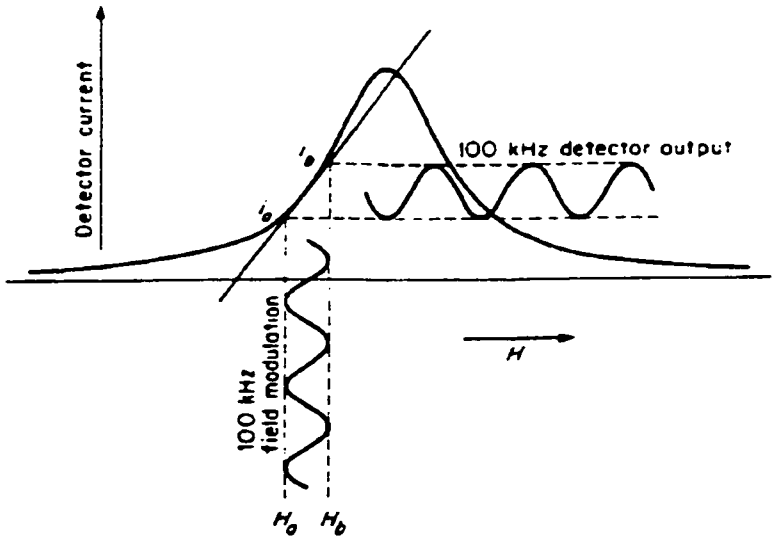

Fig. 3.3: The effect of small amplitude 100 kHz modulation on the detector output current. The static magnetic field is modulated between the limits H_a and H_b, and the detector current varies between i_a and i_b

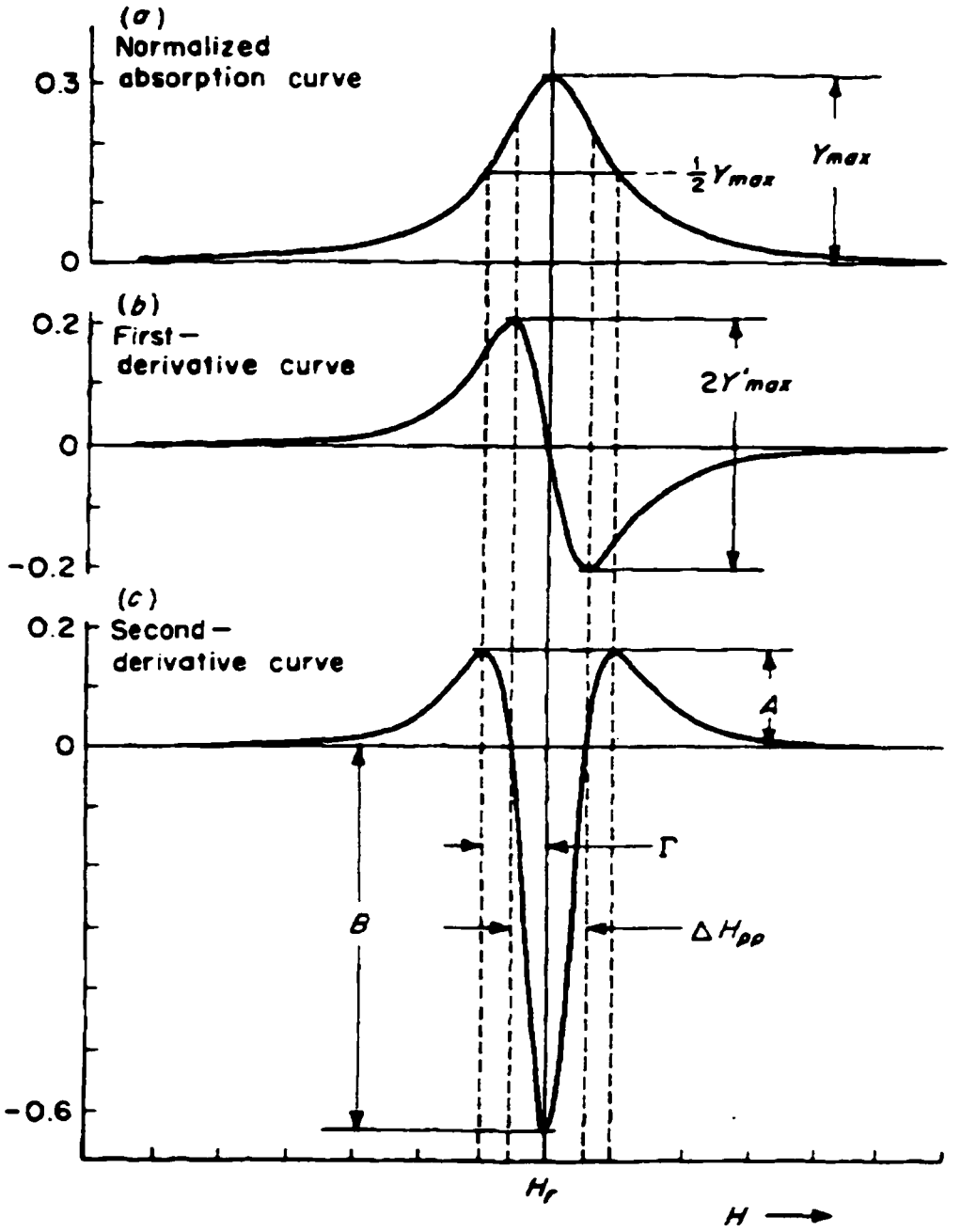

Fig. 3.4: a) absorption curve: $Y_{max} = 1/\pi\Gamma$, Γ = half-width at half-height,

b) first derivative spectrum: $2Y'_{max} = (3\sqrt{3}/4\pi)1/\Gamma^2$,

c) second derivative: $A = Y_{max}(1/2\Gamma^2)$, $B = -Y_{max}(2/\Gamma^2)$, $\Delta H_{pp} = (2/\sqrt{3})\Gamma$.

The oscillating magnetic field causes transitions, for example, from the upper +1/2 spin state to the lower −1/2 spin state, as well as in the opposite direction. The first transition involves the emission of microwaves and the second the absorption of microwaves. EPR experiments are carried out on samples containing an enormous number of unpaired electrons. If the population of electrons is thought of as being divided into two populations, the +1/2 population and the −1/2 population, then when the two populations are equal there will be as much emission as absorption of microwaves and consequently no EPR signal. Therefore, to have an absorption spectrum in EPR the net population of the −1/2 state must be higher than the +1/2 state. At thermal equilibrium the ratio of the two populations is given by [Bersohn and Baird, 1966],

$$N_{-1/2}/N_{+1/2} = \exp[(E_{-1/2} - E_{+1/2})/kT] = \exp(g\mu_0 B/kT) \qquad [3.6]$$

where k is the Boltzmann constant (1.38×10^{-23} J/K), g is the Landé splitting factor (≈ 2), B the magnetic field, μ_0 is the permeability of free space ($4\pi \times 10^{-7}$ N/A^2), and T is the temperature expressed in the Kelvin scale.

The greater the ratio $N_{-1/2}/N_{+1/2}$, the stronger is the absorption signal recorded by the EPR spectrometer. In Eq. [3.6] there is a temperature dependence on the population ratio, that is, as the temperature decreases the population ratio increases and the absorption signal is stronger. From this it can be seen that the signal intensity varies inversely as the absolute temperature [Bersohn and Baird, 1966]. For example, a first derivative spectral line seen at liquid nitrogen temperature (77K) is approximately four times more intense than a spectral line at room temperature (300K).

The magnitude of the magnetic field and the width of the magnetic field sweep are predetermined by the user. They depend greatly upon the sample that is under investigation, and are set through the field controller. The field controller makes use of the Hall effect in order to generate and monitor the intensity of the magnetic field. The poles of the magnet are made of copper wire, and the magnetic field is established by the flow of an electric current through the copper windings.

The Hall effect is a potential difference that is measured perpendicular to the flow of the current in a conductor, in this case a Hall probe, when the probe is placed in a magnetic field. The potential across the probe is given by,

$$E_z = \frac{-J_z B_y}{nq} \quad , \quad R_H = \frac{1}{nq} \qquad [3.7]$$

where, R_H is called the Hall coefficient, and is a function of the number of charge carriers n, and q being the charge of the electron [Young and Freedman, 2000]. The number of carriers depends on both the geometry and material of the Hall probe. The integrity of the field is maintained by comparing the Hall voltage at the pole face, to a reference voltage for that particular field strength, which determines the current flowing through magnet.

All the components associated with the microwave excitation and detection, as well as the control console electronics are referred to as the microwave-bridge. The microwave source is a klystron, although some spectrometers use a Gunn diode as a microwave source instead [ER Series Users Manual, 1983].

The stability of the microwave frequency is dependent upon how well "locked" the klystron frequency is to the cavity frequency. A feedback loop, consisting of a circulator and an isolator, measures the amount of power going from the klystron to the cavity, any power that is reflected back from the cavity is attenuated. When the microwave frequency is locked to the cavity resonant frequency, there will be a maximum power transfer. For a frequency mismatch, power will be reflected away from the cavity. When the klystron frequency is well matched to the cavity resonance frequency, a sharp absorption dip will appear at the center of the resonance mode. The sharpness of the dip, and how low the tip is relative to the baseline, are indicators of how efficiently the microwave power is being transferred into the cavity, and coupled to the sample. The klystron frequency can be adjusted over a small range, for a given beam voltage, by varying the reflector voltage applied to it [Poole, 1967]. In this manner the klystron can be tuned over the entire range of the resonance mode. Varian and OKI are two leaders in klystron fabrication. An illustration of a typical OKI klystron is given in Fig 3.5.

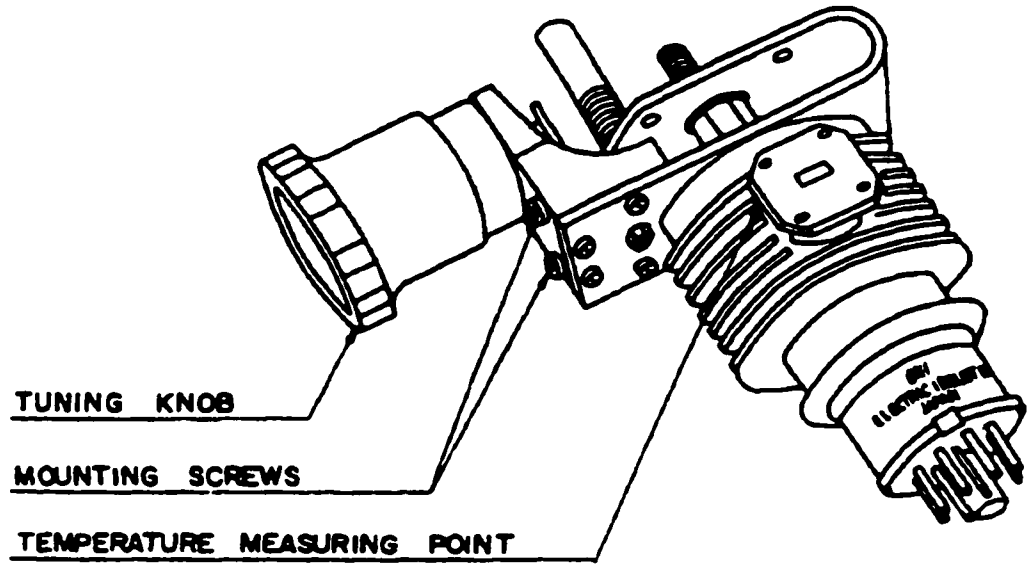

Fig. 3.5: OKI brand Q-band (≈ 35 GHz) klystron. This particular model uses a "forced air" cooling system, as opposed to a "cold water" cooling system.

The microwave cavity, or as it is sometimes referred to, the microwave probe, is used to hold the sample. It is also the geometry of the cavity that determines the operating frequency, and the sensitivity of the spectrometer. In some cases the cavity itself may limit the experimental "freedom" of the user, in other words the cavity being used can dictate whether or not a particular experiment can be performed.

The geometry of the cavity is designed in such a way so that standing wave patterns, called modes are formed by the microwave radiation. A "normal mode" of an oscillating system is one in which all the particles of the system move sinusoidally with the same frequency [Young and Freedman, 2000]. The modes are called transverse electric (TE), if the electric field is zero along the major axis of the cavity, and transverse magnetic (TM), when the magnetic field is zero along the major axis [Wertz and Bolton,

1972, ER Series Users Manual, 1983]. This is illustrated in Fig. 3.6, for a TE_{102} cavity below [Wertz and Bolton, 1972]. This cavity differs from the TE_{104} in that it has only two half-wavlengths along the principle axis. Standing waves are desirable because the energy density associated with them is much higher than for travelling waves. One needs only to think of sound waves, and how the change in the number of standing waves changes the pitch of the sound being produced. The cavity should be designed in such a manner so that a one-half wavelength of the microwave frequency being used corresponds to one of the cavity dimensions. Wavelength and frequency are related by the following expression,

$$c = \lambda \upsilon \qquad [3.8]$$

where c is the speed of light, and λ the wavelength. The frequency for which this occurs is called the fundamental resonance frequency. The numerical subscripts refer to the number of half wavelengths along the other two axes.

Microwave cavities are also rated by the efficiency with which they can integrate microwave energy. This efficiency is characterized by the quality factor Q, and is given by [Wertz and Bolton, 1972],

$$Q = \frac{2\pi(\text{maximum microwave power stored in cavity})}{\text{energy dissipated per cycle}} \qquad [3.9]$$

Since the amount of microwave power stored in the cavity, is directly related to the number of standing waves, it is in general possible to increase Q by increasing the cavity volume. The amount of energy dissipated depends upon the absorption characteristics of the particular material of which the cavity is fabricated. A highly reflective silver coating

is applied to the inside walls of the cavity in order to minimize losses due to cavity wall absorption. The reflective properties are further enhanced, by applying a thin coating of gold over the silver to prevent oxidation.

The coupling of the microwave energy into the cavity is done through a small opening called the *iris*. The iris serves the purpose of impedance matching the microwave energy incident on the cavity, with the energy inside the cavity. That is to say, the iris prevents any energy to be reflected back to the microwave source from the cavity. A maximum of energy transfer takes place when there is an impedance match. There is an electronically adjustable screw, which allows for small adjustments for optimal impedance matching. The size and type of sample has an influence on the setting of the screw.

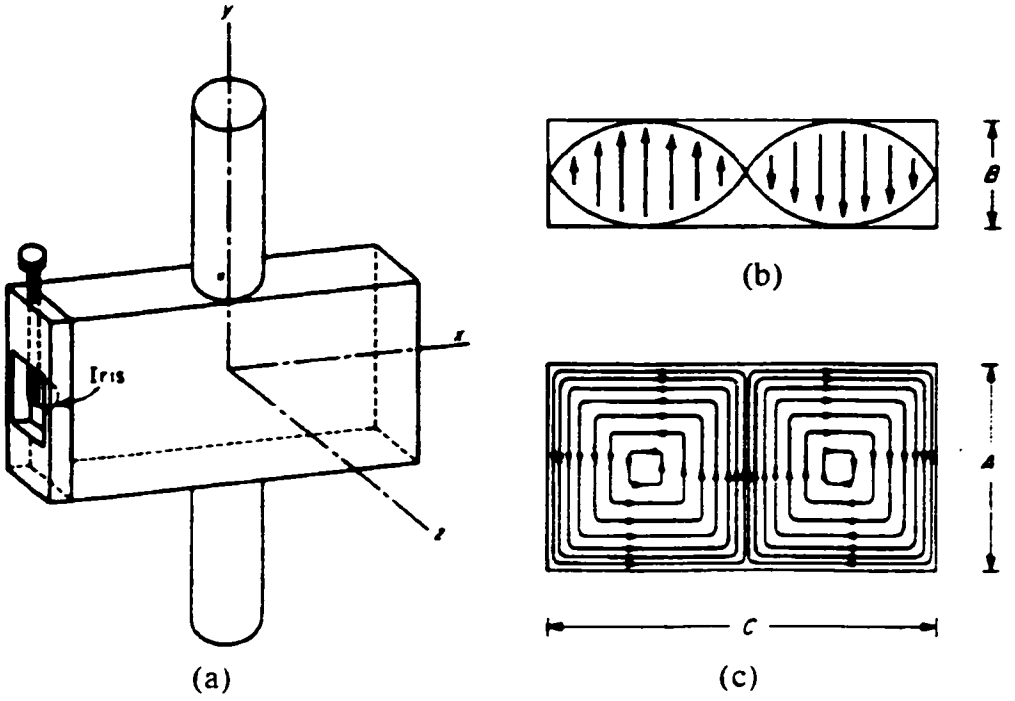

Fig. 3.6: The TE_{102} rectangular microwave cavity. (a) The iris couples the microwave energy into the cavity. The amount of microwave coupling can be adjusted by the screw at the top of the cavity. (b) The electric field boundary in the xz-plane. There is a one half-wavelength correspondence between points of equal field intensity, but opposite phase. (c) The magnetic flux in the xy-plane. The dimension of *A* is approximately one half-wavelenghth, and *C* is exactly two half-wavlengths. The *B* dimension is not critical, but should be kept at less than one half-wavelegth.

The electromagnet is designed to provide a uniform, controllable magnetic field over the sample volume. The magnet pole faces are nine inches in diameter and the spacing between them can be varied for the specific experimental application. The magnet is made of two low impedance coils connected in series. Two thermo-switches connected to a water flow detection device protect the coils from overheating.

Although it is not a physical part of a working spectrometer, a cold, filtered water supply is essential for the operation of the klystron and the electromagnet. The magnet power supply is designed to automatically shut down in the event of a disruption of the cooling water flow. A Varian 9-inch magnet is shown in Fig. 3.7.

The components discussed above apply, in general, also to Q-band spectrometers. The only variations being the waveguide, and cavity dimensions, the magnetic field intensity, and the klystron microwave source. A typical Q-band waveguide assembly is shown in Figs. 3.8 and 3.9.

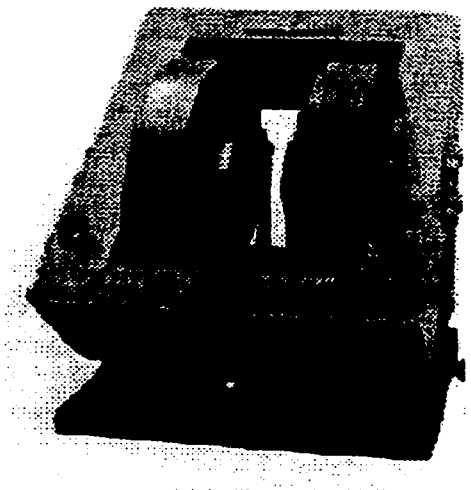

Fig. 3.7: The Varian V-3400 9-inch rotatable magnet Weight of the magnet is 1016 kg.

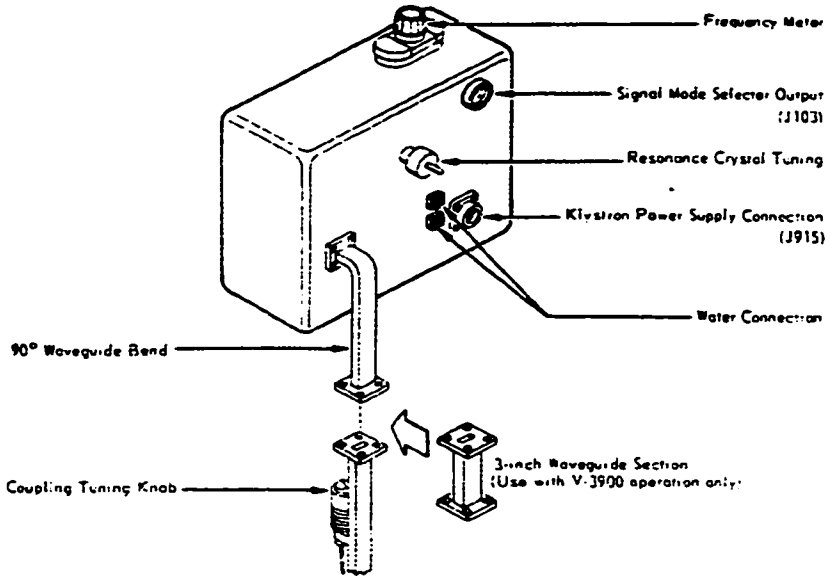

Fig. 3.8: Q-band microwave bridge and waveguide assembly.

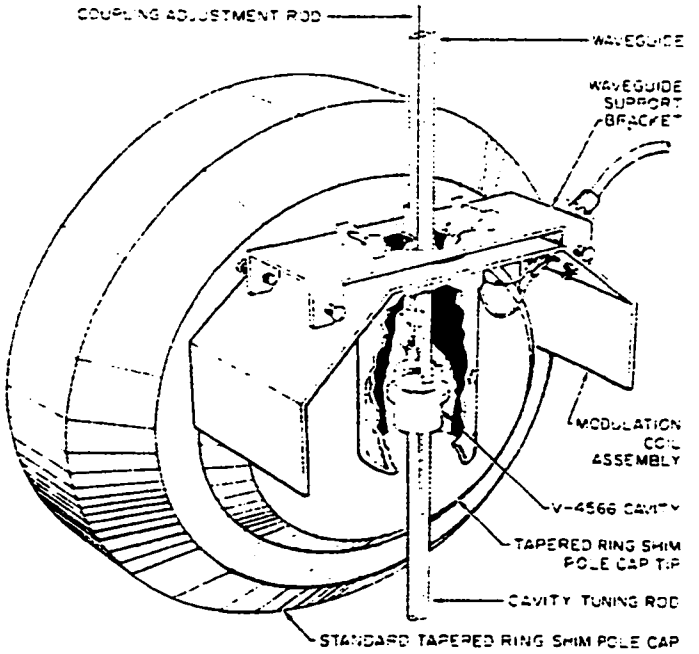

Fig. 3.9: Modulation coil assembly and Q-band cavity assembly with one of the magnet pole faces shown.

In what follows the details of the two commercial spectrometers, Bruker and Varian, used to collect data on the Mn^{2+} doped $NH_4Cl_{0.9}I_{0.1}$ mixed crystal are described.

3.3 The Bruker ER Series Spectrometer

The particular Bruker ER series X-band spectrometer used in these experiments consists of the following components: a signal channel, field controller, time base, microwave controller, microwave bridge, klystron, microwave cavity, electromagnet, and a cold filtered water supply. [ER Series Users Manual, 1983].

3.3.1 Signal Channel ER022.

The signal channel console allows the user to choose between 100 kHz and 12.5 kHz for the modulation frequency, depending on the circumstances of the experiment. The peak-to-peak modulation adjustment selects the modulation amplitude in the cavity at the sample, and is incremented in 2dB steps.

The second resonator selection is used in conjunction with the TE_{104} double cavity. It allows the user to select between the first or second cavity, and channels the modulated output from either cavity to the signal detector and amplifier.

The receiver gain level determines the sensitivity of the signal amplifier. The overload indicator will be activated when the modulation output power or the signal amplifier is saturating.

The receiver output time constant controls the frequency response of the output signal by a selection of the RC filter time constant. The signal-to-noise ratio can be greatly enhanced by selecting an appropriate time constant.

The offset switch is used to center the signal output level on the XY recorder or computer.

The phase of the receiver frequency can be adjusted in 90° intervals by setting the phase selector switch to the desired phase. The receiver phase can also be "fine" tuned in steps of 0.1° by use of the phase fine-adjust control.

3.3.2 Field Controller ER031M.

The field controller allows the user to set the magnetic field center and the sweep width. The magnetic field data can be entered with a maximum resolution of 0.1 Gauss. The entries are made by pressing the appropriate buttons on an alpha-numeric keypad.

3.3.3 Time Base ER001.

The time base unit is the component that provides the timing control required for data acquisition. The timing is achieved by using a 4.096 MHz quartz oscillator, which can be scaled by frequency dividers as needed. Its main function is to synchronize the field sweep timing with that of an external data display, such as a chart recorder or computer. The sweep time determines the record time of data accumulation in seconds. It corresponds to the total time required to vary the magnetic field between the limits set by the field controller. The sweep rate (time/Gauss) is determined by the total sweep time per sweep divided by the total sweep width.

3.3.4 Microwave Controller ER048H

In the standby position, power is applied to the klystron filament but the beam and reflector voltages remain off. Should the spectrometer be left on standby for a period exceeding 30 minutes the filament voltage will be turned off in order to prolong the

klystron lifetime. The microwave attenuation is adjusted by a thumb screw mechanism, and is used to establish the microwave mode on the spectrometer's oscilloscope. The absorption dip of the incident microwave power is found by adjusting the frequency control of the klystron, and once found the attenuation is further reduced to allow a maximum power transfer from the klystron to the sample. As the attenuation is reduced the tip of the dip will be lowered towards the baseline of the microwave mode.. Fine-tuning can be made by electronically raising or lowering the iris screw.

3.4 Varian V-4503 Spectrometer

The Q-band spectrometer used in this research consisted of the following components

3.4.1 V-4500-10A EPR Control Unit

The control unit allows the user to monitor the klystron resonator current, and also any deviations of the klystron frequency from that of the cavity. The current flowing through the crystal detector in the microwave-bridge is also indicated. The klystron reflector voltage adjustments can also be made on this unit.

3.4.2 V-4250B Sweep Unit

The sweep unit allows the user to select from variable frequencies, 20, 40, 80, 200 and 400 Hz, which are then amplified and applied to the modulation coils. The x-axis of the oscilloscope is also driven by these frequencies. The sweep unit also allows for external modulation by providing input jacks at the back of the console.

3.4.3 V-4240B Sweep Amplifier Unit

This unit serves to amplify the frequencies produced by the sweep unit, ensuring sufficient power to the cavity modulation coils.

3.4.4 V-4560 100kHz Field Modulation Control Unit

To obtain optimum signal-to-noise ratio the modulation coils should driven at the highest frequency possible as the detector noise varies inversely with the modulation frequency. The 100 kHz modulation frequency was used for these experiments. The spectrometer's sensitivity is increased by a factor of 15 when using 100 kHz modulation as opposed to 400 Hz.

Typical spectrometer settings used in these experiments are given in Table 3.1.

Table 3.1: Typical X and Q-band spectrometer settings

	X-band	Q-band
Microwave Power	12 dB	17 dB
Microwave Frequency	9.58 GHz	36.02 GHz
Modulation Frequency	100 kHz	100 kHz
Modulation Amplitude	5 G (peak-to-peak)	5 G (peak-to-peak)
Receiver Gain	5×10^3	1.2×10^4
Time Constant	500 ms	1 s
Center Field	6500 G	7000 G
Sweep Width	7000 G	11000 G
Sweep Time	1 ks	1 ks
Diode Current	200 μA	200 μA

3.5 Low Temperature Cryostats

The boiling point of liquid nitrogen is 77.3K. This extreme cold will burn skin on contact, and great care should be taken in handling liquid nitrogen. Flexible or soft materials will become hard when exposed to liquid nitrogen and are easily breakable. Should liquid nitrogen be spilled on cryogenic or vacuum equipment, it will freeze the rubber O-rings and cause a loss in vacuum.

For the low temperature measurements carried out in this work the following cryostats were employed.

3.5.1 Bruker Variable Temperature Unit

The temperature control unit has a variable temperature range of 64K to 800K for EPR studies. The required temperature at the sample is regulated by a thermocouple that senses the heat exchange between the sample and the heater. The selected temperature is maintained by a gas flow that pressurizes the dewar containing liquid nitrogen. The themocouple which is placed close to the sample detects any changes in the voltage of the temperature selected.

The liquid nitrogen is evaporated by the heater thereby producing the nitrogen gas flow needed for the low temperature regulation [Bruker Technical Manual VTU, 1990].

3.5.2 Oxford Variable Temperature Flow Unit

A vacuum pump system is needed for laboratory scale continuous-flow-cryostats (CFC), in order to pump out the liquid nitrogen transfer tube, and to set up a pressure gradient along the nitrogen flow line so that the flow of nitrogen can be controlled [Oxford Instruments Operating Manual ESR 9, 1978].

The vacuum pressure for laboratory scale cryostat systems is generally around 10^{-4} Torr (10^{-1} microns). In order to reach this pressure both a mechanical rotary pump (pumping speed of 50L/min), and oil diffusion pump (pumping speed 10L/s) are used. The rotary pump is used to reduce the pressure to a point where the diffusion pump can start to operate, generally around 1 Torr or less, and the diffusion pump will then further reduce the pressure to about 10^{-5} Torr or less.

CFC operate on the principle of the controlled continuous transfer of a coolant such as liquid nitrogen from a storage vessel to a vacuum insulated sample space. The

temperature at the sample can be maintained at any point within the CFC range by controlling the flow of liquid nitrogen and the power to the electrical heater attached to the heat exchanger. The flow of nitrogen is produced by establishing a pressure difference , with the gas flow pump, between the storage vessel and the nitrogen return line. The nitrogen gas flow is monitored on the flow controller.

The temperature is measured by a temperature sensor attached to the heat exchanger. This apparatus maintains the temperature of the cavity as close as possible to the "set point" by maintaining a balance between the heat lost by the system to its surroundings and the heat provided by the heater. By alternately heating and cooling the cavity an average temperature is established that is very close to the user defined "set point". In this regard, in order to obtain an accurate measurement of the sample volume temperature, the thermocouple must be in good contact with the sample volume, and be isolated from every part of the system that is at a different temperature [Oxford Instruments Operating Manual ESR 9, 1978]. A typical CFC system is shown in Fig. 3.10.

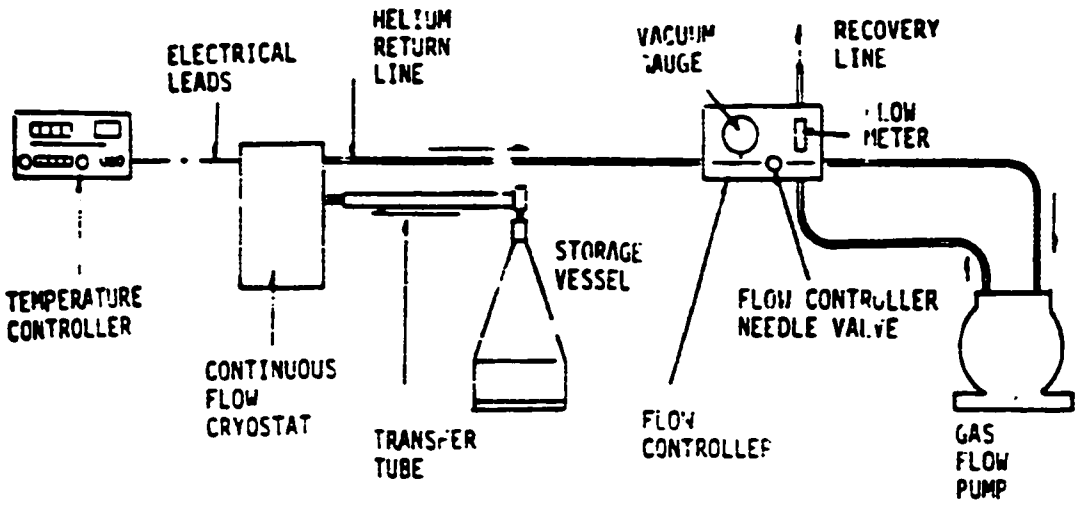

Fig. 3.10: Block diagram of a typical continuous-flow-cryostat system.

Chapter 4

Preparation of Single Crystal of $NH_4Cl_{0.9}I_{0.1}$ and Experimental Data

In this chapter the preparation of the crystal as prepared by Dr. P Chand of the Indian Institute of Technology, Kanpur, India will be presented, as well as the experimental results obtained following a multi-frequency, multi-temperature strategy.

4.1 Sample preparation

The method most commonly used in the growth of ammonium halides is by the slow evaporation of a saturated aqueous mother-solution under a constant temperature [Chand and Upreti, 1983]. It was found that solutions left in lighted areas did not produce good quality crystals, believed to be due to photo-decomposition of the compound, leading to bleeding of iodine into the mother-solution resulting in crystals being dark and malformed. Crystals grown in a very dark, temperature controlled (±0.5°C) environment were clear and cubic, and of a relatively large size. The evaporation rate was kept slow by addition of urea (2% by weight) to the mother-solution. An x-ray analysis of the crystals grown in this manner showed that the urea did not adversely contaminate the crystal lattice [Chand and Upreti, 1983].

The Mn^{2+} ion was introduced by adding 0.5% manganese dichloride ($MnCl_2$) by weight of $NH_4Cl_{0.9}I_{0.1}$ to the mother-solution. The crystal was mounted onto a quartz

support rod with some Dow-Corning vacuum grease, and attached to a Varian E-229 goniometer. When the crystal was not being tested, it was stored in a small container of mineral oil. The BCC structure of $NH_4Cl_{0.9}I_{0.1}$ is shown in Fig. 4.1.

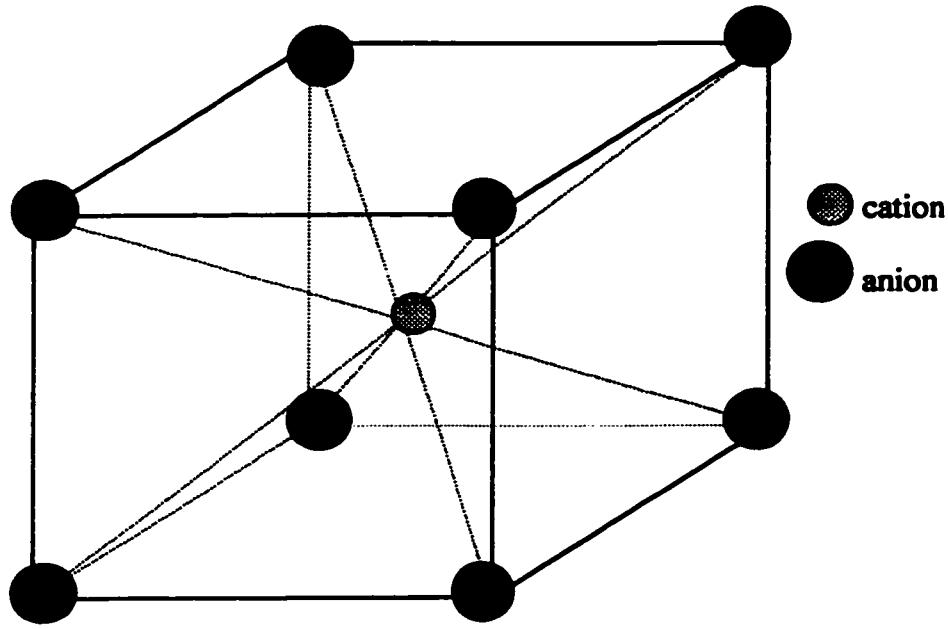

Fig. 4.1: The BCC lattice structure showing the central cation surrounded by eight anions.

4.2 Experimental Data

4.2.1 X-band

The first experiment was carried out using the Bruker X-band spectrometer at room temperature (295K), and the $NH_4Cl_{0.9}I_{0.1}$ crystal rotated in the (001) or equivalent plane. The quartz support rod and crystal were then mounted onto a goniometer and attached to the cavity. The length of quartz was adjusted such that the crystal attached to

it was in the position of highest microwave concentration. Once the crystal has been attached to the cavity an initial attempt is made at tuning the spectrometer. This is achieved first by lowering the microwave attenuation and establishing a klystron resonance mode, and secondly a good coupling, by an *iris*, of the incident microwave power and the sample in the cavity. When a sharp dip in the resonance mode of the klystron is obtained, a maximum standing wave power condition exists. This is shown in Fig. 4.2 [Poole, 1967].

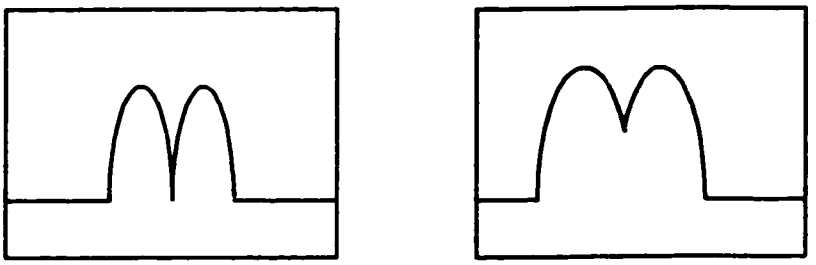

Fig. 4.2: a) On resonance: there is a maximum power transfer from the klystron to the sample. (High standing wave density within the cavity)
b) Off resonance: there is low power transfer from klystron to sample. (Low standing wave density within the cavity)

Once a good coupling has been established, the crystal's magnetic z-axis, that is the axis parallel to the applied magnetic field, is found by taking spectra at different crystal angles relative to the applied field, by rotating the goniometer. The orientation at which the spectrum shows a maximum overall splitting of lines is defined to be the z-axis

of the crystal. The magnetic z, x, and y axes, are therefore defined to be those directions of the magnetic field for which the overall splitting of the EPR line positions exhibit extrema, that is along the [100], [010], or [001] directions corresponding to the cube edges of the crystal. Of these the splitting is largest for **B** || z-axis, and smallest for **B** || y, or x-axis. The spectrum for **B** || z-axis is shown in Fig. 4.3. Each group of lines consists of a sextet, and are about 11 G peak-to-peak per line.

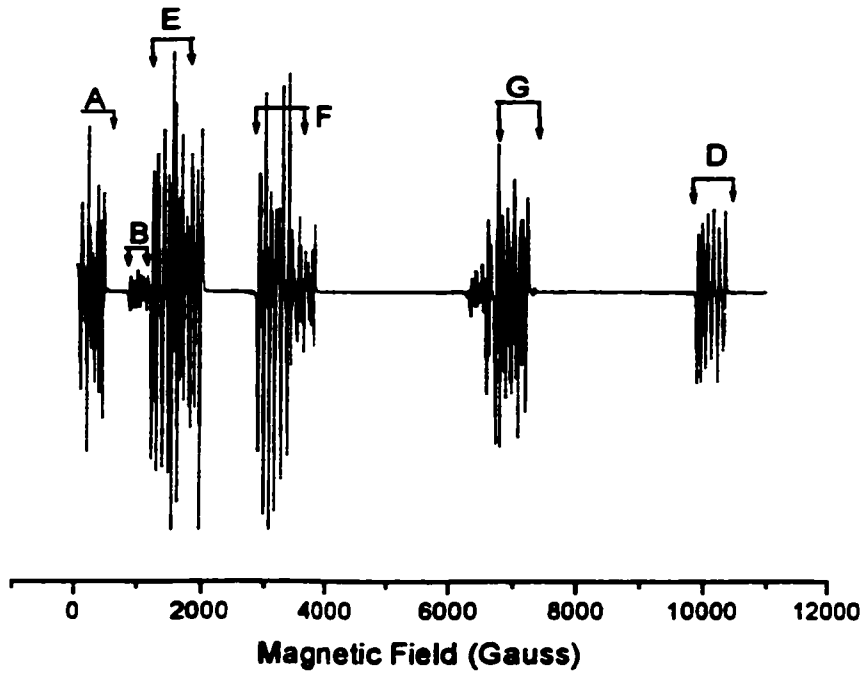

Fig 4.3: The spectrum of Mn^{2+} in $NH_4Cl_{0.9}I_{0.1}$ for **B** || z showing the largest splitting of line positions. The group of lines marked A, B, D, correspond to the z-x spectrum, while those marked E, F, G, correspond to the x-y spectrum.

The group of lines marked as E, F, G, in Fig. 4.3, do not show any angular variation as the crystal is rotated from [100] to [010] in the (001) plane. The groups marked as A, B, D, in Fig. 4.3, show angular dependence and the A, B group moved to higher magnetic field values as the crystal was rotated. This same group of lines is shown in Fig. 4.4 for an angular orientation of 45 degrees, that is **B** is at 45 degrees relative to z.

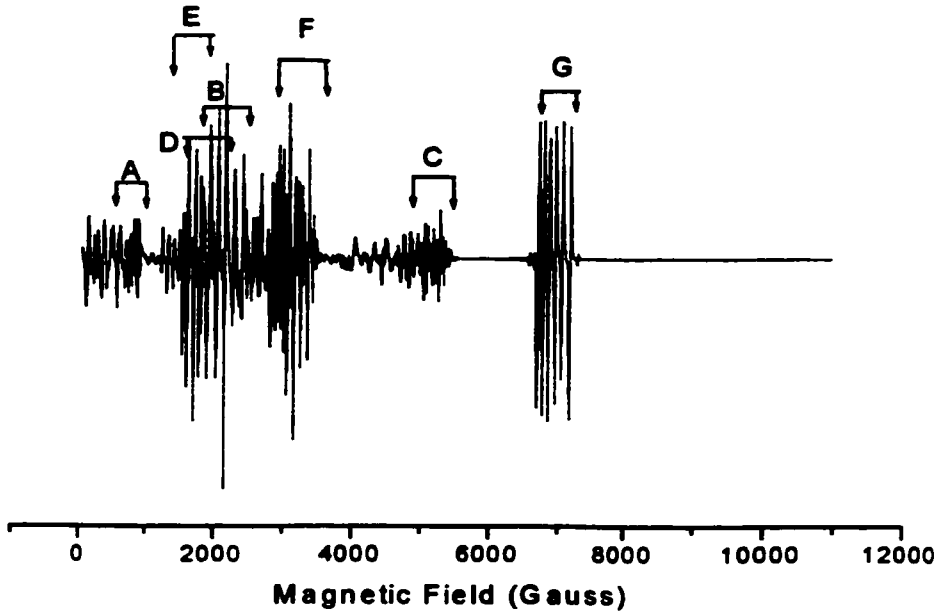

Fig. 4.4: The spectrum for an angle of 45 degrees from the z-axis. The group of lines marked A, B, C, D have shifted position from that of Fig. 4.3, while those marked E, F, G have not.

The group of lines marked as C in Fig. 4.4 showed an interesting characteristic as the crystal was rotated. For **B** || z the intensity of these lines was very small, and they first moved to higher fields up to about 30 degrees off the z-axis and then started to decrease

in field strength to the point where their position was no longer discernable in the spectrum.

All the crystal faces (100), (010) and (001) were found to be equivalent as far as the angular behavior of the EPR spectra was concerned. The EPR spectrum became quite complex as the crystal was rotated away from the z-axis due to the increasing overlap of other line positions, making it impossible to follow all the group of lines through the full angular variation of the crystal.

From the resulting angular variation, and the shifting of the line positions of the fine structure group in the (001) plane from [100] to [010] shows the existence of three types of magnetically equivalent sites, with their axes along the [100], [010], and [001] directions [Chand and Upreti, 1983]. The angular variation of the EPR spectrum of Mn^{2+} in $NH_4Cl_{0.9}I_{0.1}$ is given in Fig. 4.5 (z-spectrum). Lines not showing any angular dependence are given in Fig. 4.6 (x-y-spectrum). Spectra were recorded at angular intervals of two degrees from **B** || z to **B** || z +12°, then every four degrees thereafter up to **B** || z + 78°, and finally every two degrees up to **B** || z + 90°. This approach was used because the line positions for angles close to **B** || z have a greater influence on the SHP than those for angles farther away from **B** || z. The spectrum repeats itself at every 90° interval (z = z + 90°). This is shown in Fig. 4.7.

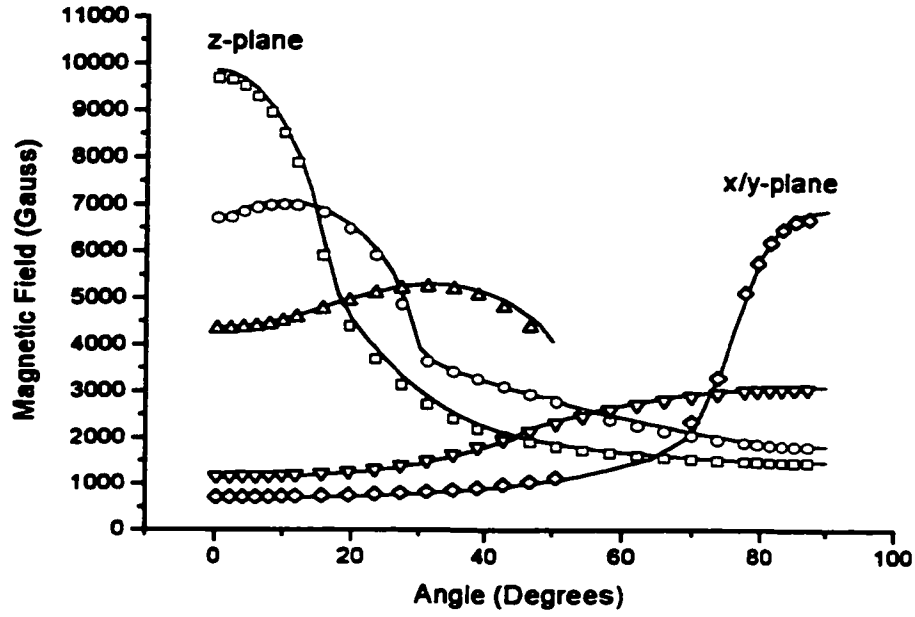

Fig. 4.5: The angular variation of Mn^{2+} in the (001) plane. The solid lines represent the computed values, and the circles, squares, triangles and diamonds are from experiment.

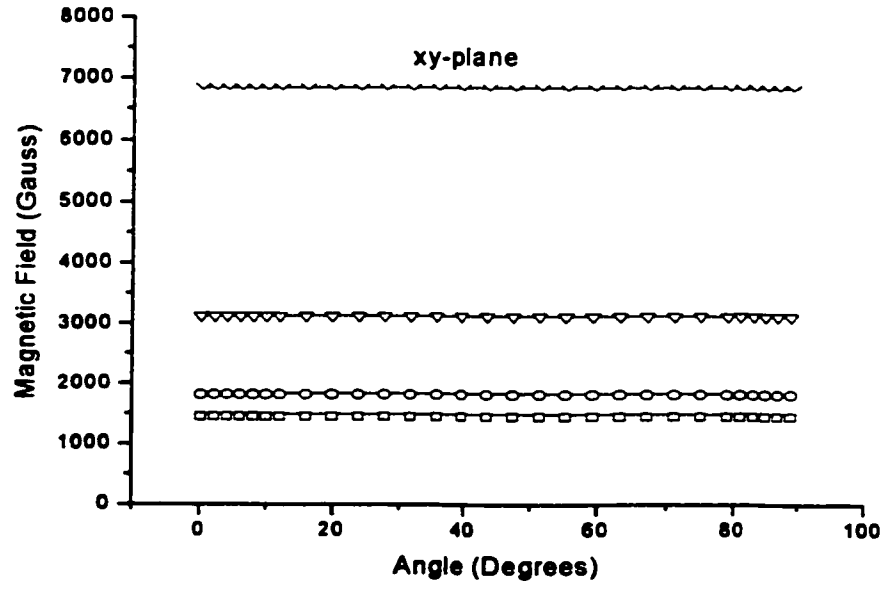

Fig. 4.6: The angular variation in the xy-plane showing the constant line positions.

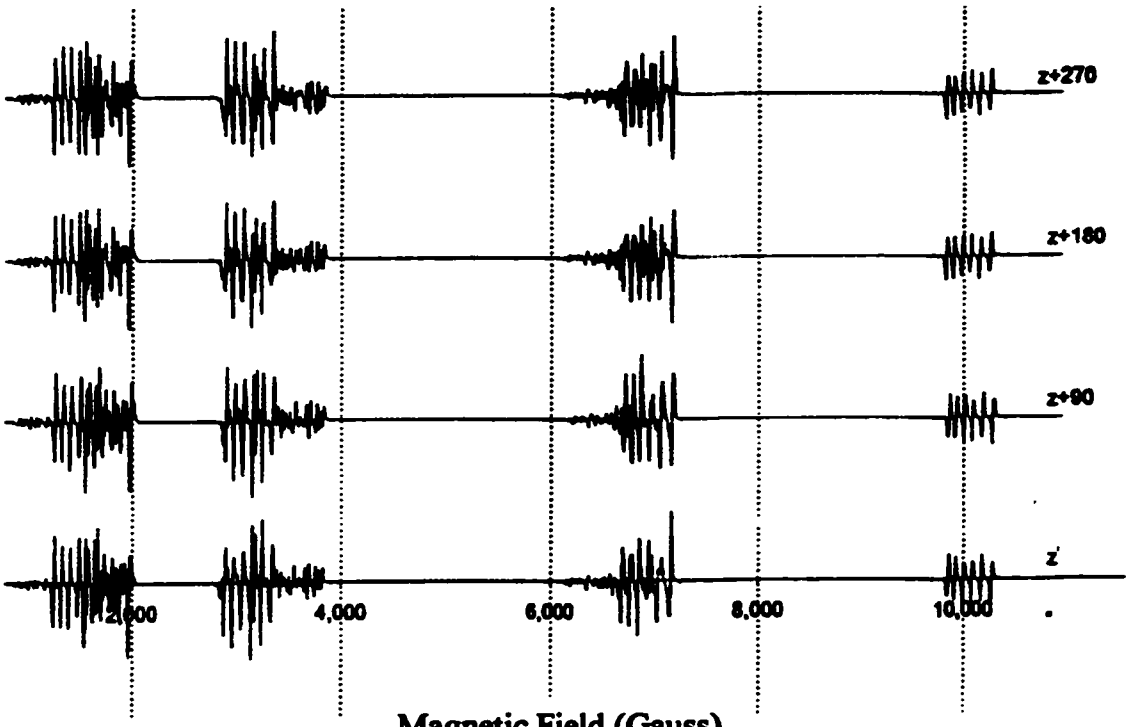

Fig. 4.7: A comparison of spectra starting at **B** || z (bottom spectrum), at 90° intervals showing that they are equivalent, verifying that the crystal has cubic symmetry. The intensities of the lines are indicated in arbitrary units.

The line positions for low magnetic fields were quite difficult to resolve due to the many fine-structure forbidden transitions, $\Delta M \neq \pm 1$, where M is the electronic magnetic quantum number. The intensities of forbidden transitions become quite high and they over shadow those of the allowed transitions [Forman and van Wyk, 1966]. The energy levels for **B** || z are shown in Fig. 4.8, and for **B** $\perp$ z in Fig. 4.9. The allowed transitions are those corresponding to an energy equal to the incident microwave frequency, and with $\Delta M = 1$ and $\Delta m = 0$. The fine structure forbidden transitions correspond to changes in the nuclear quantum number m by ± 1 [Abragam and Bleaney, 1970].

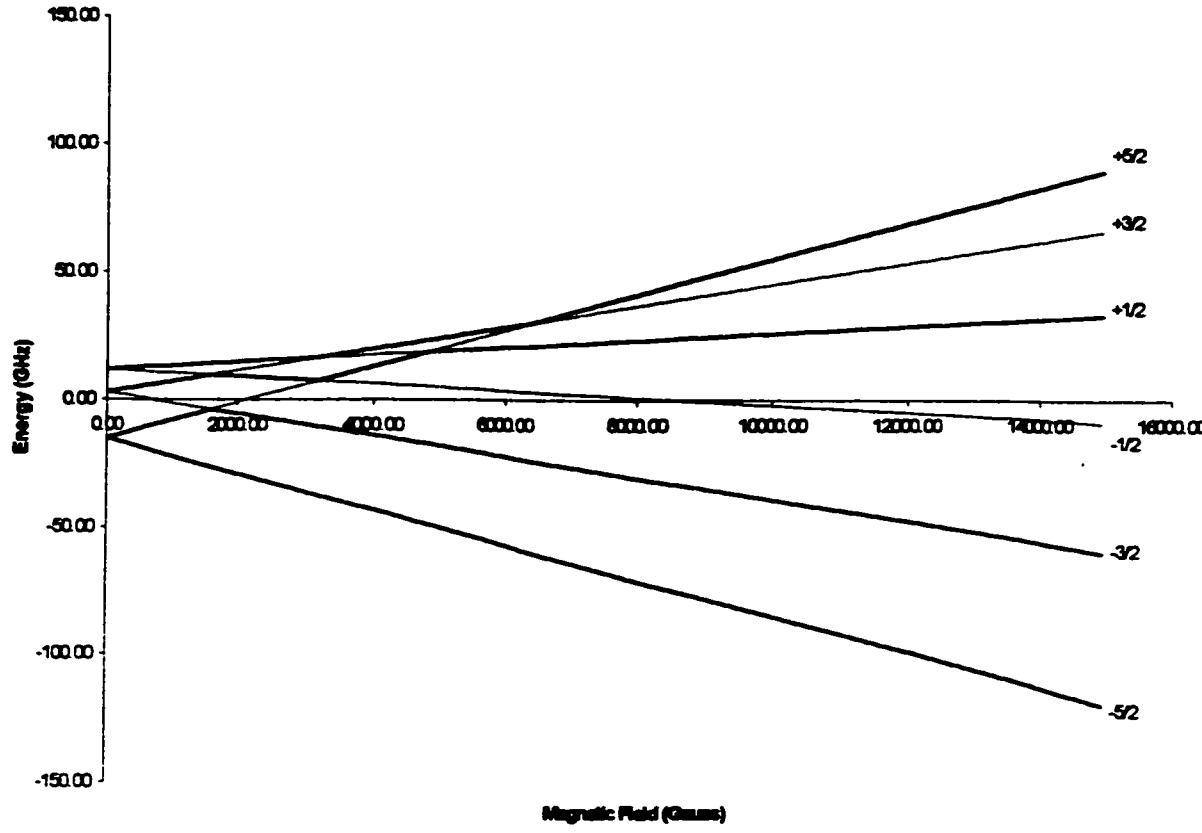

Fig. 4.8: Zeeman energy levels for **B** || z.

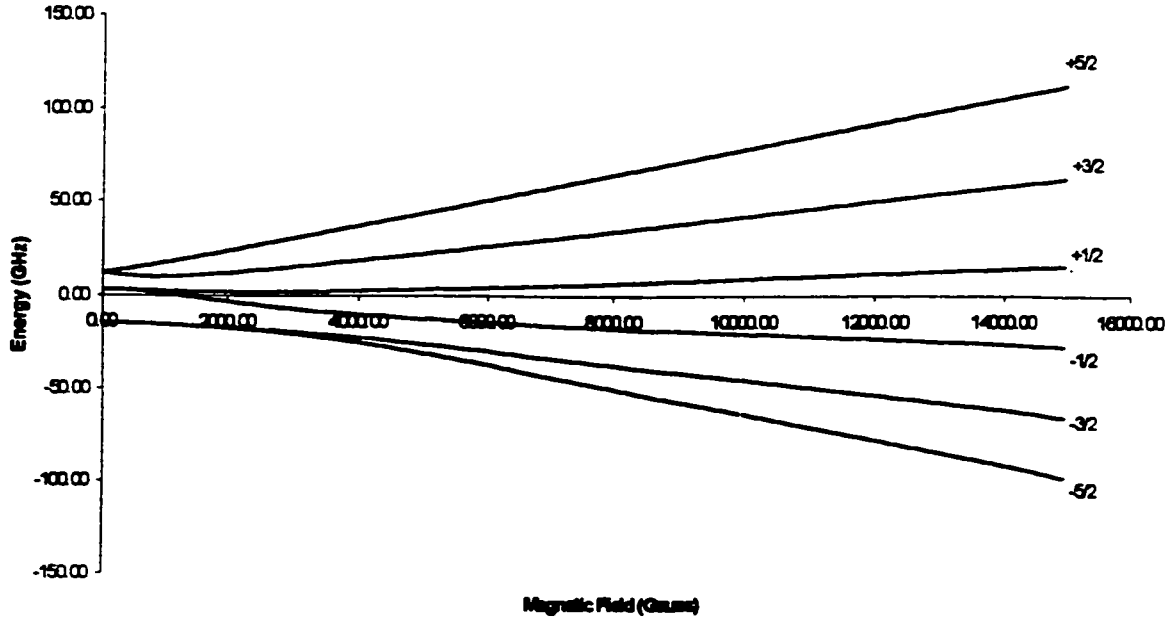

Fig. 4.9: Zeeman energy levels for **B** ⊥ z.

4.2.2 Q-band

The Q-band Zeeman energy levels are spread further apart than they are for X-band. This is owing to the fact that the Q-band microwave frequency being used here is approximately 3.5 times higher than the X-band klystron frequency of about 9.6 GHz. This higher frequency accordingly corresponds to higher magnetic field values for the electronic transitions, thereby separating the energy levels to such a degree as to allow one to distinguish quite readily between the forbidden and allowed transitions. The angular variation for Q-band is given in Fig. 4.10.

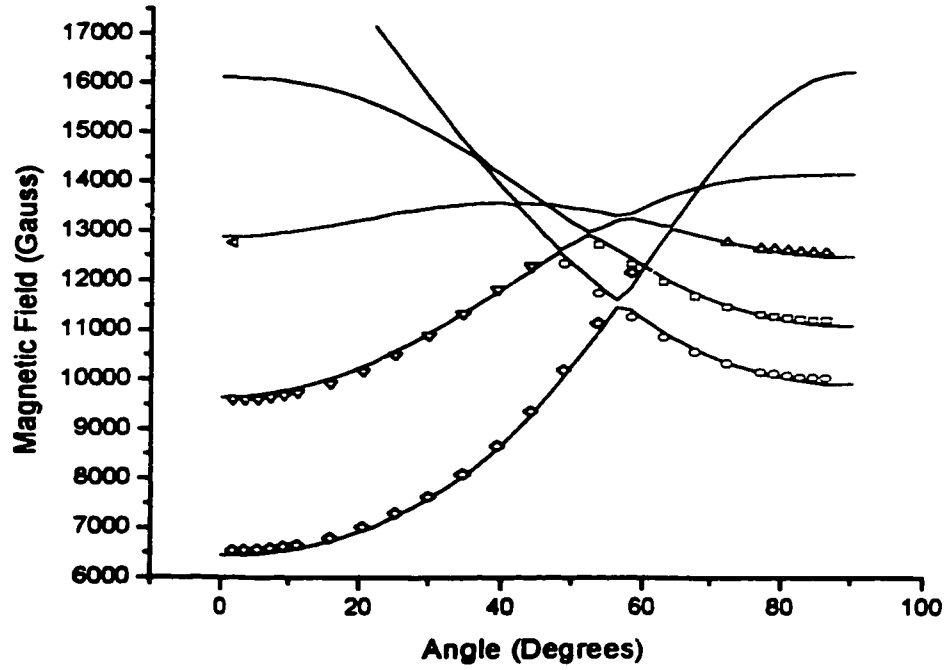

Fig. 4.10: The angular variation of Mn^{2+} in the (001) plane at Q-band. The solid lines represent the computed values, and the circles, squares, triangles and diamonds are from experiment.

The following two models have been proposed in order to explain the existence of the three axially symmetric magnetic sites [Chand and Upreti, 1983],

(i). The substitution of Mn^{2+} for NH_4^+, and in order to maintain overall charge neutrality, a vacancy at the next nearest cation site.

(ii). The substitution of Mn^{2+} for NH_4^+, and the substitution of two Cl^- ions with two OH^- ions along the cubic axis of the crystal.

All equivalent distortions in the above models occur with equal probability, so that 1/3 of the symmetric centers will have their axes along [100], 1/3 along [010] and the remaining 1/3 along the [001] direction. From experiment it was determined, to within experimental error, that the x and y-axes are equivalent, so that $g_{xx} = g_{yy} = g_\perp$. Therefore, for **B** parallel to either the [100], [010], or [001] directions the x-y spectrum becomes relatively more intense (theoretically about twice as much) than the z-x or z-y spectrum. All three centers will give identical overlapping spectra along the [111] direction, resulting in a single spectrum [Chand and Upreti, 1983].

At zero-field, the difference between the energy levels of the electron depends upon the ZFS parameter b_2^0. The quantity b_2^0 is the interaction energy of the spins of the electrons when the magnetic field **B** is in the z direction [Bersohn and Baird, 1966]. From the value $|b_2^0|$, the average separation between two electrons with opposite spin can be estimated. When axial symmetry is present [Abragam and Bleaney, 1970]

$$\left(b_2^0\right)_x = \left(b_2^0\right)_y = -1/2\left(b_2^0\right)_z = -1/3b_2^0 \qquad [4.1]$$

where,

$$\left(b_2^0\right)_{\alpha\alpha} = -\lambda^2 \sum_{M \neq 0} \frac{\left|\langle M'|L_\alpha|M\rangle\right|^2}{E_M - E_{M'}} \qquad [4.2]$$

where, $\alpha = x, y, z$, λ is the spin-orbit interaction constant, and L_α is the orbital angular momentum operator [Pake and Estle, 1973].

$$\sum_\alpha \left(b_2^0\right)_{\alpha\alpha} = 0 \qquad [4.3]$$

For Mn^{2+} in $NH_4Cl_{0.9}I_{0.1}$, the value of b_2^0 has been observed to be unusually large, indicating a strong axial distortion due to the presence of extra charge in the proximity of the paramagnetic ion [Chand and Upreti, 1983]. By model (i), it would indicate the presence of a charge compensating vacancy at the next nearest cation site. It has been found that for the alkali-halides, the equivalent sites associated with the OH^- impurity ligand, also have a large b_2^0 value compared to that of the pure ligands Cl^- or I^-. This suggests model (ii) for the strong axial distortion. As the crystal was grown from slightly aqueous solution, there was the possibility of the formation of $Mn(OH)_2$ due to the dissociation of H_2O [Chand and Upreti, 1983, Forman and van Wyk, 1967]. The OH^- ligands seem to make large distortions to the cubic environment possible, however, Chand and Upreti (1983) report having heat treated their crystal (430K), and cooled to liquid nitrogen temperature (77 K), and found no differences in the EPR spectra. This leads to the conclusion that the OH^- radical is not responsible for the large axial distortion. Forman and van Wyk (1966) report that for the NH_4Cl crystal doped with

Mn^{2+}, the spin-Hamiltonian given is consistent with a vacancy at the next nearest neighbor cation site. This same approach will be applied to the $NH_4Cl_{0.9}I_{0.1}$ crystal.

The observed spectra at Q-band are consistent with the existence of three axially symmetric magnetic sites, where the spectra also repeated themselves at 90° intervals. The analysis and interpretation of the Q-band spectra, confirm a large b_2^0 value as was found with X-band.

4.3 Evaluation of spin-Hamiltonian Parameters

The spin-Hamiltonian parameters as given by Eq. [2.7] rewritten here,

$$\mathcal{H} = \mu_B g(B_x S_x + B_y S_y + B_z S_z) + B_2^0 O_2^0 + B_4^0 O_4^0 + A(S_x I_x + S_y I_y + S_z I_z) \quad [4.4]$$

were evaluated using the least-squares fitting (LSF) procedure as outlined by Misra (1999). This method provides a quick, accurate procedure for the analysis of EPR data. In this procedure, the magnetic field values where transitions occurred for different orientations of the magnetic field relative to the crystal axis are used simultaneously, including the forbidden transitions for which $\Delta M \neq 1$. The computer program developed by Dr. Misra using the LSF technique in the evaluation of the SHP is given in Appendix C.

In the LSF, a mathematical criterion is used to arrive at a set of final parameters in an iterative manner, beginning with a set of initial parameters [Misra, 1999]. For the analysis of EPR data, one is interested in evaluating the SHP from the resonant magnetic field values obtained from one (preferably more than one) orientation of the external magnetic field. The set of P parameters described by the column vector $\bar{v}^m$ obtained from the iteration for which the chi-square value S` is at the absolute minimum, can be

obtained from a set of initial parameters which are described by the column vector $\vec{v}^i$ as follows,

$$\vec{v}^m = \vec{v}^i - \hat{E}^{-1}\vec{F} \qquad [4.5]$$

where $\vec{F}$ is the column vector whose elements are the first derivatives of S` evaluated at $\vec{v}^i$ , and $\hat{E}$ is the matrix containing the second derivatives of S` evaluated at $\vec{v}^m$. The value of chi-square is defined as,

$$S` = \sum_M (f_M(x_M, \vec{v}) - V_M)^2/\sigma^2_M \qquad [4.6]$$

where V_M is the experimental value for a given experimental variable x_M. The σ_M is a weight factor determined from standard deviation, and $f_M(x_M, \vec{v})$ is the calculated value with parameters $\vec{v}$ corresponding to the experimental value V_M.

Initially, the values of $\vec{v}^m$ are not known, therefore the elements of $\hat{E}$ are evaluated with respect to $\vec{v}^i$, from which a new set of parameters described by $\vec{v}^f$ is obtained,

$$\vec{v}^f = \vec{v}^i - (\hat{E})^{-1}\ \vec{F} \qquad [4.7]$$

In the fitting, done by the computer software designed by Dr. Misra, Eq. [4.7] is used in an iterative manner until a sufficiently small value for S` is obtained [Misra, 1999]. The chi-square function for EPR data is given by

$$S` = \sum_M [(|\Delta E_M| - h\upsilon_M)^2 /\sigma^2_M] \qquad [4.8]$$

where $\Delta E_M = E_M - E_{M'}$. The energies E_M and $E_{M'}$ are obtained by substituting the numerical values of the parameters, and the resonant magnetic field value B_M into Eq. [4.4], and diagonalizing it on the computer [Misra, 1999].

As mentioned above, in order to apply the LSF method the first and second derivatives of S` (with respect to the parameters) are needed. These are given here,

$$\frac{\partial S`}{\partial a_j} = 2\sum_M \frac{\Delta E_M}{|\Delta E_M|}\frac{(|\Delta E_M| - h\upsilon_M)}{\sigma_M^2}\left(\frac{\partial E_M}{\partial a_j} - \frac{\partial E_{M'}}{\partial a_j}\right) \qquad [4.9]$$

$$\frac{\partial^2 S`}{\partial a_j \partial a_l} = 2\sum_M \frac{1}{\sigma_M^2}\left(\frac{\partial E_M}{\partial a_j} - \frac{\partial E_{M'}}{\partial a_j}\right)\left(\frac{\partial E_M}{\partial a_l} - \frac{\partial E_{M'}}{\partial a_l}\right) + \frac{\Delta E_M}{|\Delta E_M|}(|\Delta E_M| - h\upsilon_M)\left(\frac{\partial^2 E_M}{\partial a_j \partial a_l} - \frac{\partial^2 E_{M'}}{\partial a_j \partial a_l}\right) \qquad [4.10]$$

These can be evaluated numerically by using Feyman's theorem as outlined in Misra (1999), and according to which

$$\frac{\partial E_M}{\partial a_j} = \langle \psi_M | (\partial \mathcal{H}/\partial a_j) | \psi_M \rangle \qquad [4.11]$$

or in a form more convenient for computer evaluation [Misra, 1999],

$$\frac{\partial E_M}{\partial a_j} = \mathrm{Tr}[\partial \mathcal{H}/\partial a_j (|\psi_M\rangle \otimes \langle \psi_M|)] \qquad [4.12]$$

where $|\psi_M\rangle \otimes \langle \psi_M|$ is the (2S + 1) x (2S + 1) matrix found by taking the outer-product of the column vector $|\psi_M\rangle$ with itself, and $\partial \mathcal{H}/\partial a_j$ are the spin operators proportional to either the components of $\vec{S}$ or O_l^m in Eq. [4.4]. Tr stands for "the trace of a matrix", that is, the sum of the diagonal elements of the matrix.

The evaluation of SHP from EPR data by using the LSF technique, can be done by using the following steps [Misra, 1999]

(i). By using second-order perturbation theory, an estimate is made for the initial parameters (non-zero)

(ii). Fit the greatest number of data points possible from different magnetic field orientations. The more line positions are fitted, the smaller the parameter error becomes. For each resonant field value B_M, the elements of the SH matrix are determined using the $\vec{v}^i$. By using an adequate computer subroutine the eigenvalues E_M, and eigenvectors $|\psi_M>$ should be calculated.

(iii). By using the results of (ii), calculate chi-square, the first derivative, and second derivative.

(iv). Determine the matrices $\hat{E}$ and $\vec{F}$ as outlined above.

(v). Calculate the eigenvalues and eigenvectors of $\hat{E}$. Calculate, using Eq. [4.7], a new set of parameters with the initial set found in (i), and then compute a new S`. If this "new" S` is smaller than the "old" S`, and consistent with experimental uncertainties, end the computation, otherwise Misra (1999) gives other strategies such as the use of *interpolated fields*, where the theoretical fields are computed, using a set of initial parameters, corresponding to the actual resonant fields. However, it may be simpler to calculate theoretical frequencies instead, by the use of *interpolated frequencies*, where the computed frequencies are proportional to the energy differences between the levels participating in resonance.

For each calculated spectrum the mean square deviation (SMD) is calculated using,

$$SMD = \sum_{M} (|\Delta E_M| - h\upsilon)^2 \qquad [4.13]$$

where ΔE_M is the energy difference of the two levels participating in resonance at the M^{th} resonant field value. The LSF technique was successfully applied in the interpretation of the experimental data amassed for the $NH_4Cl_{0.9}I_{0.1}$ crystal. The final output data (SHP), as determined by the LSF method, are given in Table 4.1 for different temperatures and microwave frequencies.

The SHP of Chand and Upreti (1983) X-band and (1984) Q-band for Mn^{2+} in the pure NH_4I crystal with FCC structure, along with those of Forman and van Wyk (1966) for Mn^{2+} in the pure NH_4Cl crystal with BCC structure are given in Table 4.2 for comparative purposes.

Table 4.1: Spin-Hamiltonian parameters for $NH_4Cl_{0.9}I_{0.1}$

Frequency (GHz)	9.6193	9.6965	35.87	36.06	9.6193 + 35.87
Temp (K)	295	120	295	77	295
# Lines fit	216	222	288	288	504
$g_{\|\|}$	2.0062 ± 0.00021	1.9984 ± 0.00019	2.0141 ± 0.00005	2.0446 ± 0.000067	2.0160 ± 0.000031
$g_{\perp}$	1.9991 ± 0.00012	1.9986 ± 0.00013	2.0104 ± 0.00004	2.0162 ± 0.000031	2.0102 ± 0.000032
b_2^0 (GHz)	-4.5274 ± 0.00073	-4.6362 ± 0.00068	-4.5771 ± 0.00022	-4.7003 ± 0.00027	-4.5672 ± 0.00012
b_4^0 (GHz)	.000812 ± 0.00035	0.00035 ± 0.000006	0.013 ± 0.00014	0.036 ± 0.00015	0.0111 ± 0.00012
A (GHz)	-0.24387 ± 0.00033	-0.23733 ± 0.00032	-0.25406 ± 0.00023	-0.24859 ± 0.00023	-0.24834 ± 0.00019
B (GHz)	-0.24193 ± 0.00034	-0.23888 ± 0.00034	-0.25523 ± 0.00031	-0.24987 ± 0.00024	-0.24852 ± 0.00022
SMD	0.24485	0.61396	0.35903	0.53491	0.13496

Table 4.2: Spin-Hamiltonian parameters for NH_4Cl and NH_4I.

Host	$g_{\|\|}$	$g_{\perp}$	b_2^0 (GHz)	b_4^0 (GHz)	A (GHz)	B (GHz)
NH_4Cl	2.0012	2.0012	-4.7728	0.0064	-0.26379	-0.26797
NH_4I: X-band	2.0014	2.0028	-4.7966	0.0168	-0.26797	-0.26797
NH_4I: Q-band	2.0003	2.0004	-4.4809	0.00028	-0.24414	-0.24885

Chapter 5

Analysis of Experimental Data

In this chapter an attempt is made to analyze the Mn^{2+} zero-field-splitting parameter in $NH_4Cl_{0.9}I_{0.1}$ using the superposition model of Newman (1971).

5.1 The Superposition Model

The experimentally determined spin-Hamiltonian parameters (SHP) can be analyzed by making use of the superposition model (SM), originally proposed by Newman (1971). The SM makes the assumption that the SHP can be expressed as the sum of the ionic contributions due to individual ions within the crystal lattice. The spherical symmetry of the ions allows one to represent the contribution from each ion as a cylindrically symmetric field if the z-axis is taken along the symmetry axis of the coordinated ions. The SM approach takes into account only the nearest-neighbor interactions, being the predominant contributors to the SHP, and neglects the effects of the more distant ions.

Knowledge of the crystal structure is required in order to determine the exact spatial location of the ions within it. This is important because the SM analysis in this work is based upon the interaction of the Mn^{2+} ion with the surrounding Cl^- ligands. Due to the fact that there is a "charge compensation" (Mn^{2+}: NH_4^+) effect, and a difference in ionic size between the host ion and the impurity ion, there will be some local distortion in the crystal about the Mn^{2+} ion. There is an abundance of chemical-bond data available in

publications, notably that by Pauling (1939) which were exploited in the calculations of bond distances and lattice distortions in this work.

The crystal investigated here is the mixed ammonium chloride-iodide ($NH_4Cl_{0.9}I_{0.1}$) crystal, doped with 0.2% concentration of Mn^{2+}. The valence of the NH_4 cation is +1, and it has an ionic radius of 1.43 Å [Pauling, 1939]. As the crystal is electrically neutral, the valence of the Cl, and I anions are –1 each. The ionic radii for the Cl and I ions are 1.81 Å and 2.20 Å respectively [Pauling, 1939]. There will result some local distortion within the crystal where a mono-valent $(NH_4)^+$ cation has been replaced by the divalent Mn^{2+} cation, because the latter has a different valence, and a different ionic radius of 0.81 Å [Pauling, 1939].

To apply the SM to the Mn^{2+}-doped $NH_4Cl_{0.9}I_{0.1}$ crystal, the Mn^{2+} cation will here be assumed to be at the origin (0,0,0) of a coordinate system located within the crystal. Then one of the anions Cl^{-1} or I^{-1}, say the i^{th}, called a ligand ion, will be located at some position (R_i, θ_i, ϕ_i) relative to this cation. The variable R_i is the bond length between the impurity cation and one of its nearest neighbor anions. The angular coordinates (θ_i, ϕ_i) are the azimuthal and polar angles respectively, that the anion-cation bonds make relative to the axial plane of the crystal. For cubic crystals, such as $NH_4Cl_{0.9}I_{0.1}$, which is assumed to have the BCC structure (NH_4Cl has BCC structure [Kittel, 1961]), the polar coordinate ϕ is not required due to the axial symmetry of the crystal.

The NH_4Cl crystal has a BCC structure, and a lattice constant, a, of 3.87 Å

[Kittel, 1961]. A representation of the BCC structure is given in Fig. 5.1. When the crystal consists of mixed anions, as is the case for $NH_4Cl_{0.9}I_{0.1}$, 9 out of 10 anion lattice sites will be occupied by the Cl^- ion, and the tenth site by the I^- ion if there is uniform doping. This is shown in Fig. 5.2. In this work the SM will first be applied to the $NH_4Cl_{0.9}I_{0.1}$ crystal with different possible anion configurations assuming that the local coordination of the Mn^{2+} ion is the same as that of the NH_4^+ ion, except for a vacancy in the former case. Then it will be applied to both to the NH_4Cl and NH_4I crystals separately for comparative purposes. Based upon the results obtained for these two crystals a confirmation can be made to the assumption as to whether $NH_4Cl_{0.9}I_{0.1}$ has BCC structure or the FCC structure of NH_4I.

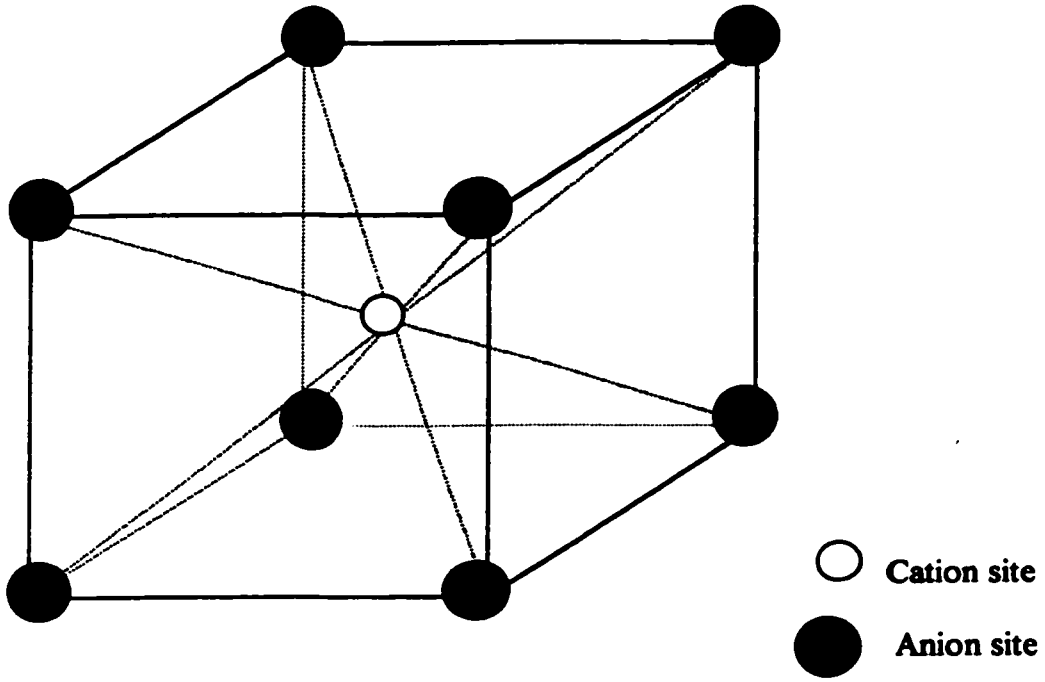

Fig. 5.1: A unit cell of the BCC lattice structure of the NH_4Cl crystal. The body-centered cation is surrounded by 8 coordinated anion ligands.

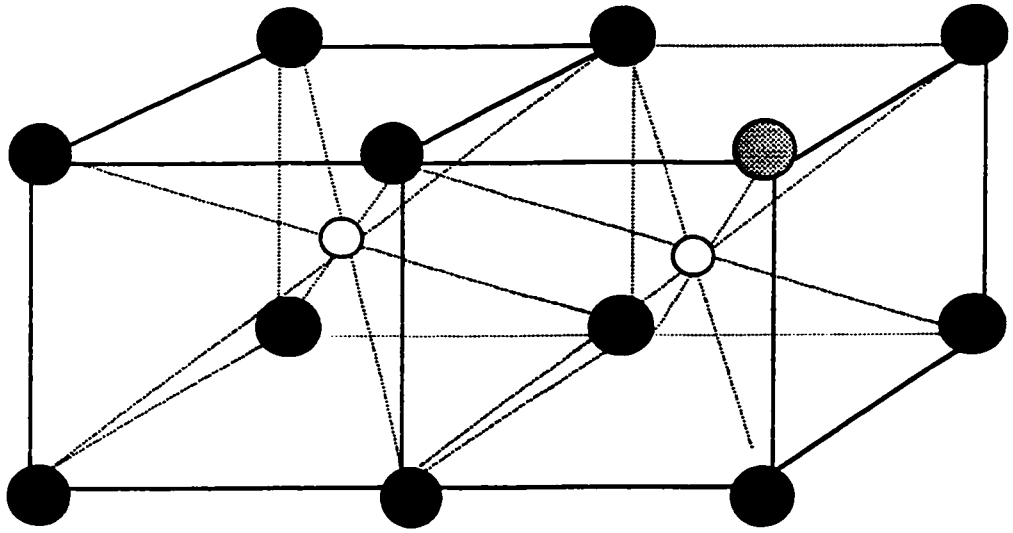

Fig. 5.2: A possible arrangement of the ions for the $NH_4Cl_{0.9}I_{0.1}$ crystal with BCC structure. The iodine ion is shown in gray, and the chlorine ion in black.

In the SM, the contribution of the i^{th} coordinated ligand to the SHP, B_n^m is expressed as,

$$K_n^m(\theta_i, \phi_i)\ \bar{b}_n(R_i) \qquad [5.1]$$

where the variable $\bar{b}_n(R_i)$ is called the intrinsic parameter, representing the contribution to the crystal field from a single ligand at a distance R_i from the origin (0,0,0) [Newman, 1971, Newman and Urban, 1975]. The K_n^m are called the coordination factors. They depend on the angular position of the ligand with respect to the defined origin within the crystal. Specifically, for cubic symmetry the only required coordination factors are:

$$K_2^0(\theta) = \tfrac{1}{2}(3\cos^2\theta - 1) \qquad [5.2]$$

$$K_4^0(\theta) = \tfrac{1}{8}(35\cos^4\theta - 30\cos^2\theta + 3) \qquad [5.3]$$

As there are multiple ligands at the distance R in a given cubic crystal, the zero field splitting parameters (ZFS), are expressed as a sum of the contributions of the various ligands i:

$$b_n^m = \sum_i K_n^m\ (\theta_i, \phi_i)\ \bar{b}_n(R_i) \qquad (i = 1, 2, 3, ...) \qquad [5.4]$$

with

$$\bar{b}_n(R_i) = \bar{b}_n(R_0)(R_0/R_i)^{t_n} \qquad [5.5]$$

where R_0 is the anion-cation bond distance taken along the direction of the Mn^{2+}-nearest neighbor vacancy. This direction will be hereby defined to be the z-direction for the Mn^{2+} doped $NH_4Cl_{0.9}I_{0.1}$ crystal. In Eq. [5.5], R_i is the impurity cation-anion distance for the ith ligand, and t_n is the power law exponent. It is usually taken as 7 ± 1 for Mn^{2+} [Newman, 1971, Newman and Urban, 1975, Newman and Siegel, 1976, Rubio and Cory, 1978,

Rubio et al., 1979, Oseguera et al., 1980, Lehmann, 1980, Weltner and van Zee, 1985, Heming and Lehmann, 1987, Jain and Lehmann, 1990, Wen-Chen, 1993].

In this work the determination of the impurity ligand distance will be made by taking into account the effect of charge compensation due to the difference in the ionic charge of the host, and impurity cation. This difference in ionic charge leads to a vacancy at the next nearest cation site in order to maintain electrical neutrality.

In EPR, the SHP, b_n^m, are determined experimentally using the LSF technique. Specifically, for a cubic crystal these are the parameters b_2^0 and b_4^0. For these parameters, Eqs. [5.4] and [5.5] yield

$$b_2^0 = \sum_i \tfrac{1}{2}(3\cos^2\theta_i - 1)\,\bar{b}_2(R_0)(R_0/R_i)^{t_2} \qquad [5.6]$$

$$b_4^0 = \sum_i \tfrac{1}{8}(35\cos^4\theta_i - 30\cos^2\theta_i + 3)\,\bar{b}_4(R_0)(R_0/R_i)^{t_4} \qquad [5.7]$$

In order to express b_2^0 , and b_4^0 in the form given by Eqs. [5.6] and [5.7] respectively, the values of $\bar{b}_2(R_0)$ and $\bar{b}_4(R_0)$ should be determined from the SHP and the configuration of the ligands. To this end one needs to know the bond length R_0. This is described in the following section.

5.2 Estimation of the Bond Length R_0

The ammonium chloride (NH_4Cl) crystal has the BCC lattice structure, while NH_4I has the FCC structure. It is expected that there will be a good probability that the mixed $NH_4Cl_{0.9}I_{0.1}$ crystal will also have the BCC structure due to the predominantly large content of Cl^- ions versus I^- ions (9:1 rato).

In order to estimate bond lengths in a host crystal one needs to know how the substitution of a host cation, NH_4^+, by the impurity cation Mn^{2+} effect the integrity of the host crystal in the vicinity of the impurity cation. At equilibrium, the attractive and repulsive coulomb forces cancel each other out completely, and the crystal is electrically neutral. If one were to think of ions as small spheres, the bond distance might simply be the sum of the radii of the anion and cation provided that they are touching each other (tight-binding). However, this is generally not the case [Pauling, 1939]. The combination of Coulomb forces, ionic radii, and type of ions, ultimately determines the structure of a crystal, and the size of the unit cell. In some cases, the equilibrium condition leads to anion-cation overlap, that is $R_0 < R_{anion} + R_{cation}$, while there are cases where the equilibrium condition requires that $R_0 > R_{anion} + R_{cation}$, due to either strong cation-cation, or anion-anion interaction [Pauling, 1939].

The NH_4Cl and NH_4I crystals may crystallize into either the BCC or FCC structure when external influences such as temperature affect the equilibrium condition [Pauling, 1939]. (However, in this work the crystal structures as published by Kittel (1961) will be used, that is, NH_4Cl has BCC structure, and NH_4I has FCC structure). The inter-ionic distances for BCC structure are about 3% greater than for FCC structure. This particularity is exploited in a manner such that given the bond length for the FCC structure, the bond length in the BCC structure can be calculated. The calculations carried out here to find the bond lengths for the BCC structure were based on the FCC structure. The FCC structure is shown in Fig. 5.3.

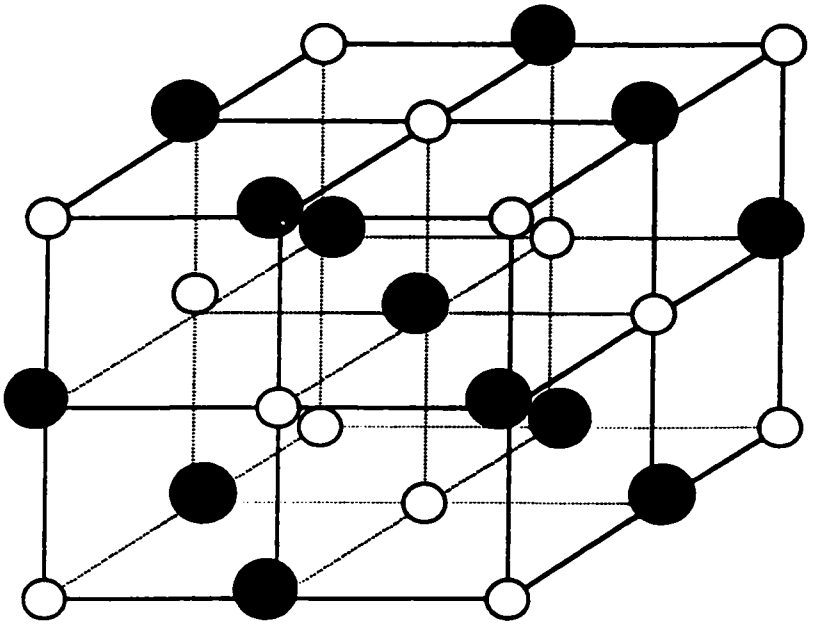

Fig. 5.3: The face-centered-cubic lattice. The large spheres are anions and the small ones cations.

The procedure described by Pauling, (1939) is described as follows.

The total potential energy of a crystal with FCC structure may be written as [Pauling, 1939],

$$V = -\frac{Ae^2 z^2}{R} + \frac{Be^2}{R^n} \qquad [5.8]$$

In Eq. [5.8], A is the Madelung constant, B is the repulsive Coulomb coefficient, the variable z^2 accounts for the valence of the ions, e is the electron charge, R is the anion-cation bond length and n is the Born exponent, or as in some publications the repulsive potential exponent. The attractive Coulomb force is accounted for in the e^2 term.

At equilibrium, the attractive and repulsive Coulomb forces are balanced. The value of R (called R_0) at which this occurs is found by differentiating Eq. [5.8] with respect to R and equating to zero [Pauling, 1939].

$$dV/dR = \frac{Ae^2z^2}{R^2} - \frac{nBe^2}{R^{n+1}} \qquad [5.9]$$

and at equilibrium,

$$\frac{Ae^2z^2}{R_0^2} - \frac{nBe^2}{R_0^{n+1}} = 0 \qquad [5.10]$$

from which R_0 can be found,

$$R_0 = \left(\frac{nB}{Az^2}\right)^{\frac{1}{n-1}} \qquad [5.11]$$

The Madelung constant depends upon the type of crystal structure; it can be determined by taking the sum of the charge distribution of the particular crystal structure. R is of vital importance to SM calculations, since the Madelung constant is dependent upon the crystal structure, and according to Eq. [5.8] the potential energy is a function of R. Determination of the Madelung constant will be discussed in further detail below. The Born exponent, n, can be estimated from the compressibility data of a crystal [Kittel, 1961], and it is given by the following relationship,

$$n = 1 + \frac{18R_0^4}{Ke^2A} \qquad [5.12]$$

where the compressibility K is a function of the change in volume of the crystal with a change in pressure. It is given by,

$$K = -\frac{dV}{Vdp} \qquad [5.13]$$

For most crystals the value of $n \approx 9$ is used [Pauling, 1939, Kittel, 1961]. If one now takes into account the sizes of the individual ions, Eq. [5.8] becomes,

$$V = -\frac{Ae^2}{R} + \beta Be^2 \frac{(r_+ + r_-)^{n-1}}{R^n} + \beta Be^2 \frac{(2r_+)^{n-1}}{(\sqrt{2}R)^n} + \beta Be^2 \frac{(2r_-)^{n-1}}{(\sqrt{2}R)^n} \qquad [5.14]$$

where β is an ionic-interaction constant. It has values of 1, 1.25, 0.75, respectively, for anion-cation interaction, for cation-cation interaction, for anion-anion interaction [Pauling, 1939]. The variables, r_+ and r_-, are the radii of the cation and anion respectively. In order to determine the distance R_0, one needs to minimize V as given by Eq. [5.14]. Thus, by differentiating Eq. [5.14] with respect to R one obtains [Pauling, 1939],

$$R_{0FCC} = (r_+ + r_-)F(\rho) \qquad [5.15]$$

in which $F(\rho)$ is a function of the ionic radii ratio

$$\rho = \frac{r_+}{r_-} \qquad [5.16]$$

and it has the form

$$F(\rho) = \left(\frac{6nB}{A}\right)^{\frac{1}{n-1}} \left\{1 + \frac{1.25}{(\sqrt{2})^n}\left(\frac{2\rho}{\rho+1}\right)^{n-1} + \frac{0.75}{(\sqrt{2})^n}\left(\frac{2}{\rho+1}\right)^{n-1}\right\}^{\frac{1}{n-1}} \qquad [5.17]$$

The factor 6 in Eq. [5.17] takes into account the six nearest neighbors in the FCC lattice. A plot of $F(\rho)$ vs ρ is given in Fig. 5.4 [Pauling, 1939].

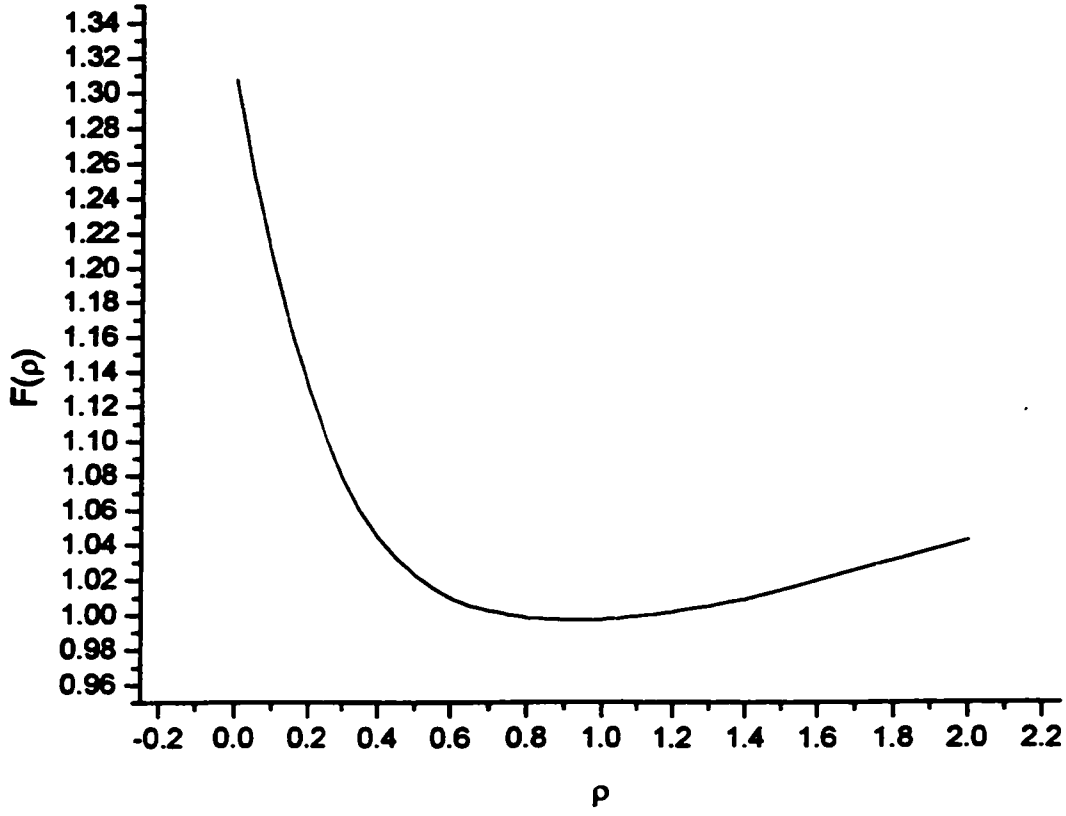

Fig. 5.4: A plot of $F(\rho)$ versus ρ. $\rho = \frac{r_+}{r_-}$, $R_0 = (r_+ + r_-)F(\rho)$, for crystals with FCC structure.

According to what has been published in the past, for the vast majority of ionic crystals n $\approx$ 9, and the value nB = 0.262 was chosen so that for $\rho = 0.75$, $F(\rho) = 1$ [Pauling, 1939, Kittel, 1961]. These particular values were chosen mainly because for many crystals with NaCl structure, which is FCC, the anion-cation radii ratio is very close to 0.75. Therefore for crystals having this particular ionic ratio, the equilibrium bond distance, R_0, is just the sum of the radii of anion and cation [Pauling, 1939].

In order to apply Eq. [5.15], which is based on FCC structure, one needs to recalculate R_0 for the assumed BCC structure for $NH_4Cl_{0.9}I_{0.1}$ crystal. As was mentioned above, NH_4Cl, and NH_4I, may crystallize into either the FCC or the BCC lattice structure, depending upon the conditions present when the crystal was formed [Pauling, 1939]. The relationship between the two possibilities is given by,

$$\frac{R_{0BCC}}{R_{0FCC}} = \left(\frac{B_{BCC}}{B_{FCC}} \bullet \frac{A_{FCC}}{A_{BCC}} \right)^{\frac{1}{n-1}} \qquad [5.18]$$

Given the inter-ionic bond distance of one structure, the Madelung constant of both, and repulsive coefficient of both, for example, it is now a simple matter to calculate using Eq. [5.18] the ionic bond distance R_{0BCC} or R_{0FCC} from that of the other [Pauling, 1939].

The bond distances for NH_4Cl and NH_4I will now be calculated for both BCC and FCC lattice arrangements respectively. Starting with Eq. [5.16], ρ for NH_4Cl is equal to,

$$\rho = r_+/r_- = 1.43/1.81 = 0.79 \qquad [5.19]$$

and now putting this value into Eq. [5.17],

$$F(\rho) = \left(\frac{6(.262)}{1.74756} \right)^{\frac{1}{8}} \left\{ 1 + \frac{1.25}{\left(\sqrt{2}\right)^9} \left(\frac{2(.79)}{.79+1} \right)^8 + \frac{0.75}{\left(\sqrt{2}\right)^9} \left(\frac{2}{.79+1} \right)^8 \right\}^{\frac{1}{8}} = 0.9986 \qquad [5.20]$$

Putting this value into Eq. [5.15], one obtains

$$R_{0FCC} = 0.9986(1.43 + 1.81) = 3.24\,\text{Å} \qquad [5.21]$$

The value obtained in Eq. [5.18] is for FCC structure, and it is now possible by using Eq. [5.18], to calculate R_0 for the BCC structure.

$$R_{0BCC} = 3.24\,\text{Å}\ (1.322)^{1/8} = 3.355\,\text{Å} \qquad [5.22]$$

Similarly the bond distance for the NH_4I crystal, for both the FCC and BCC structures can be calculated. The results are listed in Table 5.1. The repulsive potential coefficient B, is equal to 8 for BCC structure, and 6 for FCC structure [Pauling, 1939].

Table 5.1: Crystal structure data for ammonium chloride and ammonium iodide.

Host	r_+ (Å)	r_- (Å)	ρ	$F(\rho)$	R_{0FCC} (Å)	R_{0BCC} (Å)
NH_4Cl	1.43	1.81	0.79	0.9986	3.24	3.355
NH_4I	1.43	2.20	0.65	1.0056	3.65	3.81

5.3 Madelung Constant

It was felt that a brief discussion of the Madelung constant should be included here because of the role the Madelung constant plays in determining the equilibrium distance R_0, and given the importance of R_0 in the application of the SM. Its importance is justified because the value of the Madelung constant varies with the type of crystal structure as can be seen in Eq. [5.18]. It may be evaluated by taking into account the contribution of the ionic charges situated on a cubic unit cell of a particular crystal. The charges on cube faces are shared between 2 unit cells, on edges between 4 unit cells, and at corners between 8 unit cells, this method of summing the net charge contribution of successive unit cells was first developed by Evjen [Kittel, 1961]. A two dimensional representation is given below in Fig. 5.5.

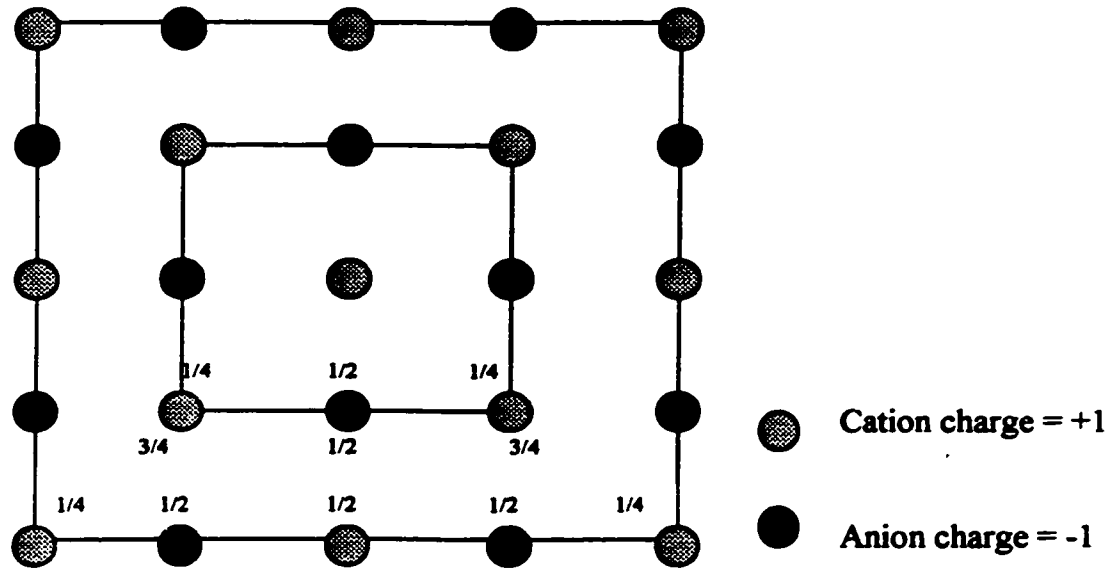

Fig. 5.5: A two-dimensional representation of the Evjen method for determining the Madelung constant.

At the boundary of the inner square we have a total charge of 4(1/2) - 4(1/4) = 1. Similarly for the outer square 4(1/2) - 4(3/4) - 4(1/2) + 8(1/2) - 4(1/4) = 0. Applying the same approach to a three dimensional FCC lattice one obtains,

$$A = n_1(1/2)/1 - n_2(1/4)/\sqrt{2} + n_3(1/8)/\sqrt{3} \qquad [5.23]$$

where n_1, n_2, n_3 are the total number of ions per cube on its faces, edges, and corners respectively, so that for a FCC unit cube with $n_1 = 6$, $n_2 = 12$, and $n_3 = 8$, A = 1.45 is obtained. If the next cube enclosing the smaller one is taken into account a more accurate value of A = 1.75 was obtained for the FCC structure. If even more successive cubes are included in the calculation, a value which is very close to the accepted value of 1.74756, which has been calculated using the Ewald method, may be obtained [Kittel, 1961]. The value of the Madelung constant for the BCC structure is 1.76267 [Pauling, 1939].

5.4 Mixed Ammonium Chloride-Iodide Host Crystal: NH_4Cl Structure

First the SM will be applied to the situation where the iodine ion is not part of the cubic unit cell surrounding the Mn^{2+} ion, so that all the ligand contributions come only from the chlorine ions. Secondly the assumption will be made that the iodine ion is part of the unit cell surrounding the Mn^{2+} ion, at an anion site on the side nearest to the cationic vacancy, and finally for the third situation, on the side furthest away from the cationic vacancy. The reason for doing this is because the exact location of the iodine anion is not known. There are 8 anion sites surrounding the central cation in BCC structure, and it was felt that the probability that the iodine anion could occupy any one of these sites was high enough to warrant the approach described above. This is shown in Fig. 5.6. In the "normal" BCC lattice, all the anion sites are equal and homogenous, so that the four anion sites on the right of Fig. 5.1 are the same as those on the left side. The same can be said for the four on top and the four on the bottom. In Fig. 5.6, cube 2 will be taken as the one undergoing lattice distortions due to the next nearest cation site vacancy in the adjoining cube to the right (cube 3). The chlorine ions are shown in black, the iodine in light gray, the manganese in white, ammonium in dark gray, and the vacancy as a square at the cationic site of cube 3. Cube 1 is assumed to consist of NH_4^+ ions and Cl^- ions only.

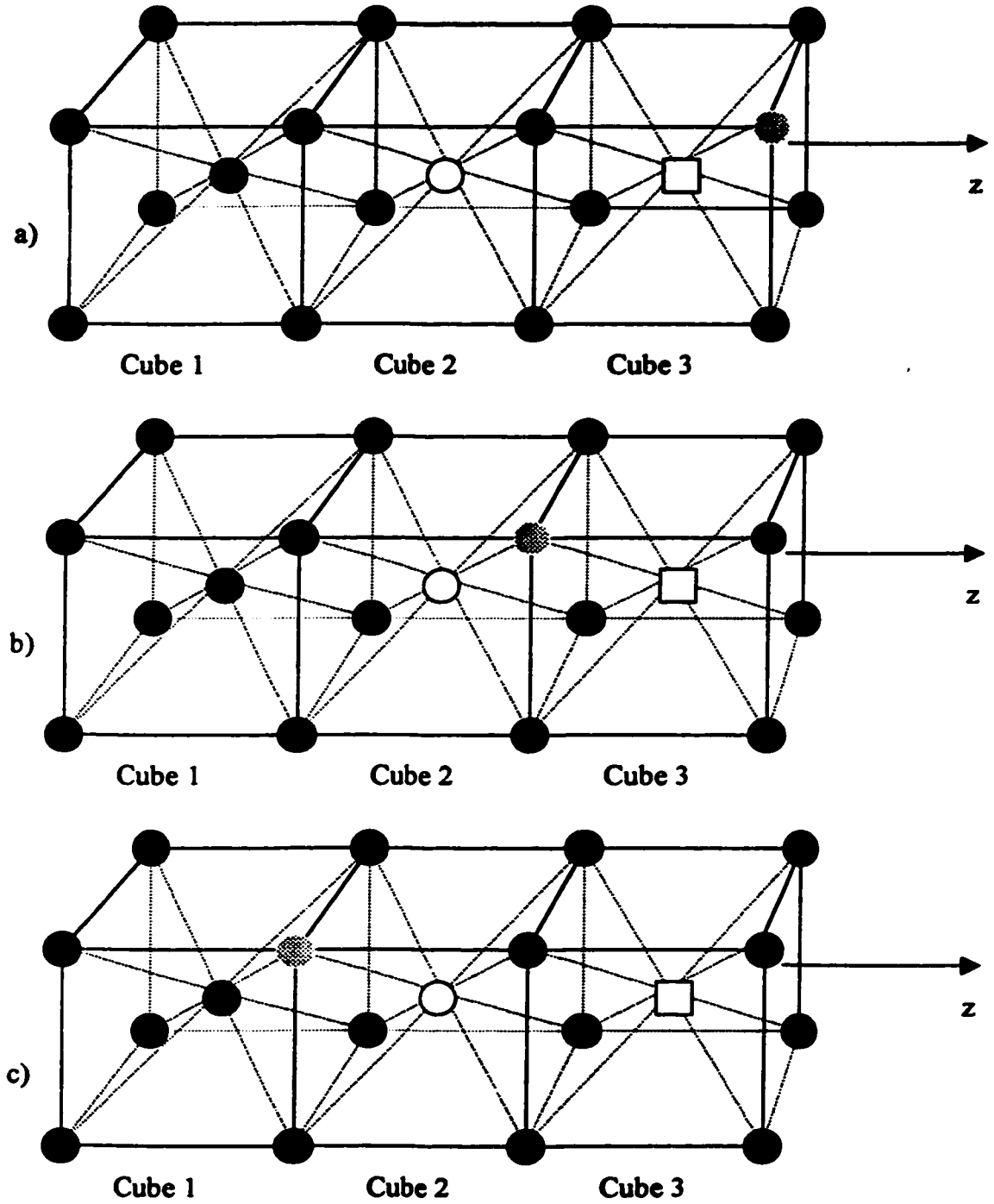

Fig. 5.6: Possible lattice configurations: a) Mn^{2+} ion surrounded by 8 Cl^- ions, b) Mn^{2+} ion surrounded by 7 Cl^- ions and one I^- ion on the side closest to vacancy, c) Mn^{2+} ion surrounded by 7 Cl^- and one I^- ion on the side farthest from vacancy.

The SM will now be applied to the situation as illustrated in Fig. 5.6a), where the assumption has been made that the Mn^{2+} ion is surrounded only by Cl^- ions as ligands.

5.4.1 a) $Cl^- = 8$, $I^- = 0$

A 2 dimensional representation of the lattice distortions due to charge compensation is given in Fig. 5.7. Because of the symmetry of the crystal the perspective shown in Fig. 5.7 can be taken as directly head on looking into the crystal, or directly overhead looking down into the crystal.

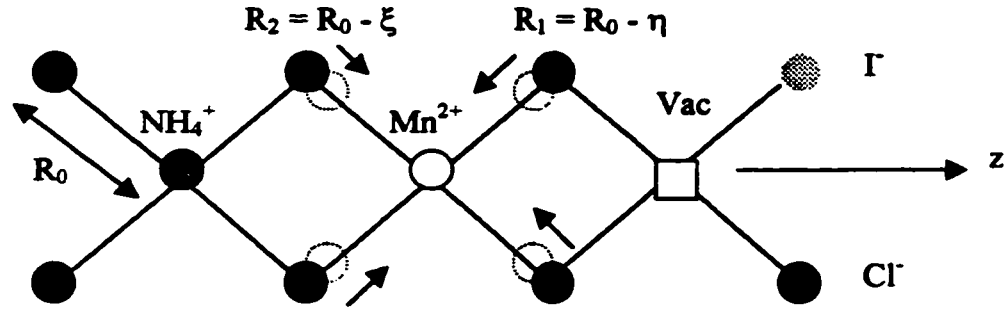

Fig. 5.7: A two-dimensional representation of the lattice distortion due to charge compensation for the BCC structure assuming that the Mn^{2+} ion is surrounded only by Cl^- ions. The angle between the ligands in this structure is 70.36 degrees. ξ and η are the distortion parameters, modifying the bond length from R_0 to R_2 and R_1 respectively. The cation sites illustrated are actually situated below the plane of the paper.

Due to the difference in cationic charges, the assumption is made that in order to maintain electrical neutrality, the next nearest cation site is vacant [Rubio and Cory, 1978, Oseguera *et al.*, 1980]. The resulting effect of the cationic substitution, and the next nearest cation site vacancy, will be to produce local site distortions about the impurity Mn^{2+} ion, changing the bond lengths.

In the BCC structure there are 8 ligands oriented about the central cation. These ligands will not be equally displaced by the vacancy at the next nearest cation site. The distortion induced by the Mn^{2+}ion causes the ligand distances to vary from that of the undisturbed lattice. The anions situated further away from the vacancy site will be less displaced from their initial positions. This is due to the NH_4^+ cation exerting an attractive force on these anions. However, this is not the case for the anions situated closer to the vacancy site, as they have a much smaller force exerted upon them from that side. The z-axis is taken along the direction of the vector drawn from the impurity cation to the vacancy site. Only the nearest neighbor interactions are taken into account here, as contributions from more distant ions are negligible [Newman, 1971].

Accordingly, the distances R_1 and R_2 as shown in Fig. 5.7 can now be estimated using the results published by Rubio and Cory (1978), and those of Oseguera *et al.* (1980). They applied the charge –compensation stratagem to several different alkali-halide crystals doped with Mn^{2+}. The results obtained by them are listed in Table 5.2.

Table 5.2: The alkali chloride crystal bond distances and distortion parameters.

Host	R_0 (Å)	η(Å)	ξ(Å)	R_1/R_2
LiCl	2.5648	0.0993	0.0623	0.9852
NaCl	2.8201	0.1585	0.0862	0.9735
KCl	3.1465	0.2293	0.0836	0.9524
RbCl	3.2740	0.2548	0.0737	0.9434

The values of the distortion parameters η and ξ determining R_1 and R_2: $R_1 = R_0 - \eta$, $R_2 = R_0 - \xi$, were estimated by Mott and Littleton (1938), and by Reitz and Gammel (1951). The method they developed is for calculating the polarisation around any lattice site in a polar crystal containing an excess of charge, and to obtain the *work* required to form vacancies (of either polarity) in alkali-halide crystals. A plot of η versus R_0 from the values given in Table 5.2 is given in Fig. 5.8. A plot of R_1/R_2 versus R_0 is given in Fig. 5.9. From these graphs the distortion parameters for the assumed BCC structure of $NH_4Cl_{0.9}I_{0.1}$ will here be estimated.

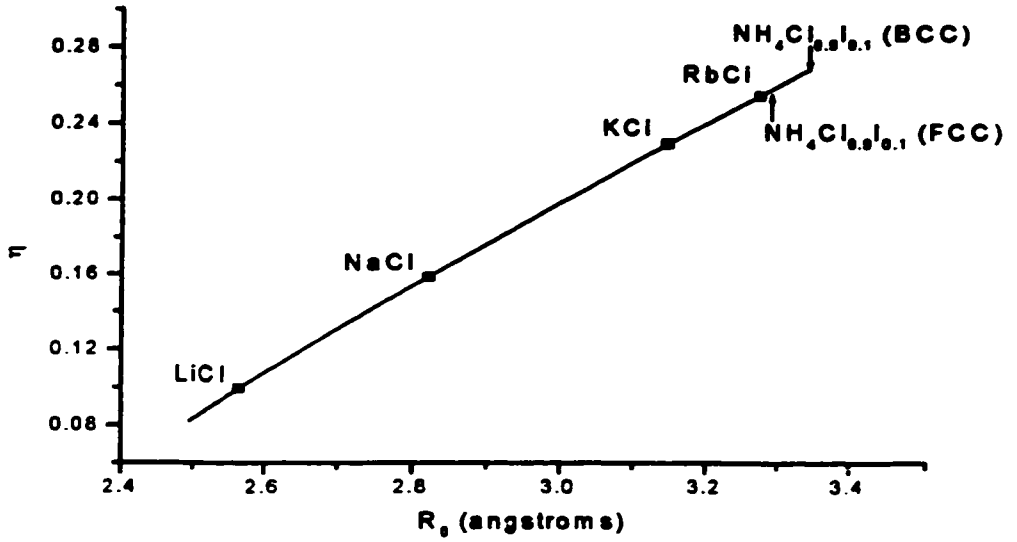

Fig. 5.8: A graph of the distortion parameter η versus the bond distance R_0 for the alkali chlorides.

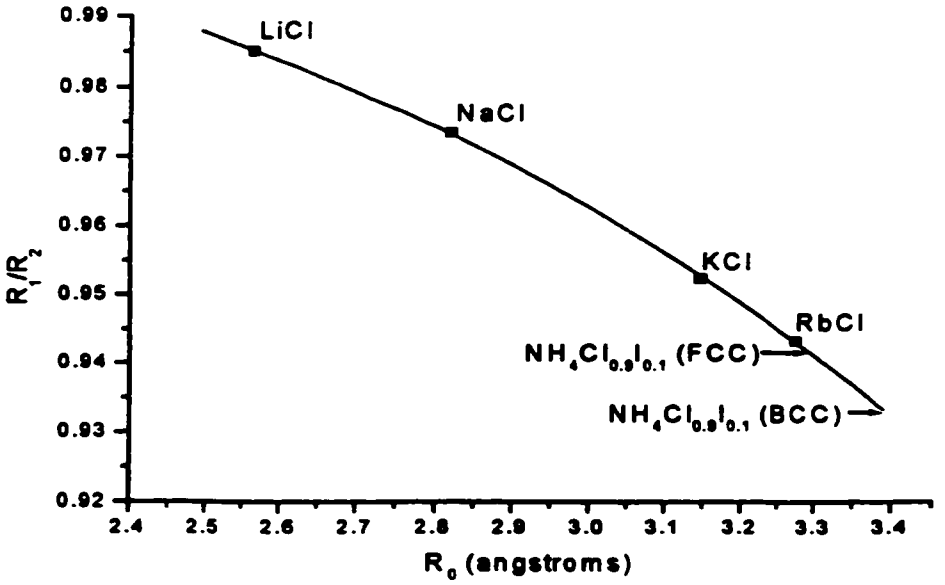

Fig. 5.9: A plot of the ratio of the distorted bond distances R_1 and R_2 versus R_0.

The bond distance R_0 for $NH_4Cl_{0.9}I_{0.1}$ was determined to be 3.39 Å, and from Fig. 5.8 the distortion parameter η was estimated to be 0.27 Å resulting in a value for R_1

$$R_1 = 3.355 - 0.27 = 3.12\,\text{Å} \qquad [5.24]$$

The radius ratio R_1/R_2, from Fig 5.9 was estimated to be 0.9315, so that

$$R_2 = (1/0.9315)3.12 = 3.35\,\text{Å} \qquad [5.25]$$

Table 5.3 lists the necessary data required to apply the SM to $NH_4Cl_{0.9}I_{0.1}$ with assumed BCC structure.

Table 5.3: The required data necessary to apply the SM to Mn^{2+} in $NH_4Cl_{0.9}I_{0.1}$. The angle, θ_z, is the angle that the impurity-ion-ligand makes with the z-axis. The SHPs b_2^0 and b_4^0 were determined experimentally.

b_2^0 (cm^{-1})	b_4^0 (cm^{-1})	R_{0BCC} (Å)	η (Å)	R_1 (Å)	R_2 (Å)	R_1/R_2	θ_z (deg)
0.15257	0.000435	3.39	0.27	3.12	3.35	0.9315	35.18

The SHPs b_2^0 and b_4^0 can now be analyzed using the SM. In Fig. 5.7, exhibiting a 2-dimensional configuration of the Cl^- ligands surrounding the Mn^{2+} ion, the z-axis is taken along the impurity-vacancy direction, which is also the direction of axial symmetry of the crystal. The number of nearest ligands at distance R_1 is 4, and the number of ligands at distance R_2 is also 4. In this case, an estimation of the angles between the

impurity-ligand bond and the z-axis gives $\theta_1 \approx \theta_2 \approx 35.18°$. Using Eqs. [5.4] and [5.5] one can express,

$$b_2^0 = K_2^0 \bar{b}_2(R_1) + K_2^0 \bar{b}_2(R_2) \qquad [5.26]$$

$$\bar{b}_2(R_2) = \bar{b}_2(R_1)(R_1/R_2)^{t_2} \qquad [5.27]$$

Substituting now the values listed in Table 5.3, the intrinsic parameter $\bar{b}_2(R_1)$ is estimated following the definition of the coordination factor K_2^0 given by Eq. [5.2].

$$0.15257 = 4/2(3\cos^2(35.18) - 1)\ \bar{b}_2(R_1) + 4/2(3\cos^2(35.18) - 1)\ \bar{b}_2(R_2) \qquad [5.28]$$

which results in

$$0.15257\ cm^{-1} = 2\ \bar{b}_2(R_1) + 2\ \bar{b}_2(R_2) \qquad [5.29]$$

$$\bar{b}_2(R_1) = 0.047\ cm^{-1} \qquad [5.30]$$

Now using Eq. [5.3] for K_4^0, the intrinsic parameter $\bar{b}_4(R_1)$ may be evaluated in a similar fashion.

$$0.000435 = 4/8(35\cos^4(35.18) - 30\cos^2(35.18) + 3)\bar{b}_4(R_1) + 4/8(35\cos^4(35.18) - 30\cos^2(35.18) + 3)\ \bar{b}_4(R_2) \qquad [5.31]$$

resulting in

$$\bar{b}_4(R_1) = -0.0002\ cm^{-1} \qquad [5.32]$$

where Eq. [5.27] has been rewritten as

$$\bar{b}_4(R_2) = \bar{b}_4(R_1)(R_1/R_2)^{t_4},\ t_4 = 7 \pm 1 \qquad [5.33]$$

5.4.1 b) $Cl^- = 7$, $I^- = 1$ (on vacancy side)

The SM will now be applied to the situation as illustrated in Fig. 5.6b), where the assumption has been made that the Mn^{2+} ion is now surrounded by 7 Cl^- ions, and one I^- ion as ligands. In this scenario the iodine anion is assumed to be at a site on the same side as the cationic vacancy relative to the Mn^{2+} cation. Therefore there will be two different bond distances "R_1" on the vacancy side, three of them due to the Cl^- ions and one due to the I^- ion. This is illustrated in Fig. 5.10.

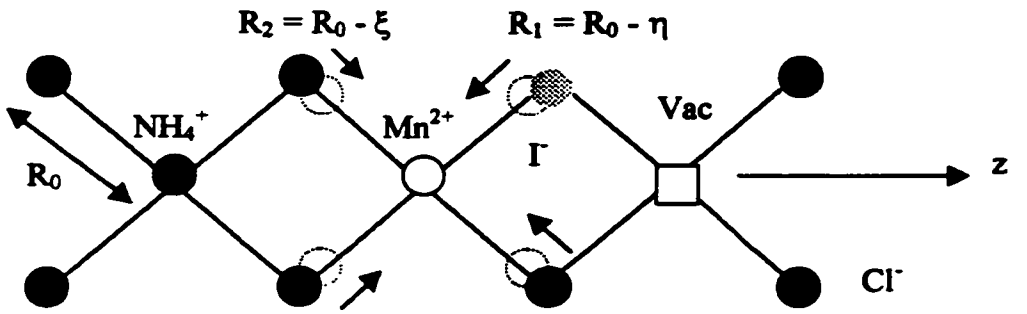

Fig. 5.10: A two-dimensional representation of the lattice distortion for BCC structure assuming that the Mn^{2+} ion is surrounded by 4 Cl^- ions at distance R_2, 3 Cl^- ions at distance R_1, and 1 I^- ion at distance R_1 .

In this case, the position of the I^- cannot be ignored. Although it has the same electronic charge as the Cl^- ion, its radius is different, 2.20 Å as compared to 1.81 Å for Cl^-. This difference in radius will affect the bond length. Thus the I^- ion's contribution to the intrinsic parameter for Mn^{2+}-Cl^- must be taken into account. The strategy adopted in this

work is to assume that the I^- ion is at a distance proportional to the atomic masses of chlorine and iodine ions

$$R_{II} = R_{ICl} - (M_{Cl}/M_I) = 3.12 - (35/127) = 2.84\,\text{Å} \qquad [5.34]$$

and that its contribution will be included in the calculation for the intrinsic parameter $\bar{b}_2(R_1)$. Recalling the result obtained for the intrinsic parameter $\bar{b}_2(R_1) = 0.047\ cm^{-1}$, in Eq. [5.30], and $\bar{b}_4(R_1) = -0.0002$, a comparison can be made with the results obtained here.

In order to relate the intrinsic parameter $\bar{b}_2(R_1)$ as a function of R_1 only, the following relations are used in the calculations as well as Eq. [5.27], and Eq. [5.33]

$$\bar{b}_2(R_{II}) = \bar{b}_2(R_{ICl})(R_{ICl}/R_{II})^7 \qquad [5.35a]$$

$$\bar{b}_4(R_{II}) = \bar{b}_4(R_{ICl})(R_{ICl}/R_{II})^7 \qquad [5.35b]$$

the following determinations are made,

$$0.15257\ cm^{-1} = 3/2(3\cos^2(35.18) - 1)\ \bar{b}_2(R_1) + 1/2(3\cos^2(35.18) - 1)\ \bar{b}_2(R_{II}) + 4/2(3\cos^2(35.18) - 1)\ \bar{b}_2(R_2) \qquad [5.36]$$

resulting in,

$$0.15257\ cm^{-1} = 3/2\ \bar{b}_2(R_1) + 1/2\ \bar{b}_2(R_{II}) + 2\ \bar{b}_2(R_2) \qquad [5.37]$$

which yields,

$$\bar{b}_2(R_1) = 0.041\ cm^{-1} \qquad [5.38]$$

and in a similar manner the intrinsic parameter,

$$\bar{b}_4(R_1) = -0.000334\ cm^{-1} \qquad [5.39]$$

5.4.1 c) $Cl^- = 7$, $I^- = 1$ (opposite the vacancy side)

In the final case investigated here the SM will now be applied to the situation as illustrated in Fig. 5.6c), where the assumption has been made that the Mn^{2+} ion is again surrounded by 7 Cl^- ions, and one I^- ion as ligands. However for this situation the iodine anion is assumed to be at a site on the opposite side of the cationic vacancy relative to the Mn^{2+} cation. Therefore, now there will be two different bond distances "R_2" on the vacancy side, three of them due to the Cl^- ions and one due to the I^- ion. This is illustrated in Fig. 5.11.

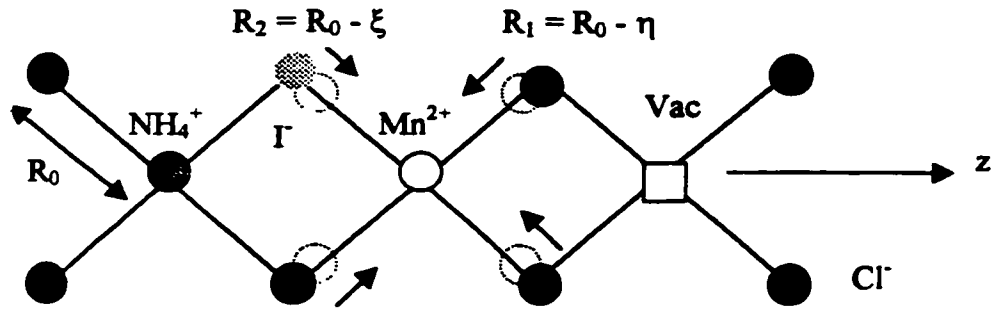

Fig. 5.11: A two-dimensional representation of the lattice distortion for BCC structure assuming that the Mn^{2+} ion is surrounded by 3 Cl^- ions and 1 I^- ion at distance R_2, and 4 Cl^- ions at distance R_1.

In Fig. 5.11, the distance of the iodine ion from the Mn^{2+} cation should now be greater than was the case in the previous section. This stems from the fact that there is now a NH_4^+ cation "attracting" the mixed ligands towards it, and compensating, to a degree, the

"attractive" force of the Mn^{2+} cation on the opposing side of the unit cell. A calculation for R_{2I} gives,

$$R_{2I} = R_{2Cl} - (M_{Cl}/M_I) = 3.35 - (35/127) = 3.07\,\text{Å} \qquad [5.40]$$

The calculations for the intrinsic parameters $\bar{b}_2(R_1)$ and $\bar{b}_4(R_1)$, following the same method as in the previous sections yielded the following results:

For the intrinsic parameter $\bar{b}_2(R_1)$,

$$0.15257\ \text{cm}^{-1} = 4/2(3\cos^2(35.18) - 1)\ \bar{b}_2(R_1) + 1/2(3\cos^2(35.18) - 1)\ \bar{b}_2(R_{2I}) + 3/2(3\cos^2(35.18) - 1)\ \bar{b}_2(R_2) \qquad [5.41]$$

leading to

$$\bar{b}_2(R_1) = 0.0398\ \text{cm}^{-1} \qquad [5.42]$$

and for the intrinsic parameter $\bar{b}_4(R_1)$,

$$\bar{b}_4(R_1) = -0.000319\ \text{cm}^{-1} \qquad [5.43]$$

5.5 Mixed Ammonium Chloride-Iodide Host Crystal: NH_4I Structure

For the sake of intellectual curiosity, and also as a means for comparison with established results for Mn^{2+} with Cl^- ligands, the SM will now be applied to the situation where the $NH_4Cl_{0.9}I_{0.1}$ crystal has the FCC structure of NH_4I. In this type of structure the central cation is surrounded by 6 anions. A 3-dimensional representation of a FCC lattice is given in Fig. 5.12. Unlike the case for BCC structure, four possible I^- ligand orientations shall be investigated for the FCC structure.

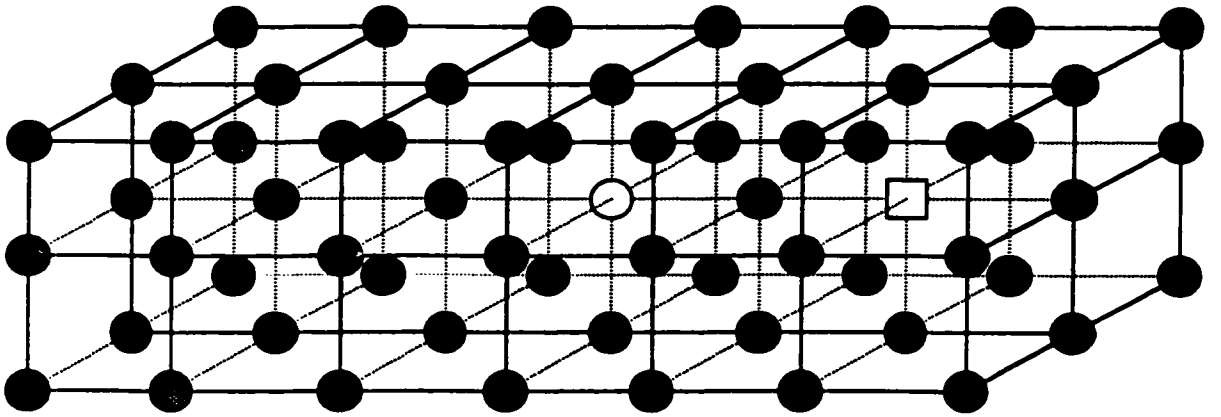

Fig. 5.12: A 3-dimensional representation of a FCC lattice. The Mn^{2+} cation is shown as the white circle, and the charge compensating vacancy as the white square.

The distortion parameter η and the radius ratio R_1/R_2 will be estimated in the same manner as for the BCC structure of NH_4Cl. The calculations are not repeated here but are summarised in Table 5.4.

Table 5.4: The required data necessary to apply the SM to Mn^{2+} in $NH_4Cl_{0.9}I_{0.1}$ for the assumed FCC structure of NH_4I.

$b_2^0(cm^{-1})$	$b_4^0(cm^{-1})$	$R_{0FCC}(\mathring{A})$	$\eta(\mathring{A})$	$R_1(\mathring{A})$	$R_2(\mathring{A})$	R_1/R_2	θ_1 (deg) θ_2
0.15257	0.000435	3.28	0.256	3.024	3.20	0.943	0 90

5.5.1 a) $Cl^- = 6$, $I^- = 0$

A 2 dimensional representation of the lattice distortions due to charge compensation is given in Fig. 5.13. Again due to the symmetry of the crystal the perspective shown in Fig. 5.13 can be taken as directly head on looking into the crystal, or directly overhead looking down into the crystal.

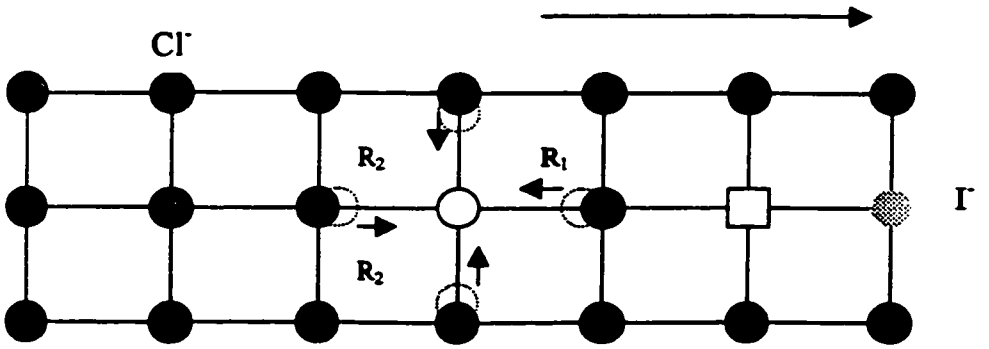

Fig. 5.13: A two-dimensional representation of the lattice distortion for FCC structure assuming that the Mn^{2+} ion is surrounded by 5 Cl^- ions at distance R_2 (1 ion is coming out of the page, and 1 is going into the page), and 1 Cl^- ion at distance R_1.

Using the data obtained and tabulated in Table 5.4, although not all the steps are included in this section, the same approach will be applied to the FCC structure as was the case for the BCC structure, and the result thus obtained for the intrinsic parameters and $\bar{b}_4$ are respectively,

$$0.15257 = 1/2(3\cos^2(0) - 1)\ \bar{b}_2(R_1) + 4/2(3\cos^2(90) - 1)\ \bar{b}_2(R_2) + 1/2(3\cos^2(0) - 1)\ \bar{b}_2(R_2) \quad [5.44]$$

resulting in

$$\bar{b}_2(R_1) = 0.458\ \text{cm}^{-1} \quad [5.45]$$

and for $\bar{b}_4$

$$0.000435 = 1/8(35\cos^4(0) - 30\cos^2(0) + 3)\bar{b}_4(R_1) + 4/8(35\cos^4(90) - 30\cos^2(90) + 3)\bar{b}_4(R_2) + 1/8(35\cos^4(0) - 30\cos^2(0) + 3)\bar{b}_4(R_2) \quad [5.46]$$

leading to the result

$$\bar{b}_4(R_1) = 0.00016\ \text{cm}^{-1} \quad [5.47]$$

5.5.1 b) $Cl^- = 5$, $I^- = 1$ (on side nearest to vacancy)

A 2 dimensional representation of the lattice distortions due to charge compensation is given in Fig. 5.14 with this time the iodine ion at a anion site which is on the side of the vacancy. Again, due to the symmetry of the crystal the perspective shown in Fig. 5.14 can be taken as directly head on looking into the crystal, or directly overhead looking down into the crystal.

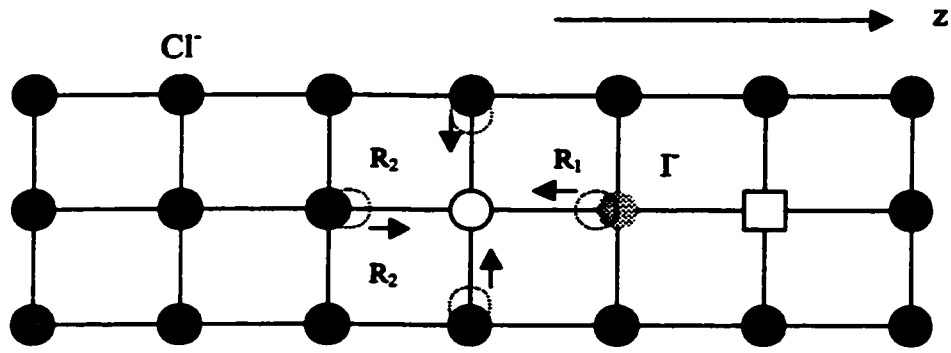

Fig. 5.14: A two-dimensional representation of the lattice distortion for FCC structure assuming that the Mn^{2+} ion is surrounded by 5 Cl^- ions at distance R_2 (1 ion is coming out of the page, and 1 is going into the page), and 1 I^- ion at distance R_{II}.

It is again necessary to calculate the bond distance due to the iodine ion. Making use once more of Eq. [5.34] with the appropriate values one obtains for R_I,

$$R_{II} = R_{ICl} - (M_{Cl}/M_I) = 3.024 - (35/127) = 2.75\,\text{Å} \qquad [5.48]$$

Resulting in,

$$\bar{b}_2(R_I) = 0.537\ \text{cm}^{-1} \qquad [5.49]$$

and $$\bar{b}_4(R_I) = 0.000121\ \text{cm}^{-1} \qquad [5.50]$$

5.5.1 c) Cl^- = 5, I^- = 1 (on side farthest from vacancy)

In this situation the iodine ion is located at an anion site on the side directly opposite the cationic vacancy. This is shown in Fig. 5.15. Once again, due to the

symmetry of the crystal, the perspective shown in Fig. 5.15 can be taken as directly head on looking into the crystal, or directly overhead looking down into the crystal.

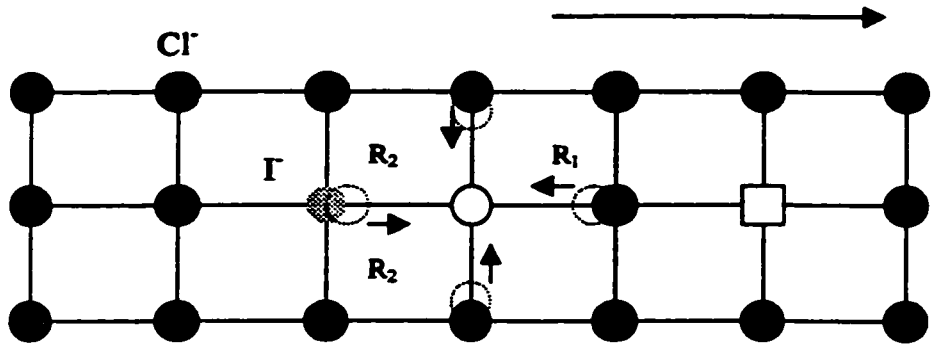

Fig. 5.15: A two-dimensional representation of the lattice distortion for FCC structure assuming that the Mn^{2+} ion is surrounded by 4 Cl^- ions at distance R_2 (1 ion is coming out of the page, and 1 is going into the page), 1 Cl^- ion at distance R_1, and the I^- ion at distance R_{2I}.

It is again necessary to calculate the bond distance due to the iodine ion. Making use once more of Eq. [5.34] with the appropriate values one obtains for R_{2I},

$$R_{2I} = R_{2Cl} - (M_{Cl}/M_I) = 3.20 - (35/127) = 2.93 \text{ Å} \qquad [5.51]$$

Resulting in,

$$\bar{b}_2(R_1) = 0.100 \text{ cm}^{-1} \qquad [5.52]$$

and $$\bar{b}_4(R_1) = 0.000113 \text{ cm}^{-1} \qquad [5.53]$$

5.5.1 d) $Cl^- = 5$, $I^- = 1$ (with I^- off the z-axis)

In this situation the iodine ion is located at an anion site, with bond length R_{2I}, not on the z-axis of the crystal. This is shown in Fig. 5.16.

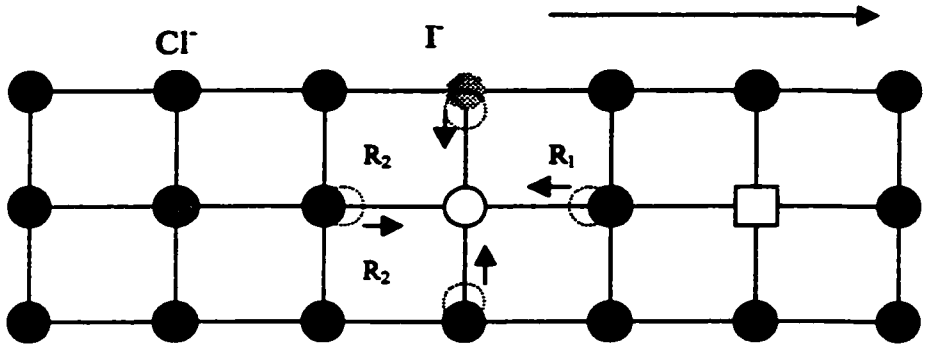

Fig. 5.16: A two-dimensional representation of the lattice distortion for FCC structure, assuming that the Mn^{2+} ion is surrounded by 4 Cl^- ions at distance R_2 (1 ion is coming out of the page, and 1 is going into the page), 1 Cl^- ion at distance R_1, and the I^- ion at distance R_{2I} off the z-axis of the crystal.

This ligand arrangement results in the following values for the intrinsic parameters,

$$\bar{b}_2(R_1) = -0.600 \text{ cm}^{-1} \qquad [5.54]$$

and $$\bar{b}_4(R_1) = 0.000152 \text{ cm}^{-1} \qquad [5.55]$$

5.6 Summary of the Results Obtained

In this chapter the SM was applied to the mixed ammonium chloride-iodide host crystal, first for the most "probable" situation where the lattice is assumed to have the BCC structure of NH_4Cl and with three possible lattice-ligand orientations. Secondly, as a matter of intellectual curiosity, the SM model was applied to the "not-so-probable" situation that the ammonium chloride-iodide crystal has the FCC structure of NH_4I, and with four possible lattice ligand orientations.

A comparison of the intrinsic parameters, $\bar{b}_2$ and $\bar{b}_4$ obtained in this work for BCC structure, show a good consistency with the values published by Heming and Lehmann (1987), and to those of Jain and Lehmann (1990). It is of interest to note that the inclusion of the iodide ion in the calculations for the intrinsic parameter, does not greatly affect the value of $\bar{b}_2$ when it is "moved" from one anion site to another for the BCC structure. This is most likely due to the fact that the iodide ion is "outnumbered" three-to-one on any given side of the BCC lattice, and it's contribution or lack thereof, to the overall magnitude of the intrinsic parameter $\bar{b}_2$ is negligible. However, for the case of the FCC structure, this "averaging" no longer applies as the iodide ion is "isolated" at any given anion site relative to the Mn^{2+} ion, and therefore it's effect on the evaluation of $\bar{b}_2$ can not be taken lightly or ignored. The results obtained are given in Table 5.5. Included are the intrinsic parameters as calculated for NH_4Cl and NH_4I based on the SHPs b_2^0 and b_4^0 of Forman and van Wyk (1966), and Chand and Upreti (1983) respectively. The calculations carried out for the intrinsic parameters of NH_4Cl and NH_4I are given in Appendix A.

Table 5.5: A summary of the results obtained for the SM as applied to the mixed ammonium chloride-iodide crystal. The results evaluated for ammonium chloride, and ammonium iodide are also included for comparison.

Host	$NH_4Cl_{0.9}I_{0.1}$ (BCC)	$NH_4Cl_{0.9}I_{0.1}$ (FCC)	NH_4Cl (BCC)	NH_4I (FCC)
$b_2^0(cm^{-1})$	0.15257	0.15257	0.14974	0.15043
$b_4^0(cm^{-1})$	0.000435	0.000435	0.00021	0.00056
$\bar{b}_2(cm^{-1})$	a) 0.047 b) 0.041 c) 0.398	a) 0.458 b) 0.537 c) 0.100 d) –0.6	0.045	0.633
$\bar{b}_4(cm^{-1})$	a) -0.0002 b) –0.000334 c) –0.000319	a) 0.00016 b) 0.000121 c) 0.000113 d) 0.000152	-0.000181	0.000193

Chapter 6

Conclusions

The EPR X-band and Q-band study of Mn^{2+} in $NH_4Cl_{0.9}I_{0.1}$ at 295 K, 120 K, and 77 K has been presented here. The spin-Hamiltonian parameters describing the EPR spectra of Mn^{2+} in $NH_4Cl_{0.9}I_{0.1}$ obtained by fitting resonance line positions for several crystal angles relative to a magnetic field, closely resemble those of NH_4Cl and NH_4I in spite of their different crystal structures. The conclusion to be drawn from the resulting spin-Hamiltonian parameters is that they are consistent with the model of the Mn^{2+} ion entering substitutionally for a NH_4^+ ion at a cationic site in the crystal. The overall charge neutrality of the crystal being maintained by having a vacancy at the next nearest NH_4^+ lattice position, and the lattice distortions induced by the vacancies in the three crystals accounting for the similarities of the SHPs.

The spin-Hamiltonian parameters were then analyzed by using the superposition model. The superposition model was first applied to the "most probable" BCC lattice structure for $NH_4Cl_{0.9}I_{0.1}$, and then to the "least probable" FCC structure. From the resulting intrinsic parameters two conclusions may be drawn. First, the intrinsic parameters determined for $NH_4Cl_{0.9}I_{0.1}$ for the assumed BCC structure are consistent with those of other publications for Mn^{2+} with Cl^- ligands. However, similar calculations carried out for the FCC structure resulted in values for the intrinsic parameters inconsistent with published values for Mn^{2+} with Cl^- ligands. In order to verify the

validity of the methods employed for the $NH_4Cl_{0.9}I_{0.1}$ FCC calculations, the SM was applied to the FCC structure of NH_4I and the results were found to be consistent for Mn^{2+} with I^- ligands. Therefore, the second conclusion to be drawn from the SM calculations is that the results obtained for the intrinsic parameters show that $NH_4Cl_{0.9}I_{0.1}$ has the BCC lattice structure of NH_4Cl.

For future work it would be interesting to study crystals with varying concentrations of chloride and iodide, especially the $NH_4Cl_{0.5}I_{0.5}$: Mn^{2+} crystal, and to study the spectra of these crystals in order to determine which structure each would have, BCC or FCC. It would also be of interest to carry out measurements at higher microwave frequencies, as the resulting splitting of energy levels are easier to interpret than for low microwave frequencies where degeneracies of energy levels at low fields lead to spectra that are difficult to analyze.

Appendix A

The SM calculations for the NH_4I and NH_4Cl host crystals are given here.

A.1 Ammonium Iodide

To be able to apply the SM, one needs to determine the bond length R_0 for the NH_4I crystal, which has the FCC lattice structure. Using Eq. [5.16], the value of 0.65 is obtained for ρ in the NH_4I crystal, where the ionic radii of the NH_4^+ cation and the I^- anion are $r_+ = 1.43\,\text{Å}$ and $r_- = 2.20\,\text{Å}$ respectively. With this value, one can find $F(\rho)$ from Eq. [5.17], which yields a value of 1.0056, and then by applying Eq. [5.15] one may calculate R_0. The value obtained using this method is $3.65\,\text{Å}$. The next step is to re-evaluate this bond length upon the substitution of the Mn^{2+} cation in place of the NH_4^+ cation. Due to the differences in the cationic charges, the assumption is made that in order to maintain electrical neutrality, the next nearest cation site is vacant [Oseguera *et al.*, 1980, Rubio and Cory, 1978]. This is illustrated in Fig. A.1.

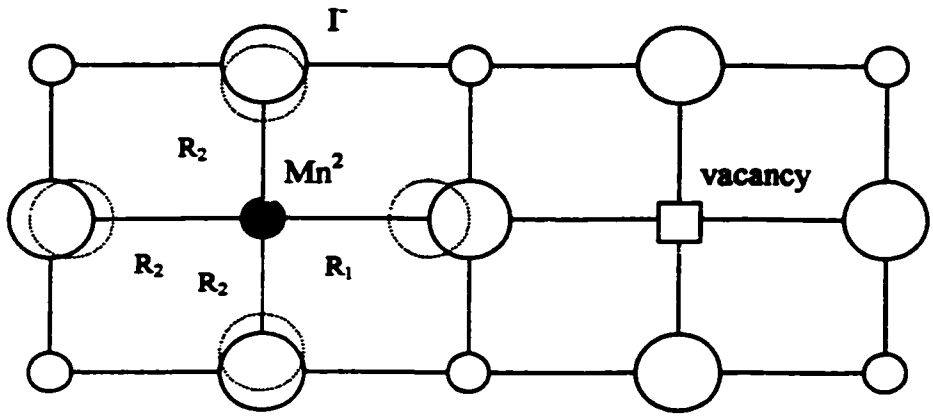

Fig. A.1: The NH_4I FCC lattice structure with distortions due to charge compensation by having nearest neighbor cation site vacant.

As was the case for the alkali-chlorides, the values for R_1 and R_2 were obtained from the work done by Oseguera *et al.*, (1980). The determination of the values of the distortion parameters, η and ξ, were made by Mott and Littleton, (1938), and by Reitz and Gammel, (1951). A plot of η versus R_0 for the alkali-iodides for the values obtained by Oseguera *et al.*, (1980) given in Fig. A.2, and was exploited in determining the value of η for the NH_4I crystal.

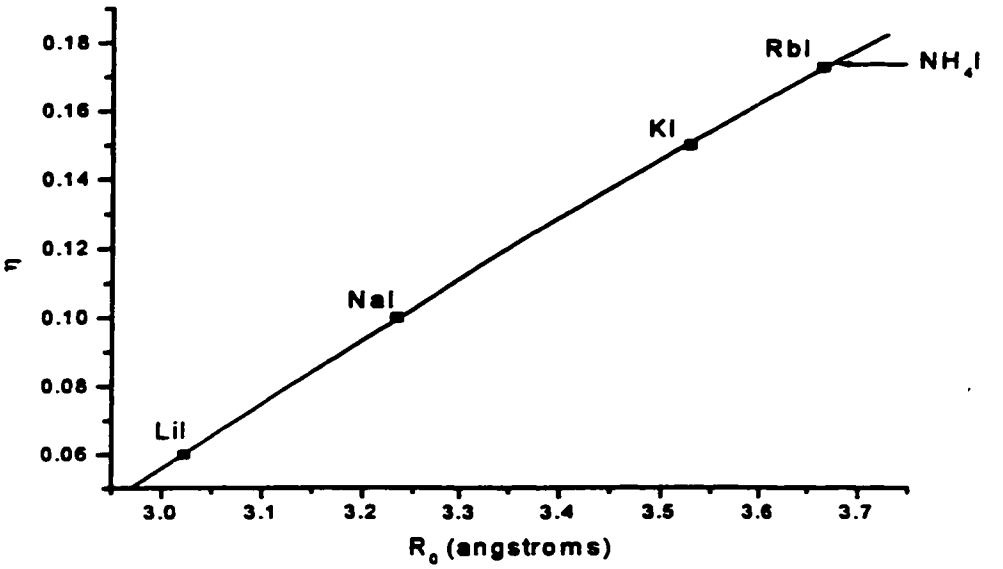

Fig. A.2: A plot of the distortion parameter η versus the intrinsic bond distance R_0 for several alkali iodide crystals.

For the NH_4I crystal, which has $R_0 = 3.65$ Å the value obtained for η is 0.1669 Å, so that

$$R_1 = (3.65 - 0.16996) = 3.48 \text{ Å} \qquad [A.1]$$

By again making use of the ratios R_1/R_2 of Rubio and Cory, (1978), it was found that they decrease for increasing R_0 in the alkali iodides. This removes the need to calculate the second distortion parameter ξ explicitly. A plot of R_1/R_2 versus R_0 for the alkali iodides of Rubio and Cory, (1978) is given in Fig. A.3.

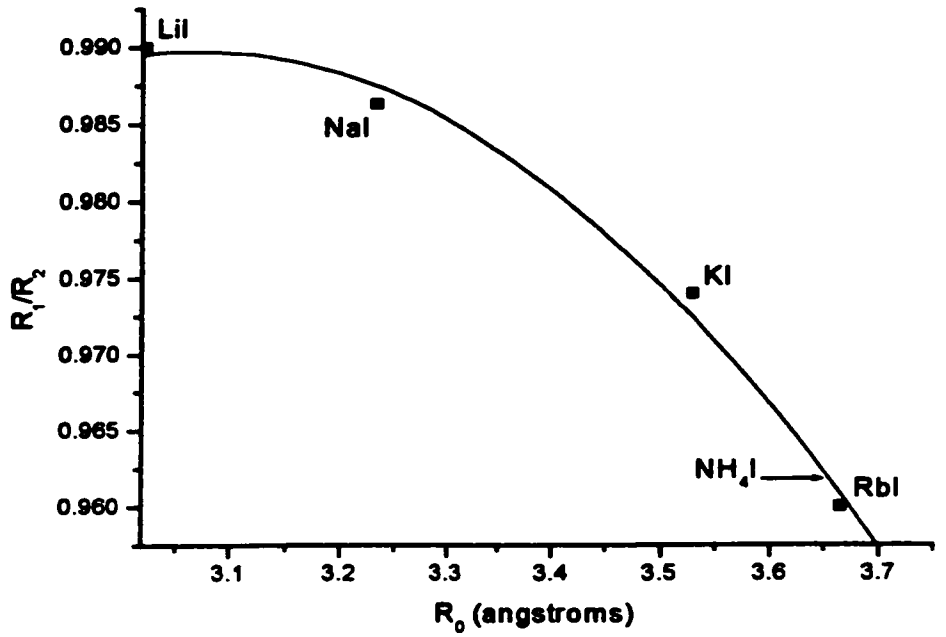

Fig. A.3: A plot of the ratio of the distorted bond distances versus the intrinsic bond distance for the alkali iodides.

From Fig. A.3 it was found that the ratio R_1/R_2 for the NH_4I bond distance of 3.65 Å is 0.962, which yields a value for R_2 of 3.62 Å, which would mean that the value of ξ is 0.03 Å. All the necessary ingredients have now been acquired in order to apply the SM to the NH_4I Mn^{2+} doped crystal.

In Fig. A.1, the z-axis is taken along the impurity-vacancy direction. The number of nearest neighbor ions at distance R_1 is one, and there are 5 next nearest neighbors at the distance R_2. Two of these impurity-ligand bonds lay in the z-direction, while the other four are perpendicular to this direction, so that $\theta_0 = 0°$, $\theta_1 = 90°$. The reported (ZFS)

parameter for the ammonium iodide crystal is 0.15043 cm^{-1} [Chand and Upreti, 1983]. Therefore in using this value the following results are obtained,

$$0.15043 = 1/2(3\cos^2(0)-1)\bar{b}_2(R_1)+1/2(3\cos^2(0)-1)\bar{b}_2(R_2)+ 4/2(3\cos^2(90)-1)\bar{b}_2(R_2) \quad [A.2]$$

$$0.15043 = \bar{b}_2(R_1)-\bar{b}_2(R_2) \quad [A.3]$$

$$0.15043 = \bar{b}_2(R_1)-\bar{b}_2(R_1)(0.962)^7 \quad [A.4]$$

$$0.15043 = 0.2375\,\bar{b}_2(R_1) \quad [A.5]$$

$$\bar{b}_2(R_1) = 0.633\ cm^{-1} \quad [A.6]$$

and for $\bar{b}_4(R_1)$

$$0.00056 = 1/8(35\cos^4(0)-30\cos^2(0)+3)\bar{b}_4(R_1)+ 1/8(35\cos^4(0)-30\cos^2(0)+3)\bar{b}_4(R_2)+ 4/8(35\cos^4(90)-30\cos^2(90)+3)\bar{b}_4(R_2) \quad [A.7]$$

which results in

$$\bar{b}_4(R_1) = 0.000193\ cm^{-1} \quad [A.8]$$

A.2 Ammonium Chloride

From Fig. 5.8, η was found to be 0.2668 for R_0 =3.335 Å. This value for R_0 was determined using the method outlined in Sec. 5.2. From these values R_1 was found to be equal to 3.0682 Å. The determination of ξ will be bypassed again exploiting the relationship between the ratio R_1/R_2 and R_0. This is given in a plot in

Fig. 5.9, and results in a ratio of 0.9369 so that $R_2 = 3.275$ Å.

$$0.14974 = 4/2(3\cos^2(35.18)-1)\bar{b}_2(R_1)+4/2(3\cos^2(35.18)-1)\bar{b}_2(R_2) \quad [A.9]$$

$$0.14974 = 2\bar{b}_2(R_1)+2\bar{b}_2(R_2) \quad [A.10]$$

$$0.14974 = 3.26\ \bar{b}_2(R_1)$$

$$\bar{b}_2(R_1) = 0.045\ cm^{-1} \quad [A.11]$$

and

$$0.00021 = 4/8(35\cos^4(35.18) - 30\cos^2(35.18) + 3)\bar{b}_4(R_1) + \quad [A.12]$$

$$4/8(35\cos^4(35.18) - 30\cos^2(35.18) + 3)\bar{b}_4(R_2)$$

resulting in

$$\bar{b}_4(R_1) = -0.000181\ cm^{-1} \quad [A.13]$$

Appendix B

The derivation of a second-order perturbation for a non-degenerate level is presented here.

The spin-Hamiltonian that most generally describes cases in practice is given by [Misra, 1985]

$$\mathcal{H} = \mathcal{H}_f + \mathcal{H}_{hf} \qquad [B.1]$$

where the fine structure term is given by

$$\mathcal{H}_f = \mu_B g(B_x S_x + B_y S_y + B_z S_z) + B_2^0 O_2^0 + B_4^0 O_4^0 \qquad [B.2]$$

and the hyperfine structure term by

$$\mathcal{H}_{hf} = A(S_x I_x + S_y I_y + S_z I_z) \qquad [B.3]$$

We assume that the equation

$$\mathcal{H}^{(0)}{}_n \psi^{(0)}{}_n = E^{(0)}{}_n \psi^{(0)}{}_n \qquad [B.4]$$

has been solved for some n [Byron and Fuller, 1992] and we are interested in finding the solution to the original problem

$$\mathcal{H}\psi_n(\lambda) = E_n(\lambda)\psi_n(\lambda) \qquad [B.5]$$

where it is assumed that the eigenstates $|\psi_n(\lambda)\rangle$, and the eigenenergies $E_n(\lambda)$ can be expanded in a power series of [Peleg *et al.*, 1998]

$$|\psi_n(\lambda)\rangle = |\psi^{(0)}{}_n\rangle + \lambda|\psi^{(1)}{}_n\rangle + \lambda^2|\psi^{(2)}{}_n\rangle + \ldots\ldots + \lambda^q|\psi^{(q)}{}_n\rangle = \sum_{q=0}^{\infty} \lambda^q|\psi^{(q)}{}_n\rangle \qquad [B.6]$$

$$E_n(\lambda) = E^{(0)}_n + \lambda E^{(1)}_n + \lambda^2 E^{(2)}_n + \ldots\ldots + \lambda^q E^{(q)}_n = \sum_{q=0}^{\infty} \lambda^q E^{(q)}_n \qquad [B.7]$$

Putting Eqs. [B.6] and [B.7] into Eq. [B.5] one obtains

$$(\mathcal{H}^{(0)} + \lambda \mathcal{H}^{(1)}) \sum_{q=0}^{\infty} \lambda^q |\psi^{(q)}_n\rangle = \sum_{p=0}^{\infty} \lambda^p E^{(p)}_n \sum_{q=0}^{\infty} \lambda^q |\psi^{(q)}_n\rangle \qquad [B.8]$$

or,

$$\sum_{q=0}^{\infty} \lambda^q \mathcal{H}^{(0)} |\psi^{(q)}_n\rangle + \sum_{q=0}^{\infty} \lambda^{q+1} \mathcal{H}^{(1)} |\psi^{(q)}_n\rangle = \sum_{p,q=0}^{\infty} \lambda^{p+q} E^{(p)}_n |\psi^{(q)}_n\rangle \qquad [B.9]$$

if we make the substitution p + q = s, and q = t, and by setting $|\psi^{(\alpha)}_n\rangle \equiv 0$ for all $\alpha = -1$, Eq. [B.9] can be rewritten in the form [Byron and Fuller, 1992]

$$\sum_{t=0}^{\infty} \lambda^t \mathcal{H}^{(0)} |\psi^{(t)}_n\rangle + \sum_{t=0}^{\infty} \lambda^t \mathcal{H}^{(1)} |\psi^{(t-1)}_n\rangle = \sum_{s=0}^{\infty} \sum_{t=0}^{s} \lambda^s E^{(s-t)}_n |\psi^{(t)}_n\rangle \qquad [B.10]$$

now, by equating the coefficients of successive powers of λ one obtains [Peleg *et al.*, 1998]

$$|\psi^{(t)}_n\rangle + \mathcal{H}^{(1)} |\psi^{(t-1)}_n\rangle = \sum_{t=0}^{s} E^{(t)}_n |\psi^{(s-t)}_n\rangle \qquad [B.11]$$

which can be written as,

$$[\mathcal{H}^{(0)} - E^{(0)}_n] |\psi^{(s)}_n\rangle = \sum_{t=1}^{s} E^{(t)}_n |\psi^{(s-t)}_n\rangle - \mathcal{H}^{(1)} |\psi^{(t-1)}_n\rangle \quad s = 0, 1, 2, \ldots. \qquad [B.12]$$

In Eq. [B.12] we have the eigenstates in terms of $|\psi^{(0)}_n\rangle$, $|\psi^{(1)}_n\rangle$, $|\psi^{(2)}_n\rangle$, $|\psi^{(s-1)}_n\rangle$, but the right hand side of the equation also contains $E^{(s)}_n$ which may cause some difficulty as $|\psi^{(s)}_n\rangle$ can not be found until $E^{(s)}_n$ is known [Kumar, 1962]. However, by taking the inner

product of both sides of Eq. [B.12] with $\langle\psi^{(0)}_n|$ the following result is obtained [Byron and Fuller, 1992],

$$\langle\psi^{(0)}_n|[\mathcal{H}^{(0)} - E^{(0)}_n]|\psi^{(s)}_n\rangle = \sum_{t=1}^{s} \langle\psi^{(0)}_n| E^{(t)}_n|\psi^{(s-t)}_n\rangle - \langle\psi^{(0)}_n| \mathcal{H}^{(1)}|\psi^{(t-1)}_n\rangle \quad [B.13]$$

it can be seen that the left hand side of Eq. [B.13] is equal to zero from Eq. [B.4] so that for s = 1, 2, 3...

$$E^{(s)}_n = \langle\psi^{(0)}_n| \mathcal{H}^{(1)}|\psi^{(s-1)}_n\rangle - \sum_{t=1}^{s-1} \langle\psi^{(0)}_n| E^{(t)}_n|\psi^{(s-t)}_n\rangle \quad [B.14]$$

So that $E^{(s)}_n$ is determined in terms of the $E^{(i)}_n$ and $E^{(ii)}_n$ which are of lower orders than s. In this manner, the set of equations implied by Eq. [B.14] can be solved by using the first (n – 1) equation providing the input for the nth equation. The first 4 equations of this group are [Byron and Fuller, 1992]

$$[\mathcal{H}^{(0)} - E^{(0)}_n]|\psi^{(0)}_n\rangle = 0 \quad [B.16]$$

$$[\mathcal{H}^{(0)} - E^{(0)}_n]|\psi^{(1)}_n\rangle = -[\mathcal{H}^{(1)} - E^{(1)}_n]|\psi^{(0)}_n\rangle \quad [B.17]$$

$$[\mathcal{H}^{(0)} - E^{(0)}_n]|\psi^{(2)}_n\rangle = -[\mathcal{H}^{(1)} - E^{(1)}_n]|\psi^{(1)}_n\rangle + E^{(2)}_n|\psi^{(0)}_n\rangle \quad [B.18]$$

$$[\mathcal{H}^{(0)} - E^{(0)}_n]|\psi^{(3)}_n\rangle = -[\mathcal{H}^{(1)} - E^{(1)}_n]|\psi^{(2)}_n\rangle + E^{(2)}_n|\psi^{(1)}_n\rangle + E^{(3)}_n|\psi^{(0)}_n\rangle \quad [B.19]$$

The first equation is just Eq. [B.4], and it provides the starting point for solving all the other equations order by order. Eq. [B.17] can give a solution for $|\psi^{(1)}_n\rangle$ only if

$$\langle\psi^{(0)}_n|[\mathcal{H}^{(1)} - E^{(1)}_n]|\psi^{(0)}_n\rangle = 0 \quad [B.20]$$

because the $|\psi^{(0)}_n\rangle$ can be written as a linear combination of the eigenvectors of $\mathcal{H}^{(1)}$ which belong to nonzero eigenvalues [Byron and Fuller, 1992]

therefore by choosing $|\psi^{(0)}_n\rangle$ to be normalized to 1, this yields,

$$E^{(1)}_n = \langle \psi^{(0)}_n | \mathcal{H}^{(1)} | \psi^{(0)}_n \rangle \qquad [B.21]$$

$$E^{(2)}_n = \langle \psi^{(0)}_n | [\mathcal{H}^{(1)} - E^{(1)}_n] | \psi^{(1)}_n \rangle \qquad [B.22]$$

$$E^{(3)}_n = \langle \psi^{(0)}_n | [\mathcal{H}^{(1)} - E^{(1)}_n] | \psi^{(2)}_n \rangle - E^{(2)}_n \langle \psi^{(0)}_n | \psi^{(1)}_n \rangle \qquad [B.23]$$

These equations give us the $E^{(i)}_n$ in terms of quantities that are known. If one were now to rewrite Eqs [B.16]-[B.19] in a manner where the $|\psi^{(1)}_n\rangle$ can be computed in terms of $|\psi^{(0)}_m\rangle$, then by taking the inner product with $|\psi^{(0)}_m\rangle$ and with $m \neq n$ one obtains for Eq. [B.17]

$$\langle \psi^{(0)}_m | [\mathcal{H}^{(0)} - E^{(0)}_n] | \psi^{(1)}_n \rangle = - \langle \psi^{(0)}_m | [\mathcal{H}^{(1)} - E^{(1)}_n] | \psi^{(0)}_n \rangle \qquad [B.24]$$

$$\langle \psi^{(0)}_m | \mathcal{H}^{(0)} | \psi^{(1)}_n \rangle - \langle \psi^{(0)}_m | E^{(0)}_n | \psi^{(1)}_n \rangle = - \langle \psi^{(0)}_m | \mathcal{H}^{(1)} | \psi^{(0)}_n \rangle - E^{(1)}_n \langle \psi^{(0)}_m | \psi^{(0)}_n \rangle \qquad [B.25]$$

now since $|\psi^{(0)}_m\rangle$ is an eigenfunction of $\mathcal{H}^{(0)}$ with eigenvalue $E^{(0)}_m$ and since the eigenvectors form an orthonormal set $\langle \psi^{(0)}_m | \psi^{(0)}_n \rangle = 0$ for $m \neq n$, one may rewrite Eq. [B.25] to obtain [Byron and Fuller, 1992],

$$(E^{(0)}_n - E^{(0)}_m) \langle \psi^{(0)}_m | \psi^{(1)}_n \rangle = \langle \psi^{(0)}_m | \mathcal{H}^{(1)} | \psi^{(0)}_n \rangle \qquad [B.26]$$

Since we are considering the nondegenerate case here $E^{(0)}_n \neq E^{(0)}_m$ as long as $m \neq n$, therefore,

$$\langle \psi^{(0)}_m = \langle \psi^{(0)}_m | \mathcal{H}^{(1)} | \psi^{(0)}_n \rangle / (E^{(0)}_n - E^{(0)}_m) \qquad [B.27]$$

applying the closure relation $\sum_m |\psi^{(0)}_m\rangle\langle\psi^{(0)}_m| = 1$ [Peleg *et al.*, 1998]to the set of orthonormal kets in Eq. [B27] we obtain

$$|\psi^{(1)}{}_n\rangle = \sum_{m \neq n} [\langle\psi^{(0)}{}_m|\mathcal{H}^{(1)}|\psi^{(0)}{}_n\rangle/(E^{(0)}{}_n - E^{(0)}{}_m)]|\psi^{(0)}{}_m\rangle \qquad [B.28]$$

which when put into Eq. [B.6] results in the first order eigenvector,

$$|\psi_n(\lambda)\rangle = |\psi^{(0)}{}_n\rangle + \lambda \sum_{m \neq n} [\langle\psi^{(0)}{}_m|\mathcal{H}^{(1)}|\psi^{(0)}{}_n\rangle/(E^{(0)}{}_n - E^{(0)}{}_m)]|\psi^{(0)}{}_m\rangle \qquad [B.29]$$

The second order correction to the energy can be obtained from Eq. [B.22]

$$E^{(2)}{}_n = \langle\psi^{(0)}{}_n|\mathcal{H}^{(1)}|\psi^{(1)}{}_n\rangle = \sum_{m \neq n} [\langle\psi^{(0)}{}_m|\mathcal{H}^{(1)}|\psi^{(0)}{}_n\rangle/(E^{(0)}{}_n - E^{(0)}{}_m)]|\psi^{(0)}{}_m\rangle \cdot$$

$$= \sum_{m \neq n} |\langle\psi^{(0)}{}_m|\mathcal{H}^{(1)}|\psi^{(0)}{}_n\rangle|^2/(E^{(0)}{}_n - E^{(0)}{}_m) \qquad [B.30]$$

and the energy, to second order is given by

$$E_n(\lambda) = E^{(0)}{}_n + \lambda\langle\psi^{(0)}{}_n|\mathcal{H}^{(1)}|\psi^{(0)}{}_n\rangle + \lambda^2 \sum_{m \neq n} |\langle\psi^{(0)}{}_m|\mathcal{H}^{(1)}|\psi^{(0)}{}_n\rangle|^2/(E^{(0)}{}_n - E^{(0)}{}_m) \qquad [B.31]$$

Or in the notation of Misra (1985)

$$E_{M,m} = g\mu_B B\ (E^{(0)}\ \text{term}) + E_f(M)\ (E^{(1)}\ \text{term}) + E_{hf}(M, m)\ (E^{(2)}\ \text{term}) \qquad [B.32]$$

Appendix C

This is a listing of the computer program, as developed by Dr. Misra, for the evaluation of the spin-Hamiltonian parameters for Mn^{2+} using the least-squares fitting method.

```
C    PROGRAM HFTUTON    (INPUT,OUTPUT,TAPE5=INPUT,TAPE6=OUTPUT)
C    NO =THE NO. OF FIRST MAG FIELD IN DATA INCLUDED IN FITTING
C    M  =NO. OF PARAMETERS
C    L4 =NO. OF ITERATIONS ALLOWED
C    Q1 =MIN. VALUE OF SUM OF SQUARES FOR FITS( CHI-SQUARE
C    TOLERANCE)
C    Z(I)=MAGNETIC FIELD VALUES FOR FITS
C    B  =PARAMETER MATRIX
C    N  =NO. OF  DATA POINTS USED IN LEAST-SQARES FITTING
C    Q1 =N/10
C    Q2 =TOLERANCE ON GRAD(CHI**2) =APPROX .01
C    FM(I) = MEASURED VALUES
C    FC(I) = CALCULATED VALUES
C    ERR(I)= STANDARD DEVIATION ON FM(I) = SQRT(FM(I))
C    DIMENSIONS OF A,B IN EXAM AND MATINV SUBROUTINES SHOULD BE
C    THE SAME AS THOSE OF B2,B1 RESPECTIVELY IN THE MAIN
C    PROGRAM AND IN  CURFIT
C    ENTER THETA IN DEGREES
C    DIMENSIONS OF Q,V IN JACOBI1 SHOULD BE THE SAME AS THOSE OF
C    B3,B2 RESPECTIVELY IN CURFIT
C    NUMBER=INDEX THAT CHANGES WITH EACH NEW CASE
C    NCASES=NO. OF CASES CONSIDERED. ITS VALUE SHOULD BE
C    ENTERED.
C    IBB(II,1) AND IBB(II,2) INDICATE THE EIGENVALUES INVOLVED IN
C    RESONANCE FOR THE NO. II MAG FIELD VALUE
C    B=G=GPARRALEL,GPERPENDICULAR,B20,B22,B40,B42,B44,A,B,
C    QPRIME=0. QDOUBLEPRIME=0
     DIMENSION Z(850),FM(850),FC(850),DF(850),ERR(850),B(12),
    1B1(12),B2(12,12),IBB1(850,2),
    1ZZ(850,5),G(12,20),ZZ1(850,5),TEETA1(850,5),
    2THETA(850),GG(12,5),IBB(850,2),DELHH(850,20),DELH(850)
     DIMENSION TEETA(850,5),FREQ(20),FACTOR(20),NN(20),HN(20)
    1,Z1(850,5),ADD(20),Z2(850),IAB(30,2),ICC(30,2),DDF(850,5)
    1 ,SMDD(20),JJII(10,2),IA1(850,5),IA2(850,5),SSS(850)
     CHARACTER*(3) ABC(2)
```

```
      CHARACTER*(3) Y(4)
      CHARACTER*(3) A2
      COMMON/DATA1A/ABC,Y
      COMMON/DATA1/B1,B2,Q1,Q2,SMD,SSMD,L4
      COMMON/DATA3/Z,THETA,DELH,IBB,IBB1
      COMMON/DATA/FM,FC,DF,ERR,B,BO,HN,
     *I,L,NUMBER,N,M
      open(unit=6,file= 'mnhf1.dat',status='new')
C     CASE5= AM/ZN MN2+
C----------DATA FOR XBAND (ROOM TEMP)--------------------
      DATA(ZZ(J,5),J=1,216)/
C     Data for Z
     * 9662.5,9734.7,9815.8,9902.1,9997.6,10092.6,
     * 4143.3,4231.7,4320.7,4408.7,4497.7,4585.6,
     * 921.7,1009.6,1098.6,1188.3,1277.5,1366.6,
C     Data for Z+2
     * 9622.1,9693.7,9775.3,9862.5,9957.2,10052.4,
     * 4148.3,4236.4,4325.1,4413.8,4502.7,4590.3,
     * 921.3,1009.7,1098.4,1188.3,1277.5,1366.9,
C     Data for Z+4
     * 9482.4,9553.3,9635.7,9722.2,9817.1,9912.6,
     * 4163.5,4251.6,4340.7,4428.8,4517.3,4605.7,
     * 926.7,1014.4,1103.6,1193.4,1282.7,1371.4,
C     Data for Z+6
     * 9256.8,9328.4,9410.2,9497.6,9592.1,9687.8,
     * 4198.8,4286.4,4375.9,4466.7,4560.1,4655.0,
     * 926.7,1014.4,1108.2,1193.8,1282.4,1371.4,
C     Data for Z+8
     * 8920.4,8993.7,9075.4,9162.3,9257.3,9352.4,
     * 4233.5,4332.7,4431.1,4530.8,4629.6,4726.1,
     * 936.7,1024.3,1118.1,1203.6,1292.7,1381.6,
C     Data for Z+10
     * 8475.8,8548.3,8630.5,8717.3,8812.3,8907.7,
     * 4283.4,4383.7,4485.1,4589.7,4695.9,4800.1,
     * 946.8,1034.5,1128.9,1213.4,1302.3,1391.4,
C     Data for Z+80
     * 5021.3,5111.6,5217.8,5287.5,5375.4,5463.8,
     * 2847.6,2937.1,3025.4,3114.8,3203.7,3292.7,
     * 1288.4,1377.2,1466.3,1555.1,1644.8,1733.2,
C     Data for Z+82
     * 5666.1,5756.7,5862.1,5932.8,6020.4,6108.6,
     * 2867.8,2957.1,3045.9,3134.4,3223.4,3312.8,
     * 1283.4,1372.8,1461.7,1550.8,1639.3,1728.7,
C     Data for Z+84
```

```
     * 6106.4,6196.4,6302.7,6372.2,6460.4,6548.5,
     * 2882.3,2972.8,3060.7,3149.2,3238.6,3327.4,
     * 1278.7,1367.4,1456.3,1545.9,1634.7,1723.4,
C    Data for Z+86
     * 6401.2,6491.7,6579.5,6667.2,6755.5,6843.7,
     * 2892.9,2982.2,3070.3,3159.5,3248.7,3337.1,
     * 1273.4,1362.7,1451.2,1540.7,1629.5,1718.5,
C    Data for Z+88
     * 6571.8,6661.3,6749.5,6837.3,6925.4,7013.8,
     * 2898.6,2987.2,3075.4,3164.9,3253.7,3342.1,
     * 1268.2,1357.4,1446.2,1535.7,1624.3,1713.8,
C    Data for Z+90
     * 6627.5,6716.4,6804.3,6892.9,6980.6,7068.2,
     * 2903.7,2992.5,3080.4,3169.8,3258.7,3347.1,
     * 1268.1,1357.4,1446.2,1535.8,1624.3,1713.2/
     DATA(TEETA(J,5),J=1,216)/
     * 18*0,18*2,18*4,18*6,18*8,18*10,
     * 18*80,18*82,18*84,18*86,18*88,18*90/
C------------------DATA FOR QBAND (ROOM TEMP)----------------
C    DATA(ZZ1(J,5),J=1,288)/
C    Data for Z
     * 6036.89,6129.36,6218.41,6307.44,6396.5,6485.51,
     * 9237.79,9326.83,9415.87,9494.64,9587.11,9671.73,
     * 12506.71,12596.45,12682.75,12775.85,12865.65,12955.3,
C    Data for Z+2
     * 6036.89,6129.36,6218.41,6307.44,6396.5,6485.51,
     * 9242.7,9331.74,9420.78,9499.55,9592.02,9676.64,
     * 12511.65,12601.39,12687.69,12780.79,12870.59,12960.24,
C    Data for Z+4
     * 6051.46,6143.93,6232.98,6322.01,6411.07,6500.08,
     * 9262.32,9351.36,9440.4,9519.17,9611.64,9696.26,
     * 12521.54,12611.28,12697.58,12790.68,12880.48,12970.13,
C    Data for Z+5
     * 6058.1,6148.1,6235.75,6326.8,6415.86,6504.87,
     * 9282.94,9371.3,9461.51,9540.73,9631.94,9715.16,
C    Data for Z+6
     * 6075.76,6168.23,6257.28,6346.31,6435.37,6524.38,
     * 9291.74,9380.78,9469.82,9548.59,9641.06,9725.68,
     * 12541.3,12631.04,12717.34,12810.44,12900.24,12989.89,
C    Data for Z+8
     * 6104.91,6197.38,6286.43,6375.46,6464.52,6553.53,
     * 9330.98,9420.02,9509.06,9587.83,9680.3,9764.92,
     * 12570.95,12660.69,12746.99,12840.09,12929.89,13019.54,
C    Data for Z+10
```

```
     * 6148.63,6241.1,6330.15,6419.18,6508.24,6597.25,
     * 9384.93,9473.97,9563.01,9641.78,9734.25,9819.87,
     * 12605.55,12695.29,12781.59,12874.69,12964.49,13054.14,
C    Data for Z+15
     * 6284.5,6380.7,6470.14,6562.97,6655.8,6745.2,
C    Data for Z+20
     * 6481.57,6574.15,6666.68,6755.83,6851.82,6944.37,
C    Data for Z+25
     * 6750.34,6846.14,6941.94,7034.3,7126.69,7222.49,
C    Data for Z+30
     * 7127.63,7223.34,7320.05,7417.74,7513.44,7609.14,
C    Data for Z+35
     * 7609,7705.55,7805.56,7902.1,7997.66,8095.21,
C    Data for Z+40
     * 8206.59,8303.14,8401.14,8497.68,8594.23,8691.78,
C    Data for Z+45
     * 8942.28,9039.83,9138.83,9236.37,9332.93,9429.48,
C    Data for Z+50
     * 9804.71,9900.26,10000.26,10095.98,10190.54,10290.09,
C    Data for Z+75
     * 9825.87,9915.91,10003.95,10093.04,10185.87,10275.24,
     * 11011.3,11095.15,11185,11267,11356.39,11445.78,
     * 12325.25,12421.52,12514.36,12610.61,12704,12800.5,
C    Data for Z+80
     * 12200.58,12293.04,12379.87,12474.55,12570.43,12666.63,
     * 10873.27,10962.93,11052.58,11142.24,11224.99,11314.65,
C    Data for Z+82
     * 9642.61,9732.52,9822.27,9908.56,9998.31,10091.51,
     * 10828.81,10918.47,11008.12,11097.78,11180.53,11270.19,
     * 12177.47,12267.21,12356.96,12446.68,12536.44,12629.64,
C    Data for Z+84
     * 9608.11,9698.02,9787.77,9874.06,9963.81,10057.01,
     * 10794.23,10883.89,10973.54,11063.2,11145.95,11235.61,
     * 12152.73,12242.47,12332.22,12421.94,12511.7,12604.9,
C    Data for Z+86
     * 9578.52,9668.43,9758.18,9844.47,9934.22,10027.42,
     * 10769.56,10859.22,10948.87,11038.53,11121.28,11210.94,
     * 12132.98,12222.72,12312.47,12402.19,12491.95,12585.15,
C    Data for Z+88
     * 9563.73,9653.64,9743.39,9829.68,9919.43,10012.63,
     * 10749.77,10839.43,10929.08,11018.74,11101.49,11191.15,
     * 12118.17,12207.91,12297.66,12387.38,12477.14,12570.34,
C    Data for Z+90
     * 9558.8,9648.71,9738.46,9824.75,9914.5,10007.7,
```

```
     * 10744.83,10834.49,10924.14,11013.8,11096.55,11186.21,
     * 12113.22,12202.96,12292.71,12382.43,12472.19,12565.39/
C      DATA(TEETA1(J,5),J=1,288)/
     * 18*0,18*2,18*4,12*5,18*6,18*8,18*10,6*15,6*20,6*25,6*30,6*35,
     * 6*40,6*45,6*50,18*75,12*80,18*82,18*84,18*86,18*88,18*90/
C      Input initial spin hamiltonian parameters here
      DATA(G(J,5),J=1,11)/
     * -4.5000,-0.25000,-0.25000,2.0000,2.0000,0.0,
     * 0.0,0.0,0.0,0.0,0.0/
C      HERE ONE DEFINES THE TRANSITIONS FOR VARIOUS LINES
      DATA(IBB(J,1),J=1,216)/
C      XBAND TRANSITIONS 1st COLUMN (TEMP=ROOM)----------
     11,2,3,4,5,6,13,14,15,16,17,18,13,14,15,16,17,18,
     21,2,3,4,5,6,13,14,15,16,17,18,13,14,15,16,17,18,
     41,2,3,4,5,6,13,14,15,16,17,18,13,14,15,16,17,18,
     61,2,3,4,5,6,13,14,15,16,17,18,13,14,15,16,17,18,
     81,2,3,4,5,6,13,14,15,16,17,18,13,14,15,16,17,18,
     11,2,3,4,5,6,13,14,15,16,17,18,13,14,15,16,17,18,
     130,29,28,27,26,25,13,14,15,16,17,18,1,2,3,4,5,6,
     230,29,28,27,26,25,13,14,15,16,17,18,1,2,3,4,5,6,
     430,29,28,27,26,25,13,14,15,16,17,18,1,2,3,4,5,6,
     630,29,28,27,26,25,13,14,15,16,17,18,1,2,3,4,5,6,
     830,29,28,27,26,25,13,14,15,16,17,18,1,2,3,4,5,6,
     930,29,28,27,26,25,13,14,15,16,17,18,1,2,3,4,5,6/
C      QBAND TRANSITIONS 1st COLUMN (TEMP=ROOM)----------
     130,29,28,27,26,25,24,23,22,21,20,19,13,14,15,16,
     217,18,30,29,28,27,26,25,24,23,22,21,20,19,13,14,15,16,
     317,18,30,29,28,27,26,25,24,23,22,21,20,19,13,14,15,16,
     417,18,30,29,28,27,26,25,24,23,22,21,20,19,30,29,28,27,
     526,25,24,23,22,21,20,19,13,14,15,16,17,18,30,29,28,27,
     626,25,24,23,22,21,20,19,13,14,15,16,17,18,30,29,28,27,
     726,25,24,23,22,21,20,19,13,14,15,16,17,18,30,29,28,27,
     826,25,30,29,28,27,26,25,30,29,28,27,26,25,30,29,28,27,
     926,25,30,29,28,27,26,25,30,29,28,27,26,25,30,29,28,27,
     126,25,30,29,28,27,26,25,1,2,3,4,5,6,7,8,9,10,11,12,13,
     214,15,16,17,18,13,14,15,16,17,18,7,8,9,10,11,12,1,2,3,
     34,5,6,7,8,9,10,11,12,13,14,15,16,17,18,1,2,3,4,5,6,7,
     48,9,10,11,12,13,14,15,16,17,18,1,2,3,4,5,6,7,8,9,10,11,
     512,13,14,15,16,17,18,1,2,3,4,5,6,7,8,9,10,11,12,13,14,
     615,16,17,18,1,2,3,4,5,6,7,8,9,10,11,12,13,14,15,16,17,18/
      DATA(IBB(J,2),J=1,216)/
C      XBAND TRANSITIONS 2nd COLUMN (TEMP=ROOM)----------
     17,8,9,10,11,12,24,23,22,21,20,19,24,23,22,21,20,19,
     27,8,9,10,11,12,24,23,22,21,20,19,24,23,22,21,20,19,
```

```
     47,8,9,10,11,12,24,23,22,21,20,19,24,23,22,21,20,19,
     67,8,9,10,11,12,24,23,22,21,20,19,24,23,22,21,20,19,
     87,8,9,10,11,12,24,23,22,21,20,19,24,23,22,21,20,19,
     17,8,9,10,11,12,24,23,22,21,20,19,24,23,22,21,20,19,
     136,35,34,33,32,31,24,23,22,21,20,19,7,8,9,10,11,12,
     236,35,34,33,32,31,24,23,22,21,20,19,7,8,9,10,11,12,
     436,35,34,33,32,31,24,23,22,21,20,19,7,8,9,10,11,12,
     636,35,34,33,32,31,24,23,22,21,20,19,7,8,9,10,11,12,
     836,35,34,33,32,31,24,23,22,21,20,19,7,8,9,10,11,12,
     936,35,34,33,32,31,24,23,22,21,20,19,7,8,9,10,11,12/
C    QBAND TRANSITIONS 2nd COLUMN----------------------------
     136,35,34,33,32,31,30,29,28,27,26,25,24,23,22,21,
     220,19,36,35,34,33,32,31,30,29,28,27,26,25,24,23,22,21,
     320,19,36,35,34,33,32,31,30,29,28,27,26,25,24,23,22,21,
     420,19,36,35,34,33,32,31,30,29,28,27,26,25,36,35,34,33,
     532,31,30,29,28,27,26,25,24,23,22,21,20,19,36,35,34,33,
     632,31,30,29,28,27,26,25,24,23,22,21,20,19,36,35,34,33,
     732,31,30,29,28,27,26,25,24,23,22,21,20,19,36,35,34,33,
     832,31,36,35,34,33,32,31,36,35,34,33,32,31,36,35,34,33,
     932,31,36,35,34,33,32,31,36,35,34,33,32,31,36,35,34,33,
     132,31,36,35,34,33,32,31,7,8,9,10,11,12,13,14,15,16,17,
     218,24,23,22,21,20,19,24,23,22,21,20,19,13,14,15,16,17,
     318,7,8,9,10,11,12,13,14,15,16,17,18,24,23,22,21,20,19,
     47,8,9,10,11,12,13,14,15,16,17,18,24,23,22,21,20,19,7,8,
     59,10,11,12,13,14,15,16,17,18,24,23,22,21,20,19,7,8,9,10,
     611,12,13,14,15,16,17,18,24,23,22,21,20,19,7,8,9,10,11,12,
     713,14,15,16,17,18,24,23,22,21,20,19/
C    JJII(,1),(,2) TELL GROUPS OF 30 LINES WHICH ARE BETWEEN
C    0 AND 25 DEG. AND BETWEEN 75 AND 90 DEG. RESPECTTIVELY.
     DATA(JJII(J,1),J=1,4)/6,5,6,6/
     DATA(JJII(J,2),J=1,4)/5,6,5,5/
     DATA(FREQ(J),J=1,5)/9.6193,9.5256,9.4475,9.485,9.6193/
     DATA(FACTOR(J),J=1,5)/6.1,6.1,6.1,6.1,1.0/
     DATA(ADD(J),J=1,5)/314.,326.5,332.10,304.5,0.0/
C    To change number of lines here (5th column)
     DATA(NN(J),J=1,5)/330,330,330,330,504/
     DO 331 JJ=1,5
     NNJJ=NN(JJ)
     DO 331 J=1,NNJJ
     DELHH(J,JJ)=FACTOR(JJ)*2
 331 CONTINUE
     NZERO=5
     NUMBER=NZERO
     NCASES=5
```

```
   1 CONTINUE
C*****DEFINE HERE QUANTUM NOS. FOR VARIOUS LINES
C    FACTOR CONVERTS MMS ON GRAPH TO GAUSS
 188 FORMAT(1H1)
   8 FORMAT(1X,4HQ1 = ,E13.5,5X,4HQ2 = ,E13.5)
 137 FORMAT (3X,I2,5X,E16.6/)
 136 FORMAT(10X,19H INITIAL PARAMETERS//3X,1HJ,10X,4HB(J)//)
 135 FORMAT(1X,11H PARAMETERS//3X,1HJ,10X,4HB(J),27X,6HERRORS//)
   9 FORMAT(2X,4H HN= ,F9.4)
 140 FORMAT(3X,I2,5X,E16.6,15X,E16.6/)
 138 FORMAT(5X,14H CASE NUMBER =,I2//)
 141 FORMAT(10X,6H SMD =,E13.5//)
 235 FORMAT (15X,5(E13.5,8X)/)
     M=5
     MM=M
C    L4 IS THE TOTAL NUMBER OF ITERATIONS ALLOWED
     L4=10
     Q1=1.E-8
     Q2=1.E-40
C     BO CONVERTS GAUSS TO GHZ
     BO=92.732/(6.6252*10000.)
     IG=1
 958 CONTINUE
     WRITE (6,188)
     N=NN(NUMBER)
     HN(NUMBER)=FREQ(NUMBER)
     N1=N
     N2=216
     N3=NN(NUMBER)-N2
     DO 6661 I6=1,N2
     Z1(I6,NUMBER)=ZZ(I6,NUMBER)
6661 THETA(I6)=TEETA(I6,NUMBER)
     DO 6662 I6=1,N3
     Z1(I6+N2,NUMBER)=ZZ1(I6,NUMBER)
6662 THETA(I6+N2)=TEETA1(I6,NUMBER)
     DO 806 IJK=1,N1
     IF(NUMBER.EQ.5) GO TO 342
     IF (THETA(IJK).GT.(25.)) GO TO 807
     JYJ=JJII(NUMBER,1)
     DO 340 II=1,30
     DO 340 JJ=1,JYJ
     JJ1=(JJ-1)
     IIJJ=II+JJ1*30
     IBB(IIJJ,1)=IAB(II,1)
```

```
      IA1(IIJJ,NUMBER)=IBB(IIJJ,1)
      IBB(IIJJ,2)=IAB(II,2)
      IA2(IIJJ,NUMBER)=IBB(IIJJ,2)
  340 CONTINUE
      GO TO 342
  807 CONTINUE
      JXJ=JJII(NUMBER,2)
      DO343 II=1,30
      DO 343 JJ=1,JXJ
      JJ1=(JJ-1)
      IIJJ=II+JJ1*30+JJII(NUMBER,1)*30
      IBB(IIJJ,1)=ICC(II,1)
      IA1(IIJJ,NUMBER)=IBB(IIJJ,1)
      IBB(IIJJ,2)=ICC(II,2)
      IA2(IIJJ,NUMBER)=IBB(IIJJ,2)
  343 CONTINUE
  342 CONTINUE
  806 CONTINUE
      DO 210 LL=1,MM
  210 B(LL)=G(LL,NUMBER)
      WRITE (6,138) NUMBER
      WRITE (6,136)
      WRITE (6,137) (J,B(J),J=1,M)
      DO 3 IJK = 1,N1
      DELH(IJK)=DELHH(IJK,NUMBER)
    3 Z(IJK) = Z1(IJK,NUMBER)
      IF (NUMBER.NE.1) GO TO 20
   20 CONTINUE
      IF(NUMBER.NE.2) GO TO 21
   21 CONTINUE
      IF(NUMBER.NE.3) GO TO 22
   22 CONTINUE
      IF(NUMBER.NE.5) GO TO 6666
 6666 CONTINUE
      DO 6663 II=1,N1
 6663 CONTINUE
      IF(NUMBER.NE.4) GO TO 23
   23 CONTINUE
      WRITE(6,8)Q1,Q2
      WRITE(6,9) HN(NUMBER)
      DO 201 II=1,N1
      IF(II.LE.N2)FM(II)=HN(NUMBER)
C     To change the Qband frequency
      IF(II.GT.N2)FM(II)=35.87
```

```
 201 CONTINUE
     CALL CURFIT
     DO 202 II=1,N1
     IF(NUMBER.EQ.5) THEN
     IA1(II,NUMBER)=IBB(II,1)
     IA2(II,NUMBER)=IBB(II,2)
     END IF
     DDF(II,NUMBER)=DF(II)
 202 CONTINUE
     SMDD(NUMBER) = SSMD
     WRITE(6,188)
     WRITE(6,135)
     DO 220 LL=1,M
 220 GG(LL,NUMBER) = B(LL)
     WRITE(6,140)(J,B(J),B1(J),J=1,M)
     WRITE(6,188)
     NUMBER = NUMBER + 1
     IF ( NUMBER - NCASES) 1,1,2
   2 CONTINUE
     DO 230 LL=NZERO,NCASES
     N=NN(LL)
     IF (LL.GT.NZERO) WRITE(6,188)
     WRITE (6,138) LL
     WRITE (6,141) SMDD(LL)
     WRITE(6,302)
 302 FORMAT(15X,' IDENTIFICATION OF LINES')
     DO 300 II=1,N
     IF(Z1(II,LL))563,562,563
 563 CONTINUE
 562 CONTINUE
 300 CONTINUE
 658 FORMAT(//)
C      SSS1 IS SMD(1),THAT IS WHEN ALL(LINES)SIGMA=1
     SSS1=0.
     NEFF=0
     DO 555 ID=1,N1
     IF(Z(ID))561,560,561
 561 CONTINUE
     NEFF=NEFF+1
     SSS(ID)=DDF(ID,LL)**2
     SSS1=SSS(ID)+SSS1
 560 CONTINUE
 555  CONTINUE
     WRITE(6,3011)
```

```
      WRITE(6,301)((IL,Z(II),THETA(II),IA1(II,LL),IA2(II,LL),
     1 SSS(II)),II=1,N)
      ANEFF=FLOAT(NEFF)
      SSSAV5=SSS1*5./ANEFF
      WRITE (6,657)SSS1,SSSAV5
  657 FORMAT (10X,'SMD(1)=',E13.5,5X,'SSSAV5=',E13.5,//)
  301 FORMAT(X,I3,2X,F12.1,2X,F8.2,4X,I3,3X,I3,5X,E12.5)
 3011 FORMAT(2X,'FIELD NO.',3X,'GAUSS',4X,'ANGLE',4X,
     1'TRANSITIONS',8X,'SMD',/)
  230 WRITE (6,235) (GG(LM,LL),LM=1,11)
  708 CONTINUE
      STOP
      END
      SUBROUTINE CURFIT
C     EXAM  HANDLES ALL MATRICES OF DIMENSIONS UPTO THE DIMS.MM
C     OF A,B,C
C     THAT IS M IS LESS THAN OR EQUAL TO MM (SAME IS TRUE OF MATINV
C     AND JACOBI)
C     IN EQUIVALENCEGRAD SHOULD BE PLACED IMMEDIATELY AFTER
C     B SINCE IN FUNC B(12,2)=BB(12),GRAD(12) IN CURFIT
C     DIMENSION OF B3 SHOULD BE M*(M+1)/2
C     F O R T R A N  4
      DIMENSION FM(850),FC(850),DF(850),ERR(850),B(12),GRAD(12),
     1 B1(12),B2(12,12),B4(12,12),HN(20),ANORM1(12),F1(12,12),
     2 F2(12,12),AI(12,12),W(12),B3(12,12),
     1 X(850),D1(12),D2(12,12)
      CHARACTER*(3) ABC(2)
      CHARACTER*(3) Y(4)
      CHARACTER*(3) A2
      COMMON/DATA1A/ABC,Y
      COMMON/DATA1/ B1,B2,Q1,Q2,SMD,SSMD,L4
      COMMON/DATA/FM,FC,DF,ERR,B,BO,HN,
     *I,L,NUMBER,N,M
      COMMON/DATA2/D1,D2,GRAD,LLX
      INTEGER LDA,LDVEC,NNN
      PARAMETER(NNN=12,LDA=NNN,LDEVEC=NNN)
      COMPLEX ZP(LDA,NNN),EVEC(LDA,NNN)
      EXTERNAL EVCHF
C     EQUIVALENCE (Z,DC),(FM,DC(501)),(FC,DC(1001)),
C     1(DF,DC(1501)),(ERR,DC(2001)),(B,DC(2989)),(GRAD,DC(3001)),
C     2(B1,DC(3013)),(B2,DC(3025)),(N,DC(3169)),(L4,DC(3170)),
C     3(Q1,DC(3171)),(Q2,DC(3172)),(M,DC(3173)),(I,DC(3174)),
C     4(L,DC(3175)),(D1,DC(2501)),(D2,DC(2513)),(BO,DC(3176)),
C     5(SMD,DC(3177)),(SSMD,DC(3178)),(IBB,DC(4000)),(THETA,DC(3500))
```

```
C    6 ,(HN,DC(3179))
C    7,(S,DC(2901)),(SA,DC(2902)),(BMOD,DC(2903)),(PROD,DC(2904))
C    8,(GMOD,DC(2905)),(LE,DC(2906)),(LLX,DC(4998))
C     DATA(ABC=2HNO,3HYES),(Y=1H ,1HC,1H*,1HM)
     ABC(1)='NO'
     ABC(2)='YES'
     MM=M
     NN=N
     L1 = 0
     SA = 0.0
C     SA1 IS SA WITH SIGMA (ALL LINES)=1.
     SA1=0.
     DO 1000 J=1,MM
     B1(J)=0.0
     DO 1000 K=1,MM
 1000 B2(J,K)=0.0
     WRITE(6,901)
C     LLX=0 ALLOWS WRITING E.VALUES IN FUNC
     LLX=0
     DO 100 II = 1, NN
     I=II
     L=1
     CALL FUNC(2)
     X(II)=ERR(II)**2
 901  FORMAT(5X,10H FUNC2,210 )
     DF(II) =FM(II) - FC(II)
     DO 101 J=1,MM
     B1(J)=B1(J)-(2.0*DF(II)*D1(J))/X(II)
     DO 101 K=1,MM
  101 B2(J,K)=B2(J,K)-(2.0*(DF(II)*D2(J,K)-D1(J)*D1(K)))/X(II)
     SA1=SA1+DF(II)**2
  100 SA = SA + DF(II)**2/X(II)
C     LLX=1 OMITS WRITING E.VALUES IN FUNC
     LLX=1
C     EQZERO TELLS IF ELEMENTS OF B2,B1 ARE ZERO
     CALL EQZERO(B2,B1,M,IC1,IC2,IC3)
     WRITE(6,901)
     LM=1
     WRITE(6,5)CPU,LM
   5 FORMAT(5X,'CPU=',F8.2,'LM=',I2)
     GMOD=0.0
     DO 102 J=1,M
  102 GMOD=GMOD+B1(J)**2
     WRITE(6,243)SA,GMOD
```

```
 243 FORMAT(1X,26H'INITIAL VALUE SUM OF SQ.=E13.5,20X,17H'SQ MOD OF
      GR
     1AD =E13.5)
     WRITE(6,244) SA1
 244 FORMAT(5X,'INITIAL VALUE SUM OF SQ.(ALL SIGMA
     1 =1)=',E13.5,//)
     WRITE(6,1751)
1751 FORMAT(14H0 DERIVATIVES-)
     WRITE(6,240)(B1(J),J=1,M)
 240 FORMAT (15X,5(E13.5,8X)/)
     LLJJ=0
C***** FOLLOWING FOR CALCULATING INITIAL VALUES ONLY
C      LLJJ=1
     IF(LLJJ.NE.0) GOTO 559
     IF (SA - Q1) 110, 110, 200
 110 LE = 1
     GO TO 600
 200 S = 0.0
     GMOD = 0.0
     BMOD = 0.0
     PROD = 0.0
     A2=ABC(1)
     DO 210 J = 1, MM
     B1(J) = 0.0
     DO 210 K = 1, MM
 210 B2(J,K) = 0.0
     WRITE(6,902)
     DO 220 II = 1, NN
     I=II
     L=1
     CALL FUNC(2)
     X(II)=ERR(II)**2
902  FORMAT(5X,10H FUNC2,210 )
     DF(II) = FM(II) - FC(II)
     DO 220 J = 1, MM
     B1(J) = B1(J) - (2.0*DF(II)*D1(J))/X(II)
     DO 220 K = 1, MM
 220 B2(J,K) = B2(J,K) - (2.0*(DF(II)*D2(J,K) -D1(J)*D1(K)))/X(II)
     CALL EQZERO(B2,B1,M,IC1,IC2,IC3)
     WRITE(6,902)
     LM=2
     WRITE(6,5)CPU,LM
     DO 230 J = 1, MM
 230 GRAD(J) = B1(J)
```

```
      L1 = L1 + 1
      WRITE(6,903)
      CALL EXAM (B2,B1,M,LF)
      WRITE(6,903)
  903 FORMAT(5X,9H EXAM,230 )
      IF (LF) 250, 250, 305
  250 CONTINUE
      DO 1231 II=1,M
      DO 1231 JJ=1,M
      AI(II,JJ)=0.
 1231 B3(II,JJ)=B2(II,JJ)
      WRITE(6,904)
      DO 232 II=1,MM
      DO 232 JJ=1,MM
  232 ZP(II,JJ)=CMPLX(B3(II,JJ),AI(II,JJ))
      CALL EVCHF(NNN,ZP,LDA,W,EVEC,LDEVEC)
      CALL EVCHFN(NNN,LDA,W,EVEC,ANORM1,F1,F2)
      WRITE(6,904)
  904 FORMAT(5X,12H EVCSF,231 )
      DO 5005 IR=1,MM
      B3(IR,IR)=W(IR)
      DO 5005 JR=1,MM
 5005 B2(IR,JR)=REAL(EVEC(IR,JR))
      DO 235 K=1,MM
  235 B1(K)=B3(K,K)
      WRITE(6,240)B1
      DO 389 I5=1,MM
      AB1=ABS(B1(I5))
      IF((AB1).GT.(1.E-10)) GO TO 388
      B1(I5)=0.
  388 CONTINUE
  389 CONTINUE
      I4=5
      IF (I4.EQ.1) GO TO 912
      A2=ABC(2)
      DO 260 J = 1, MM
  260 D1(J) = 0.0
      DO 270 J = 1, MM
      DO 270 K = 1, MM
  270 D1(K) = D1(K) + B2(J,K) *GRAD(J)
      DO 275 J = 1, MM
      IF (B1(J)) 280, 290, 285
  280 B1(J) = - B1(J)
  285 D1(J) = D1(J)/B1(J)
```

```
      GO TO 275
  290 D1(J) = 0.0
  275 CONTINUE
      DO 295 J = 1, MM
  295 B1(J) = 0.0
      DO 300 J = 1, MM
      DO 300 K = 1, MM
  300 B1(J) = B1(J) + B2(J,K)*D1(K)
  305 DO 310 J=1,MM
      GMOD = GMOD + GRAD(J)**2
      BMOD = BMOD + B1(J)**2
  310 PROD = PROD + GRAD(J)*B1(J)
      IF (GMOD - Q2)  315, 315, 320
  315 LE = 2
      WRITE(6,1761) GMOD
 1761 FORMAT(5X,7H GMOD =,E13.5//)
      GO TO 600
  320 C=PROD/SQRT(BMOD*GMOD)
      IF (C) 335, 335, 400
  335 LE = 4
      GO TO 600
  400 LD = 0
      L3 = 0
      DO 410 J = 1, MM
  410 GRAD(J) = B(J) - B1(J)
      WRITE(6,905)
  450 DO 420 II = 1, NN
      I=II
      L=2
      CALL FUNC(1)
      X(II)=ERR(II)**2
  905  FORMAT(5X,10H FUNC1,450 )
      DF(II) = FM(II) - FC(II)
  420 S = S + DF(II)**2/X(II)
      LM=3
      WRITE(6,5)CPU,LM
      WRITE(6,905)
      IF (SA - S) 435, 500, 500
  435 LD = LD + 1
      WRITE(6,906)
  430 DO440 J = 1, MM
      B1(J) = B1(J)/2.0
  906  FORMAT(5X,16H BINARY CHOP,430 )
  440 GRAD(J) = B(J) - B1(J)
```

```
      WRITE(6,906)
      S = 0.0
      L3 = L3 + 1
      IF(L3-3)450,460,460
  460 LE = 5
      GO TO 600
  500 IF (LD) 505, 505, 506
  506 LD = 0
      GO TO 430
  505 DO 510 J = 1, MM
  510 B(J) = GRAD(J)
      SA = S
      IF (SA - Q1) 507, 507, 530
  507 LE = 1
      GO TO 600
  530 IF (L4) 200, 200, 900
  900 WRITE(6,920)L1,A2,L3,S,GMOD,(B(J),J=1,M)
  920 FORMAT(//,15H ITERATION NO.=I5,10X,43H  TRANSFORMATION MADE
TO PR1INCIPAL AXES = A4,10X,  18H BINARY CHOP USED=I3,6H
TIMES/1X,27H W

     2EIGHTED SUM OF SQUARES = E14.7,25X,32H  SQUARE MODULUS OF
GRADIEN

     3T = E14.7/20H  PARAMETERS B(J) -/(6E17.8)/)
      IF (L1 - L4) 200, 910, 910
  910 LE = 6
      GO TO 600
  600 DO 710 J=1,MM
      B1(J) = 0.0
      DO 710 K=1,MM
  710 B2(J,K) = 0.0
      L=1
  907 FORMAT(5X,'FUNC(2) AT 720',/)
C*****FOLLOWING FOR INITIAL VALUES ONLY
  559 CONTINUE
      WRITE(6,907)
      DO 720 II = 1, NN
      I=II
      CALL FUNC(2)
      X(II)=ERR(II)**2
      DF(II) = FM(II) - FC(II)
      DO 720 J = 1, MM
      B1(J) = B1(J) - (2.0*DF(II)*D1(J))/X(II)
```

```
      DO 720 K = 1, MM
  720 B2(J,K) = B2(J,K) - ((DF(II)*D2(J,K) -D1(J)*D1(K)))/X(II)
      CALL EQZERO(B2,B1,M,IC1,IC2,IC3)
      LM=4
      WRITE(6,5)CPU,LM
      WRITE (6,3029)
 3029 FORMAT(' GINO, I AM LOST IN MANTINV')
 3030 FORMAT('   GINO, I AM OUT OF MATINV')
      WRITE(6,3031)B2(1,1),B2(1,2),B2(1,3),B2(1,10),B2(1,11)
      WRITE(6,3032)B2(2,1),B2(2,2)
 3031 FORMAT(2X,'B2(I,J)=',5(E10.4,2X))
 3032 FORMAT(2X,'B2(I,J)=',2(E10.4,2X))
      CALL MATINV(B2,M,B1,1,DETERM)
      WRITE (6,3030)
      DO 730 J=1,MM
      IF (B2(J,J)) 2001,2002,2002
 2001 B1(J) = -SQRT(-B2(J,J))
      GO TO 730
 2002 B1(J)= SQRT(B2(J,J))
  730 CONTINUE
      DO 740 J=1,MM
      DO 740 K=1,MM
  740 B2(J,K)=B2(J,K)/(B1(J)*B1(K))
      WRITE(6,551)LE,SA
  551 FORMAT(//,13H EXIT NUMBER=I3,20X,25H WEIGHTED SUM OF
      SQUARES=E15.81//)
      SSMD = SA
  912 CONTINUE
      RETURN
      END

      SUBROUTINE FUNC(LX)
C     SUBROUTINE FUNC
      DIMENSION SZ(6,6),SX(6,6),S20(6,6),S40(6,6),S42(6,6),SU(6,6),
     1AR(6,6),SY(6,6),S22(6,6),SPX(6),S44(6,6),HN(20),S(36,36)
      DIMENSION B(12),GRAD(12),BB(12),D1(12),D2(12,12)
     1 ,Z(850),SIGN(850),SP(8,12),IBB(850,2),THETA(850)
     2 ,W(36),ZR(36,36),SR(36,36),SI(36,36),CC(36,36),A(666)
     3 ,DELH(850),ANORM2(36),F3(36,36),F4(36,36),IBB1(850,2)
     4 ,CCI(36,36),SI22(36,36),SI42(36,36),SI44(36,36)
     5 ,ZI(36,36),AI(36,36),FM(850),FC(850),DF(850),ERR(850)
      COMMON/DATA/FM,FC,DF,ERR,B,BO,HN,
     *I,L,NUMBER,N,M
      COMMON/DATA2/D1,D2,GRAD,LLX
```

```
      COMMON/DATA3/Z,THETA,DELH,IBB,IBB1
      INTEGER MDA,MDVEC,MMM
      PARAMETER(MMM=36,MDA=MMM,MDVEC=MMM)
      COMPLEX ZP(MDA,MMM),EVEC(MDA,MMM)
      EXTERNAL EVCHF
C     EQUIVALENCE (Z,DC),(B,DC(2989)),(D1,DC(2501)),(D2,DC(2513)),
C     1(M,DC(3173)),(L,DC(3175)),(I,DC(3174)),(BO,DC(3176)),
C     2(HN,DC(3179)),(IBB,DC(4000)),(THETA,DC(3500)),(FC,DC(1001))
C     3 ,(LLX,DC(4998)),(NUMBER,DC(4999)),(ERR,DC(2001))
C     B(I,L) ARE THE LITTLE B(I,L) AS IN THE SPIN HAMILTONIAN
C     FOR RELATION TO CAP.B(I,L) SEE ABRAGAM AND BLEANEY
      DATA(SP(J,1),J=1,6)/2.5,1.5,.5,-.5,-1.5,-2.5/
      DATA(SPX(J),J=1,6)/10.,-2.,-8.,-8.,-2.,10./
      DATA(SP(J,5),J=1,6)/1.,-3.,2.,2.,-3.,1./
C     ****TO BE REMOVED LATER
      DO 91 JIJ=1,6
   91 SP(JIJ,3)=SPX(JIJ)/3.
      R2=SQRT(2.0)
      R3=SQRT(3.0)
      R5=SQRT(5.0)
      R7=SQRT(7.0)
      R10=SQRT(10.0)
      SP(1,4)=R10/3.
      SP(2,4)=R2
      SP(3,4)=R2
      SP(4,4)=R10/3.
      SP(1,6)=3.*R10/20.
      SP(2,6)=-5.*R2/20.
      SP(3,6)=-5.*R2/20.
      SP(4,6)=3.*R10/20.
      SP(1,7)=1./R5
      SP(2,7)=1./R5
      SP(1,2)=R5/2.
      SP(2,2)=R2
      SP(3,2)=1.5
      SP(4,2)=R2
      SP(5,2)=R5/2.
      IF (M.LE.3) THEN
        BB(4)=2.00
        BB(5)=2.00
      END IF
      DO 117 II=1,M
      IF (L.EQ.1)BB(II)=B(II)
      IF (L.EQ.2)BB(II)=GRAD(II)
```

```
 117 CONTINUE
     IF (Z(I)) 18,21,18
  18 CONTINUE
C     PBBZ, PBBX, PBBY ARE COEFFS. MULTIPLYING S(Z), S(X),S(Y)
C     SPIN COMPONENTS
     DO 500 IX=1,6
     DO 500 JX=1,6
     SZ(IX,JX) = 0.
     SX(IX,JX) = 0.
     SY(IX,JX) = 0.
     S20(IX,JX) = 0.
     S22(IX,JX) = 0.
     S40(IX,JX) = 0.
     S42(IX,JX)=0.
     S44(IX,JX) = 0.
     AR(IX,JX) = 0.
     SU(IX,JX) = 0.
 500 CONTINUE
     DO 605 IX=1,36
     W(IX) = 0.
     DO 605 JX=1,36
     SR(IX,JX)=0.
     ZR(IX,JX)=0.
     SI(IX,JX)=0.
 605 CC(IX,JX)=0.
     DO 505 IX=1,6
     SZ(IX,IX) = SP(IX,1)
     S20(IX,IX) = SP(IX,3)
     S40(IX,IX) = SP(IX,5)
     SU(IX,IX) = 1.
 505 CONTINUE
     DO 510 IX=1,4
     IX2 = IX + 2
     S22(IX,IX2) = SP(IX,4)
     S22(IX2,IX) = SP(IX,4)
 510 CONTINUE
     DO 515 IX=1,5
     IX1=IX+1
     SX(IX,IX1) = SP(IX,2)
     SX(IX1,IX) = SP(IX,2)
 515 CONTINUE
     S42(1,3)=9.*R10/60.
     S42(2,4)=-15.*R2/60.
     S42(3,5)=S42(2,4)
```

```
      S42(4,6)=S42(1,3)
      S42(3,1)=S42(1,3)
      S42(4,2)=S42(2,4)
      S42(5,3)=S42(3,5)
      S42(6,4)=S42(4,6)
      S44(1,5)=12.*R5/60.
      S44(2,6)=S44(1,5)
      S44(5,1)=S44(1,5)
      S44(6,2)=S44(2,6)
      RD=3.14159264/180.
      TH = THETA(I)*3.14159264/180.
      CSTH =(COS(TH))
      SNTH =(SIN(TH))
      IF (THETA(I).GT.(8000.))GOTO 775
      BB(12)=0.
      PBBZ = BB(4)*BO*Z(I)*CSTH*COS(BB(12)*RD)
      PBBX = BB(5)*BO*Z(I)*SNTH
      PBBY = BB(5)*BO*Z(I)*CSTH*SIN(BB(12)*RD)
      GO TO 780
  775 CONTINUE
      PBBZ = 0.0
      PBBX = BB(5)*BO*Z(I)*CSTH
      PBBY = BB(5)*BO*Z(I)*SNTH
  780 CONTINUE
      AR(1,1)=2.5*PBBZ+10.*BB(1)/3.+BB(6)
      AR(2,2)=1.5*PBBZ-2.*BB(1)/3.-3.*BB(6)
      AR(3,3)=.5*PBBZ-8.*BB(1)/3.+2.*BB(6)
      AR(4,4)=AR(3,3)-PBBZ
      AR(5,5)=AR(2,2)-3.*PBBZ
      AR(6,6)=AR(1,1)-5.*PBBZ
      AR(1,3)=BB(10)*R10/3.+BB(11)*9.*R10/60.
      AR(2,4)=BB(10)*3.*R2/3.-BB(11)*15.*R2/60.
      AR(3,5)=AR(2,4)
      AR(4,6)=AR(1,3)
      AR(3,1)=AR(1,3)
      AR(4,2)=AR(2,4)
      AR(5,3)=AR(3,5)
      AR(6,4)=AR(4,6)
      AR(1,5)=BB(9)*R5*12./60.
      AR(2,6)=AR(1,5)
      AR(5,1)=AR(1,5)
      AR(6,2)=AR(2,6)
      AR(1,2)=R5*PBBX/2.
      AR(2,1)=AR(1,2)
```

```
      AR(2,3)=R2*PBBX
      AR(3,2)=AR(2,3)
      AR(3,4)=1.5*PBBX
      AR(4,3)=AR(3,4)
      AR(4,5)=R2*PBBX
      AR(5,4)=AR(4,5)
      AR(5,6)=R5*PBBX/2.
      AR(6,5)=AR(5,6)
      SY(1,2)=-R5*PBBY/2.
      SY(2,1)=-SY(1,2)
      SY(2,3)=-R2*PBBY
      SY(3,2)=-SY(2,3)
      SY(3,4)=-1.5*PBBY
      SY(4,3)=-SY(3,4)
      SY(4,5)=-R2*PBBY
      SY(5,4)=-SY(4,5)
      SY(5,6)=-R5*PBBY/2.
      SY(6,5)=-SY(5,6)
      AI(1,2)=SY(1,2)*PBBY
      AI(2,1)=-AI(1,2)
      AI(2,3)=SY(2,3)*PBBY
      AI(3,2)=-AI(2,3)
      AI(3,4)=SY(3,4)*PBBY
      AI(4,3)=-AI(3,4)
      AI(4,5)=SY(4,5)*PBBY
      AI(5,4)=-AI(4,5)
      AI(5,6)=SY(5,6)*PBBY
      AI(6,5)=-AI(5,6)
      DO 530 J=1,4
      J2=J+2
      SI22(J,J2)=-S22(J,J2)
      SI22(J2,J)=S22(J,J2)
      SI42(J,J2)=-S42(J,J2)
      SI42(J2,J)=S42(J,J2)
      BB(12)=0.
      AI(J,J2)=BB(12)*SI22(J,J2)+BB(12)*SI42(J,J2)
      AI(J2,J)=-AI(J,J2)
  530 CONTINUE
      DO 535 J=1,2
      J4=J+4
      SI44(J,J4)=-S44(J,J4)
      SI44(J4,J)=S44(J,J4)
      BB(12)=0.
      AI(J,J4)=BB(12)*SI44(J,J4)
```

```
      AI(J4,J)=-AI(J,J4)
  535 CONTINUE
      DO 520 IY=1,6
      DO 520 JY =1,6
      DO 520 IZ=1,6
      DO 520 JZ=1,6
      IX=(IY-1)*6+IZ
      JX=(JY-1)*6+JZ
      SR(IX,JX)=AR(IY,JY)*SU(IZ,JZ)+
     1 SU(IY,JY)*(S20(IZ,JZ)*BB(7)+S22(IZ,JZ)*BB(8))+
     2BB(2)*SZ(IY,JY)*SZ(IZ,JZ)+BB(3)*(SX(IY,JY)*SX(IZ,JZ)
     3 -SY(IY,JY)*SY(IZ,JZ))
      SI(IX,JX)=AI(IY,JY)*SU(IZ,JZ)
  520 CONTINUE
      DO 5007 IR=1,36
      DO 5007 JR=1,36
 5007 ZP(IR,JR)=CMPLX(SR(IR,JR),SI(IR,JR))
      CALL EVCHF(MMM,ZP,MDA,W,EVEC,MDVEC)
      CALL EVCHFN(MMM,MDA,W,EVEC,ANORM2,F3,F4)
      DO 5005 IR=1,36
      S(IR,IR)=W(IR)
      DO 5005 JR=1,36
      ZI(IR,JR)=AIMAG(EVEC(IR,JR))
 5005 ZR(IR,JR)=REAL(EVEC(IR,JR))
C     ** TO BE REMOVED LATER(LLX IS DEFINED IN FUNC)
      IF(LLX)992,993,992
  993 CONTINUE
  995 FORMAT(5X,'I=',I3)
  994 FORMAT(X,'W=',6E12.4)
      IF(I.NE.415)GOTO 1111
 1994 FORMAT(X,6E12.4)
 1111 CONTINUE
  992 CONTINUE
C  *****DEFINE HERE THE LINES WHOSE QUANTUM NOS. NOT DEFINED
ABOVE
      I6=I
      IF(NUMBER.NE.1) GO TO 1814
      I1=IBB(I6,1)
      I2=IBB(I6,2)
      GO TO 803
 1814 CONTINUE
      IF(NUMBER.NE.2) GO TO 815
      I1=IBB(I6,1)
      I2=IBB(I6,2)
```

```
      GO TO 803
  815 CONTINUE
      IF(NUMBER.NE.3) GO TO 816
      I1=IBB(I6,1)
      I2=IBB(I6,2)
      GO TO 803
  816 CONTINUE
      IF (NUMBER.NE.4) GO TO 817
      I1=IBB(I6,1)
      I2=IBB(I6,2)
      GO TO 803
  817 CONTINUE
      IF (NUMBER.NE.5) GO TO 818
      IF ((IBB(I6,1).EQ.0).AND.(IBB(I6,2).EQ.0)) GO TO 818
      I1=IBB(I6,1)
      I2=IBB(I6,2)
      GO TO 803
  818 CONTINUE
C*****DEFINE ABOVE THE LINES WHOSE QUANTUM NOS. NOT DEFINED
ABOVE
  802 CONTINUE
      I1=1
      I2=2
      DELMIN=ABS(ABS(W(1)-W(2))-FM(I))
      DO 85 IX=1,35
      IX1=IX+1
      DO 81 JX=IX1,36
      DELI=ABS(ABS(W(IX)-W(JX))-FM(I))
      IF(DELI-DELMIN)84,84,86
   84 DELMIN=DELI
      I1=IX
      I2=JX
      IBB(I,1)=I1
      IBB(I,2)=I2
   86 CONTINUE
   81 CONTINUE
   85 CONTINUE
  803 CONTINUE
      FC(I)=ABS(W(I1)-W(I2))
      SIGN(I)=(W(I1)-W(I2))/FC(I)
      DO 301 IY=1,6
      DO 301 JY=1,6
      DO 301 IZ=1,6
      DO 301 JZ=1,6
```

```
      IX=(IY-1)*6+IZ
      JX=(JY-1)*6+JZ
      CC(IX,JX)=BO*DELH(I)*(BB(4)*CSTH*SZ(IY,JY)*SU(IZ,JZ)+
     1 BB(5)*SNTH*SX(IY,JY)*SU(IZ,JZ))
  301 CONTINUE
      ERR(I)=0.
      DO 814 IX=1,36
      DO 814 JX=1,36
      ERR(I)=ERR(I)+CC(IX,JX)*(ZR(JX,I1)*ZR(IX,I1)
     1 -ZR(JX,I2)*ZR(IX,I2))
  814 CONTINUE
      GO TO 17
   21 CONTINUE
      FC(I)=FM(I)
      ERR(I)=1.
      SIGN(I) =1.
   17 CONTINUE
      IF(LX-1)110,110,120
  120 CONTINUE
      DO 235 IZ=1,12
      D1(IZ) = 0.0
      DO 235 JZ=1,12
  235 D2(IZ,JZ) =0.0
      IF (Z(I)) 418,217,418
  418 CONTINUE
      DO 237 KX=1,11
      DO 236 IY=1,6
      DO 236 JY=1,6
      DO 236 IZ=1,6
      DO 236 JZ=1,6
      IX=(IY-1)*6 + IZ
      JX=(JY-1)*6 + JZ
      GO TO (707,714,715,705,706,709,712,713,711,708,710),KX
  705 CC(IX,JX)=SZ(IY,JY)*SU(IZ,JZ)
      ALPHA=BO*Z(I)*CSTH
      GO TO 720
  706 CC(IX,JX)=SX(IY,JY)*SU(IZ,JZ)
      ALPHA=BO*Z(I)*SNTH
      GO TO 720
  707 CC(IX,JX)=S20(IY,JY)*SU(IZ,JZ)
      ALPHA=1.
      GO TO 720
  709 CC(IX,JX)=S40(IY,JY)*SU(IZ,JZ)
      ALPHA=1.
```

```
      GO TO 720
  714 CC(IX,JX)=SZ(IY,JY)*SZ(IZ,JZ)
      ALPHA=1.
      GO TO 720
  712 CC(IX,JX)=SU(IY,JY)*S20(IZ,JZ)
      ALPHA=1.
      GO TO 720
  710 CC(IX,JX)=S42(IY,JY)*SU(IZ,JZ)
      ALPHA=1.
      GO TO 720
  711 CC(IX,JX)=S44(IY,JY)*SU(IZ,JZ)
      ALPHA=1.
      GO TO 720
  708 CC(IX,JX)=S22(IY,JY)*SU(IZ,JZ)
      ALPHA=1.
      GO TO 720
  713 CC(IX,JX)=SU(IY,JY)*S22(IZ,JZ)
      ALPHA=1.
      GO TO 720
  715 CC(IX,JX)=SX(IY,JY)*SX(IZ,JZ)
     2 -SY(IY,JY)*SY(IZ,JZ)
      ALPHA=1.
  720 CONTINUE
      SR(JX,IX)=(ZR(JX,I1)*ZR(IX,I1)-ZR(JX,I2)*ZR(IX,I2))*
     1 SIGN(I)
C FOLLOWING TWO LINES CHANGE FROM GXX INDEPENDENT TO
GXX=GZZ
      KX1=KX
  236 D1(KX1)=D1(KX1)+CC(IX,JX)*SR(JX,IX)*ALPHA
C     FOLLOWING LINE CHANGES GXX INDEP. TO GXX=GZZ
  237 CONTINUE
  217 CONTINUE
  110 CONTINUE
      RETURN
      END
      SUBROUTINE EXAM(A,B,M,LF)
C     SUBROUTINE EXAM
C       F O R T R A N  4
      DIMENSION A(12,12),B(12),C(12)
      DO 80 J=1,M
   80 C(J)=A(J,J)
      IF(A(1,1)) 60,200,70
   60 A(1,1) =-SQRT(-A(1,1))
      GO TO 300
```

```
 70 A(1,1) =SQRT(A(1,1))
    GO TO 100
100 IF(M-1)400,400,110
110 DO 115 K=2,M
115 A(1,K)=A(1,K)/(A(1,1))
    DO 120 J=2,M
    J1=J-1
    S=A(J,J)
    DO 125 L=1,J1
125 S=S-A(L,J)**2
    IF (S) 50,200,40
 50 A(J,J) =-SQRT(-S)
    GO TO 300
 40 A(J,J) =SQRT(S)
    GO TO 130
130 IF(J-M)135,400,400
135 J2=J+1
    DO 120 K=J2,M
    S=A(J,K)
    DO 145 L=1,J1
145 S=S-A(L,J)*A(L,K)
120 A(J,K)=S/A(J,J)
400 B(1)=B(1)/A(1,1)
    IF(M-1)420,420,405
405 DO 410 J=2,M
    S=B(J)
    J1=J-1
    DO 415 L=1,J1
415 S=S-A(L,J)*B(L)
410 B(J)=S/A(J,J)
420 B(M)=B(M)/A(M,M)
    J=M-1
435 IF(J)450,450,425
425 S=B(J)
    J2=J+1
    DO 430 L=J2,M
430 S=S-A(J,L)*B(L)
    B(J)=S/A(J,J)
    J=J-1
    GO TO 435
450 LF=1
    GO TO 460
200 LF=0
    GO TO 460
```

```
 300 LF=-1
 460 DO 465 J=1,M
     A(J,J)=C(J)
     IF(J-M)470,475,475
 470 J2=J+1
     DO 465 K=J2,M
 465 A(J,K)=A(K,J)
 475 RETURN
     END

     SUBROUTINE MATINV(A,N,B,M,DETERM)
C    SUBROUTINE MATINV
C     F O R T R A N  4
C    MATRIX INVERSION WITH ACCOMPANYING SOLUTION OF LINEAR
C    EQUATIONS
     DIMENSION IPIVOT(12),A(12,12),B(12,1),INDEX(12,2),PIVOT(12)
     EQUIVALENCE (IROW,JROW),(ICOLUM,JCOLUM),(AMAX,T,SWAP)
     DETERM=1.0
     DO 20 J=1,N
  20 IPIVOT(J)=0
     DO 169 I=1,N
     WRITE(6,179)(A(I,J),J=1,N)
 169 CONTINUE
 179 FORMAT(5X,'A(I,J)=',/,6(E10.4,2X),/,6(E10.4,2X))
     DO 550 I=1,N
     AMAX=0.0
     DO 105 J=1,N
     IF(IPIVOT(J)-1)60,105,60
  60 DO 100 K=1,N
     IF(IPIVOT(K)-1)80,100,740
  80 IF(ABS(AMAX)-ABS(A(J,K)))85,100,100
  85 IROW=J
     ICOLUM=K
     AMAX=A(J,K)
 100 CONTINUE
 105 CONTINUE
     IPIVOT(ICOLUM)=IPIVOT(ICOLUM)+1
     IF (IROW-ICOLUM)140,260,140
 140 DETERM=-DETERM
     DO 200 L=1,N
     SWAP=A(IROW,L)
     A(IROW,L)=A(ICOLUM,L)
 200 A(ICOLUM,L)=SWAP
     IF(M)260,260,210
```

```
210 DO 250 L=1,M
   SWAP=B(IROW,L)
   B(IROW,L)=B(ICOLUM,L)
250 B(ICOLUM,L)=SWAP
260 INDEX(I,1)=IROW
   INDEX(I,2)=ICOLUM
   PIVOT(I)=A(ICOLUM,ICOLUM)
   DETERM=DETERM*PIVOT(I)
   MODIFY = 0
   IF (ABS(DETERM).LT.(1.E+25)) GO TO 310
   MODIFY = MODIFY + 1
   DETERM = DETERM*(1.E-10)
   WRITE(6,320) MODIFY
320 FORMAT(5X,'MODIFY=', I2)
310 CONTINUE
   A(ICOLUM,ICOLUM)=1.0
   DO 350 L=1,N
350 A(ICOLUM,L)=A(ICOLUM,L)/PIVOT(I)
   IF(M)380,380,360
360 DO 370 L=1,M
370 B(ICOLUM,L)=B(ICOLUM,L)/PIVOT(I)
380 DO 550 L1=1,N
   IF (L1-ICOLUM)400,550,400
400 T=A(L1,ICOLUM)
   A(L1,ICOLUM)=0.0
   DO 450 L=1,N
450 A(L1,L)=A(L1,L)-A(ICOLUM,L)*T
   IF(M)550,550,460
460 DO 500 L=1,M
500 B(L1,L)=B(L1,L)-B(ICOLUM,L)*T
550 CONTINUE
   DO 710 I=1,N
   L=N+1-I
   IF(INDEX(L,1)-INDEX(L,2))630,710,630
630 JROW=INDEX(L,1)
   JCOLUM=INDEX(L,2)
   DO 705 K=1,N
   SWAP=A(K,JROW)
   A(K,JROW)=A(K,JCOLUM)
   A(K,JCOLUM)=SWAP
705 CONTINUE
710 CONTINUE
740 RETURN
   END
```

```
      SUBROUTINE EQZERO(A,B,M,IC1,IC2,IC3)
      DIMENSION A(12,12),B(12)
      IC1=0
      IC2=0
      IC3=0
      DO 5 J3=1,M
      IF((ABS(B(J3))).GT.(1.E-20)) GO TO 10
      B(J3)=0.
      IC1=J3
      WRITE(6,100) IC1
   10 CONTINUE
      DO 5 J4=1,M
      IF((ABS(A(J3,J4))).GT.(1.E-10)) GO TO 15
      A(J3,J4)=0.
      IC2=J3
      IC3=J4
      WRITE(6,101) IC2,IC3
   15 CONTINUE
    5 CONTINUE
  100 FORMAT(5X, I3)
  101 FORMAT(5X,2I3)
      RETURN
      END
      SUBROUTINE EVCHFN(M,MDA,W,EVEC,ANORM1,F11,F22)
C     NORMALIZATION OF EIGENVECTORS
      COMPLEX EVEC(MDA,M),VV(M)
      REAL ANORM1(M),F11(M,M),F22(M,M),W(M),TEMP
      DO 108 I=1,M
      DO 108 J=1,M
      F11(I,J)=REAL(EVEC(I,J))
  108 F22(I,J)=AIMAG(EVEC(I,J))
      DO 1005 I1=1,M
      ANORM1(I1)=0.0
      DO 1006 J1=1,M
 1006 ANORM1(I1)=ANORM1(I1)+F11(J1,I1)**2+F22(J1,I1)**2
 1005 ANORM1(I1)=SQRT(ANORM1(I1))
      DO 1007 I1=1,M
      DO 1007 J1=1,M
      F11(I1,J1)=F11(I1,J1)/ANORM1(J1)
 1007 F22(I1,J1)=F22(I1,J1)/ANORM1(J1)
      DO 101 I2=1,M
      DO 101 J2=1,M
  101 EVEC(I2,J2)=CMPLX(F11(I2,J2),F22(I2,J2))
```

```
      M1=M
      DO 501 I9=1,M1
      I6=I9+1
      DO 501 I8=1,M1
      IF(W(I8)-W(I9))505,510,510
  505 TEMP=W(I8)
      W(I8)=W(I9)
      W(I9)=TEMP
      DO 515 I7=1,M
      VV(I7)=EVEC(I7,I8)
      EVEC(I7,I8)=EVEC(I7,I9)
  515 EVEC(I7,I9)=VV(I7)
  510 CONTINUE
  501 CONTINUE
      RETURN
      END
```

References

A. Abragam and B. Bleaney, *Electron Paramagnetic Resonance of Transition Ions*, (Clarendon Press, Oxford) (1970)

Malcolm Bersohn and James C. Baird, *An Introduction to Electron Paramagnetic Resonance*, (W. A. Benjamin, New York) (1966)

Bruker Technical Manual, (3 Ave. du General de Gaulle, Lisses) (1990)

Frederick W. Byron and Robert W. Fuller, *Mathematics of Classical and Quantum Physics*, (Dover Publications Inc., New York) (1992)

Prem Chand and G. C. Upreti, J. Chem. Phys. **78**, 5930 (1983)

Prem Chand and G. C. Upreti, J. Chem. Phys. **81**, 1650 (1984)

E. U. Condon and G. H. Shortley, *The Theory of Atomic Spectra*, (Cambridge University Press, Cambridge) (1935)

John C. Dering, Ph. D Thesis, University of Calgary, Calgary (1967)

A. Forman and J. A. van Wyk, J. Chem. Phys. **44**, 73 (1966)

A. Forman and J. A. van Wyk, Can. J. Phys. **45**, 3381 (1967)

M. Heming and G. Lehmann, Electronic Magnetic Resonance of the Solid State, edited by John A. Weil, 163 (1987)

IBM Instruments Inc., *Bruker ER Series User's Manual*, (Department 74P, Danbury, CT) (1983)

V. K. Jain and G. Lehmann, Phys. Stat. Sol. (b) **159**, 495 (1990)

Charles Kittel, *Introduction to Solid State Physics*, (John Wiley and Sons Inc., New York) (1961)

K. Kumar, *Perturbation Theory and the Nuclear Many Body Problem*, (Interscience Publishers, New York) (1962)

G. Lehmann, Phys. Stat. Sol. (b) **99**, 623 (1980)

Eugene Merzbacher, *Quantum Mechanics*, (John Wiley and Sons, Inc, New York) (1998)

S. K. Misra, Magnetic Resonance Review **10**, 285 (1986)

S. K. Misra in: *Handbook of Electron Spin Resonance*, **2**, 85, edited by Charles P. Poole Jr. and Horacio A. Farach, (Springer-Verlag, New York) (1999)

N. F. Mott and M. J. Littleton, Trans. Faraday Soc. **34**, 485 (1938)

D. J. Newman, Adv. Phys. **20**, 197 (1971)

D. J. Newman and E. Siegel, J. Phys. C: Solid State Phys. **9**, 4285 (1976)

D. J. Newman and W. Urban, Adv. Phys. **24**, 793 (1975)

OKI Reflex Klystrons, *OKI electric industry company ltd.*, (10-3, shibaura 4-chome, Minato-ku, Tokyo) (1977)

U. Oseguera V. *et al.*, J. Chem. Phys. **73**, 1132 (1980)

Oxford Instruments Operating Manual ESR 9, (Osney Mead, Oxford) (1978)

G. E. Pake and T. L. Estle, *The Physical Principles of Electron Paramagnetic Resonance*, (W. A. Benjamin, Inc, Reading, Massachusetts) (1973)

Linus Pauling, *The Nature of the Chemical Bond*, (Cornell University Press, Ithaca) (1939)

Yoav Peleg *et al.*, *Theory and Problems of Quantum Mechanics*, (McGraw-Hill, New York) (1998)

Charles P. Poole, *Electron Spin Resonance: A Comprehensive Treatise on Experimental Techniques*, (Interscience Publishers, New York) (1967)

John R. Reitz and J. L. Gammel, J. Chem. Phys. **19**, 894 (1951)

J. Rubio O. and W. K. Cory, J. Chem. Phys. **69**, 4792 (1978)

J. Rubio *et al.*, J. Chem. Phys. **71**, 4112 (1979)

VARIAN Analytical Instruments Division, (19 Brydon Dr., Rexdale, On.) (1965)

W. Weltner Jr. and R. J. Van Zee, J. Chem. Phys. **82**, 4492 (1985)

Wen-Chen Zheng, Physica B **190**, 413 (1993)

John E. Wertz and James R. Bolton, *Electron Spin Resonance: Elementary Theory and Practical Applications* (McGraw-Hill, New York) (1972)

Hugh D. Young and Roger A. Freedman, *University Physics*, (Addison-Wesley, San Francisco) (2000)